Old Dominion University

ODU Digital Commons

Diamond for Fiber-Optic Raman Spectroscopy

Jianli Zheng
Old Dominion University

Recommended Citation

DIAMOND FOR FIBER OPTIC RAMAN SPECTROSCOPY

By

Jianli Zheng

B.S. in Optical and Scientific Instrumentation Engineering, July 1984,
Zhejiang University, P. R. China
M.S. in Optical and Scientific Instrumentation Engineering, July 1987,
Zhejiang University, P. R. China

A Dissertation submitted to the faculty of
Old Dominion University in Partial Fulfillment of the
Requirements for the Degree of

DOCTOR OF PHILOSOPHY

ELECTRICAL ENGINEERING

OLD DOMINION UNIVERSITY

December 1997

Approved by:

_____
Dr. Sacharia Albin

_____
Dr. John B. Cooper

_____
Dr. Linda L. Vahala

_____
Dr. Vishnu K. Lakdawala

ABSTRACT

DIAMOND FOR QUANTITATIVE FIBER OPTIC RAMAN SPECTROSCOPY

Jianli Zheng

Old Dominion University, 1997

Director: Dr. Sacharia Albin

Raman spectroscopy is a powerful technique for molecular structural studies and concentration measurement. Being a single beam technique, the Raman intensity depends on the optical power of the excitation source, optical alignment of the system, detector response as well as species concentration. To eliminate the unwanted variations in the system and get the concentration information of the species, intensity referencing is necessary. The existing referencing methods either use a constant Raman band of the sample, or add a chemically inert material with known concentration into the sample. Unfortunately, the former method is not always applicable and the latter is not acceptable for *in situ* process monitoring. A new concept of using diamond as an intensity standard in quantitative Raman analysis is presented in this dissertation. Combined with fiber optics, a self-referenced universal Raman probe is developed. Performances of five probe designs are investigated. Results indicate that diamond-referenced probes are insensitive to the excitation power fluctuation and optical alignment. Chemical vapor deposited (CVD) diamond film is investigated as an alternative to the expensive bulk diamond. The CVD diamond referenced probe shows performance similar to the bulk diamond probe. A remote measurement is also performed with a 500-foot fiber probe, which shows the potential of long distance *in situ* concentration monitoring in an industrial environment.

ACKNOWLEDGEMENTS

I would first like to express my sincere thanks to Dr. Sacharia Albin, for his guidance, patience, friendship, and financial support during this research. His knowledge and hard work helped me overcome a variety of difficulties throughout my graduate study. His help in my education has been invaluable. I would also like to thank Dr. John B. Cooper. He has dedicated his valuable time to help me setup the Raman system and provided the chemicals for this research. He also provided insightful discussion, which has been very helpful in completing this research. Special thanks go to members of the committee, Dr. Vishnu Lakdawala and Dr. Linda Vahala, for their valuable time and assistance in bringing this research to a close.

Thanks also go to my colleagues Arnel C. Lavarias and John C. Hagwood for their help in the Photonics and Microelectronics Laboratory. Working with them has been very enjoyable and those discussions ranging from research to daily life have helped me to overcome the language barrier and accommodate the life style in this country.

Most importantly, I would like to thank my wife, Li Ding. She has provided all the support she could give and brought two boys, Kevin and Jason, to our family during the years of my graduate study, while she has also been pursuing her Master's degree.

Finally, I would like to thank my family for the years of support they have given me. Thanks!

TABLE OF CONTENTS

LIST OF TABLES

LIST OF FIGURES

Page

CHAPTER I

INTRODUCTION

This dissertation deals with the investigation of a self-referencing method for quantitative fiber optic Raman spectroscopy. The research covers three areas: Raman spectroscopy, fiber optics, and diamond technology. The goal of this research is to produce a self-referenced general-purpose fiber-optic probe for remote quantitative *in-situ* monitoring using Raman spectroscopy. The motivation and a brief review of the research are given in this chapter.

1.1 Research Background

The Raman effect was first discovered by the Indian scientist Sir C. V. Raman in 1928 [1]. This discovery lead to Asia's first Nobel Prize winner in science for him in 1930. The significance of the Raman effect was recognized immediately because this technique provides another way to investigate the ultimate structure of molecules in the medium other than the infrared (IR) spectroscopy, and it was much easier to implement compared to the IR spectrum at that time. As stated by Raman: "The universality of the phenomenon, the convenience of the experimental technique, and the simplicity of the spectra obtained enable the effect to be used as an experimental aid to the solution of a wide range of problems in physics and chemistry."

The Raman effect is an inelastic light scattering process as shown in Fig. 1.1. It can be simply described by two processes: (1) incident light is virtually absorbed by a

Incident
photon
$h\nu_0$

Molecule

Emitted
photon
$h(\nu_0 \pm \nu_m)$

Phonon
$h\nu_m$
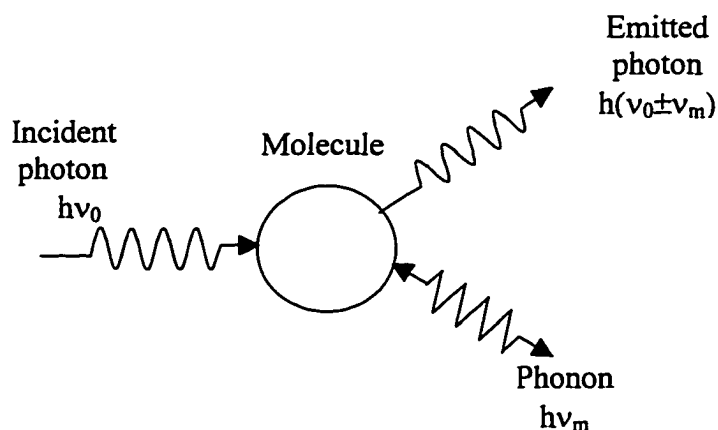
Figure 1.1   A schematic diagram of Raman effect

polarizable sample, inducing a transition from the lower electronic states to an excited or

"virtual" state, and (2) the energy is then relaxed via a transition from the virtual state to a

lower energy state by spontaneous emission of a photon and either creating or absorbing

a vibrational quantum of energy (a phonon in crystals). Thus the energy of the emitted

photon is shifted by the vibrational energy of the molecule, leading to a wavelength shift

in the scattered light. This shift is independent of the incident light, it contains the

information of the molecular structure and vibrational status.

In the first two decades after its discovery, Raman spectroscopy played a major

role in many chemical structure studies [2]. However, in the next two decades, because

of the rapid development of the commercial IR spectrometers, there was almost no major

advance in Raman instruments. In 1962, laser was first introduced by Porto and Wood in

Raman spectroscopy [3]. The appearance of laser revived the Raman technique

dramatically because lasers are ideal sources for Raman studies for its monochromatic

property and high intensity. At about the same time, developments in optical components

such as diffraction gratings, photomultiplier tubes, and photo-counting devices made a new generation of Raman spectrometers commercially possible. Their availability led to a great resurgence in this field. For many years, Raman spectroscopy has been a powerful tool for investigation of molecular vibrations and rotations. The importance of Raman spectroscopy has been further augmented by the discovery and use of resonance Raman effect [4], nonlinear Raman effects (includes hyper-Raman scattering, coherent anti-Stokes Raman scattering or

CARS, stimulated Raman scattering) [5], surface-enhanced Raman spectroscopy (SERS) [6], and Fourier transform (FT) Raman spectroscopy [7].

Although Raman spectroscopy is a very powerful tool for species identification and concentration measurement, for a long time, its application was limited in the laboratory for "off line" analysis, which means a test sample has to be brought to the laboratory to do the analysis. On-line monitoring becomes difficult because of the critical alignment requirement. This situation has changed since optical fibers have been incorporated with this technology. As shown in Fig.1.2, fiber optic sampling greatly simplifies optical alignment, and also can isolate the Raman spectrometer from the dirty and corrosive environment by transmitting the signal to the centralized control room using long optical fibers. Both excitation light and scattered light can be guided through the flexible fiber, and Raman spectrum can be easily obtained merely by immersing the fiber optic probe in the sample. In addition to that, the emergence of FT Raman using IR excitation sources provides a solution of circumventing the fluorescence problems. Thus Raman technologies are now becoming a useful tool not only for laboratory analysis, but
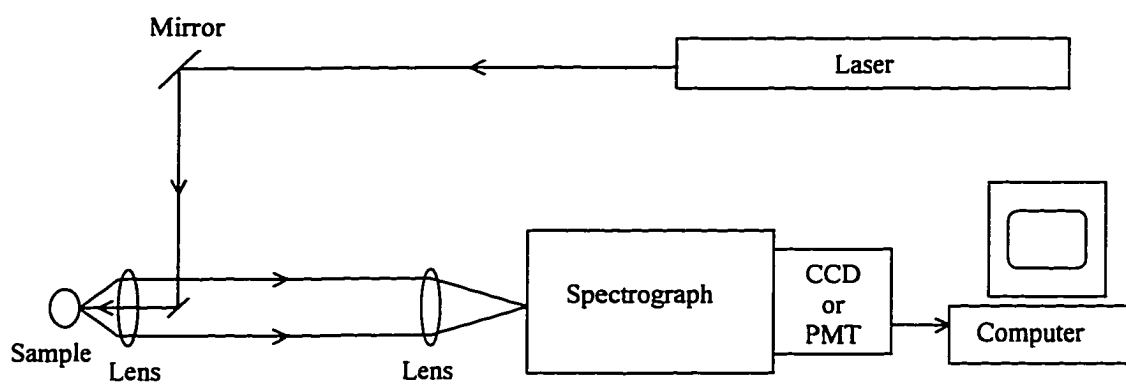
(a)
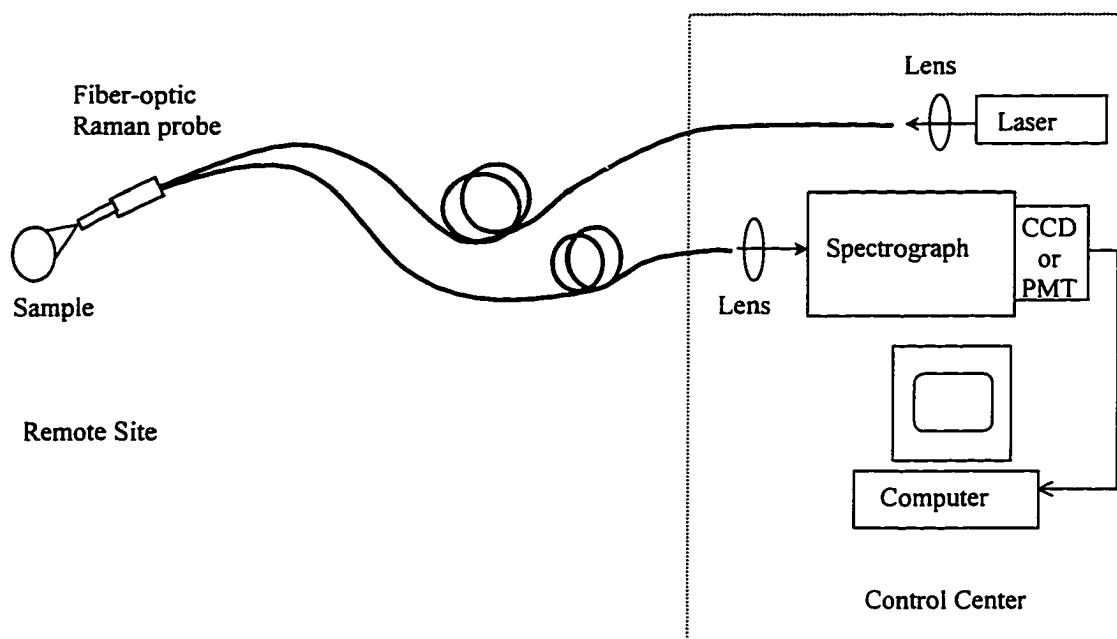
(b)

Figure 1.2   Schematic diagram of (a) a typical conventional Raman system, (b) a fiber-optic Raman system

also for remote monitoring in industrial environments. Measurements at distances of up to several hundred meters between the instruments and the industrial site can now be routinely obtained [8]. Multi-point measurement also becomes possible by multiplexing the optical fibers and having the operation of the whole system controlled by microcomputers.

The use of fiber optics in Raman spectroscopy was first presented by Trott and Furtak [9], followed by McCreery, Fleischmann, and Hendra in 1983 [10]. Subsequent developments have been reported by McCreery *et al.* [11-13]. Mullen *et al.* have used fiber optics in SERS for *in situ* monitoring of the ions in water [14], the remote sensing and high sensitivity make it useful in the environmental industry. Wang *et al.* have used fiber optic Raman spectroscopy for a direct quantitative analysis of styrene during an emulsion polymerization [15]. Fiber optics has also been combined with the FT-Raman system to eliminate the florescent problems [16-17]. One of the problems with the fiber-optic Raman system is the SiO_2 background in the Raman spectrum induced by the glass fiber. This can be solved by optimizing the probe structure [8,18] or introducing optical filters [19]. More details about fiber-optic Raman spectroscopy will be presented in Chapter III.

Fiber optics have brought Raman spectroscopy from the laboratory to the industrial environments. However, one more problem still to be solved for quantitative analysis is referencing. Since Raman spectroscopy is a single beam technique, other than the concentration of the analyte, the intensity of a Raman line is also affected by a number of factors, including incident laser power, frequency of the scattered radiation,

absorption of the materials involved in the scattering, and the response of the detection system.

To eliminate the unwanted variations in the system and get the concentration information of the species, intensity referencing is necessary. The widely used referencing technique is to introduce into the sample a small quantity of a presumably inert material with an easily detectable Raman line used as a referencing standard. As the concentration of the standard is kept constant, the relative intensity, which is the ratio of the Raman line of the interested species to the Raman line of the standard, only depends on the concentration of the interested species [20]. Unfortunately, this invasive method will contaminate the testing sample, and is usually unacceptable for *in situ* monitoring industrial process.

Diamond is a good candidate to be used as a standard. It follows all the essential requirements for the referencing standard. It is chemically inert and has a sharp narrow peak at 1332 cm^{-1} with a flat background. Unlike some soluble referencing standard, diamond does not mix with the sample. By combining diamond with fiber optics, it is quite possible to make a self-referenced fiber-optic Raman probe that can be used for non-destructive *in situ* measurement. The verification of this concept and probe design becomes the first part of this research.

One more aspect to be considered is that natural diamond is very expensive. It is usually unacceptable in commercial products. The alternative to expensive natural diamond is the chemical vapor deposited (CVD) diamond. The Raman band of CVD diamond usually is broader than natural diamond, and the background is not flat due to graphite contamination and other impurities. This may distort the Raman spectrum of the

sample. Thus another part of this research is to optimize the deposition parameters to get high quality CVD diamond with the Raman spectrum close to natural diamond.

1.2 Research Overview

A brief discussion of basic theory and application of Raman spectroscopy will be given in Chapter II. The rest of Chapter II will discuss the general referencing techniques for quantitative Raman spectroscopy, followed by an introduction of diamond properties, and the possibility of using diamond as a referencing standard for quantitative Raman spectroscopy. Chapter III presents four designs of the diamond-referenced fiber-optic Raman probe. The performances of these probes are investigated using both aqueous and organic solutions. These performances include the effect of the excitation laser power, the effect of the optical alignment, and the effect of the refractive index of the tested media. A remote sensing experiment is also conducted with a 500-foot fiber optic probe referenced with diamond. To reduce the cost of the probe, CVD diamond can replace the expensive bulk diamond. The investigation of CVD diamond is presented in Chapter IV. A microwave plasma enhanced CVD (MPECVD) system is used to grow diamond. Growth parameters are optimized by executing a series of experiments to get high quality CVD diamond. Different combinations of gases are introduced into the deposition chamber to increase the deposition rate. Finally, a fiber-optic Raman probe with CVD diamond is developed, and the experimental results are presented and compared to the results of the natural diamond probe. The last chapter will give the summary and future research directions.

CHAPTER 2

RAMAN SPECTROSCOPY AND QUANTATIVE ANALYSIS

In this chapter, the basic theory of Raman effect as well as the experimental setup for Raman spectroscopy is discussed. A brief review of the general applications of Raman spectroscopy will also be provided. The rest of this chapter will concentrate on the quantitative analysis using Raman spectroscopy. Raman spectroscopy can be used for quantitative measurement of species concentration. However, like other emission techniques, Raman spectroscopy suffers from the disadvantage of a single-beam technique that the accuracy of quantitative analysis is disturbed by the uncorrected variations in source, sample, and optics. The general techniques to solve this problem will be discussed. Finally, a new concept of using diamond as a referencing standard in fiber-optic Raman spectroscopy for quantitative analysis is presented.

2.1 Basic Principles of Raman Spectroscopy

2.1.1 Raman Theory

Raman spectroscopy involves the inelastic scattering of photons. Unlike infrared spectroscopy, which involves the actual direct transition between the two energy levels, Raman lines correspond to the transition from the initial level to the final level with the help of intermediate levels (also called virtual levels). A simplified energy level is shown in Fig.2.1. When a sample is illuminated by a beam of very intense monochromatic light, usually a laser, two types of scattering occur. One is called Rayleigh scattering, which is strong and has the same frequency as the incident light
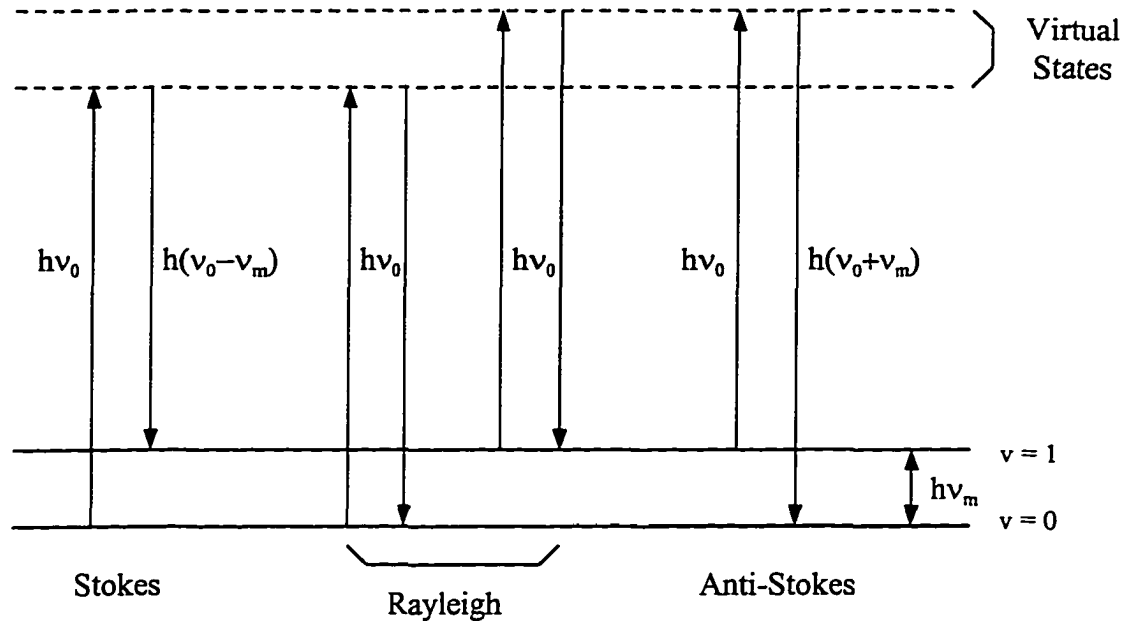
Figure. 2.1 A simplified Energy level showing the Raman effect

(v_0). The other called Raman scattering, is very weak and has frequencies $v_0 \pm v_m$, where v_m is the vibrational frequency of a molecule. The ($v_0 - v_m$) line is called Stokes scattering, and the ($v_0 + v_m$) line is called anti-Stokes scattering. Thus, Raman spectroscopy actually measures the intensity and the frequency shift of the scattered light from the incident beam, which is determined by the viberational frequency of the sample molecules. Since the probability of the molecules to stay at the ground state $v = 0$ is higher than that at the state $v = 1$, the Stokes lines are stronger than the anti-Stokes lines.

A simple explanation of Raman effect can be given by the classical theory [3][21]. When a polarizable diatomic molecule is irradiated by a beam of laser, a dipole moment P is induced by the electric field of the radiation; thus,

$$P = \alpha E = \alpha E_0 \cos 2\pi v_0 t. \tag{2.1}$$

Here $E = E_0 \cos 2\pi v_0 t$ is the electric field strength induced by the electromagnetic wave with E_0 as the amplitude and v_0 as the frequency of the laser; α is the molecular polizability which is a function of the vibrational or other motion of the nuclei. For a given normal mode of vibrational frequency v_m, and nuclear displacement q,

$$\alpha = \alpha_0 + (\frac{\partial \alpha}{\partial q}) q + \frac{1}{2}(\frac{\partial^2 \alpha}{\partial q^2}) q^2 + \dots \tag{2.2}$$

where

$$q = q_0 \cos 2\pi v_m t. \tag{2.3}$$

For small amplitude of vibration, the square term and the higher order terms can be ignored. Combining Eq.(2.2) and Eq.(2.3), we get

$$\alpha = \alpha_0 + (\frac{\partial \alpha}{\partial q}) q_0 \cos 2\pi v_m t = \alpha_0 + \alpha_l \cos 2\pi v_m t \tag{2.4}$$

where $\alpha_l = (\frac{\partial \alpha}{\partial q}) q_0$.

Substituting in Eq. (2.1),

$$P = \alpha_0 E_0 \cos 2\pi v_0 t + \alpha_l E_0 \cos 2\pi v_0 t \cos 2\pi v_m t$$

$$= \alpha_0 E_0 \cos 2\pi v_0 t + \frac{1}{2} \alpha_l E_0 \{\cos[2\pi(v_0 + v_m)t + \cos[2\pi(v_0 - v_m)t]\}. \tag{2.5}$$

According to the classical electromagnetic theory, the radiated power by an oscillating dipole is given as:

$$I = \frac{16\pi^4 v_0^4}{3c^2} P^2. \tag{2.6}$$

Combining Eq.(2.5) and Eq.(2.6), the total scattered light power from one molecule is given by:

$$I = \frac{16\pi^4 v_0{}^4}{3c^2} \{\alpha_0{}^2 E_0{}^2 \cos^2 2\pi v_0 t + \frac{1}{4}\alpha_1{}^2 E_0{}^2 \cos^2[2\pi(v_0 + v_m)t]$$

$$+ \frac{1}{4}\alpha_1{}^2 E_0{}^2 \cos^2[2\pi(v_0 - v_m)t] + \text{cross terms}\}. \tag{2.7}$$

The first term in Eq.(2.7) corresponds to the Rayleigh scattering with the dipole radiating light of frequency v_0, while the second and third terms correspond to the anti-Stokes Raman scattering with frequency $(v_0 + v_m)$ and Stokes Raman scattering with frequency $(v_0 - v_m)$, respectively. The cross terms can usually be neglected, since in most experiments, the power they propagate integrates to zero over a sufficient time interval. If $\alpha_1 = \partial\alpha/\partial q = 0$, the vibration is not Raman-active. Eq.(2.7) also shows that the Raman scattering is linearly proportional to the incident light intensity $E_0{}^2$. Obviously, the total scattered Raman intensity is proportional to the total molecules excited, or say, the concentration of the species, in the sample. This is again consistent with the experiments for normal Raman scattering.

2.1.2 Raman Experimental Setup

The typical experimental set up for normal Raman spectroscopy consists of five basic components: (1) a light source, usually a CW laser, (2) a sample illuminating system, (3) a sample holder and collection optics, (4) a dispersing optical element (monochrometer or spectrometer), and (5) a signal detection and processing system, including a photomultiplier tube or a CCD, and an output device which is now usually a personal computer. Fig.2.2 schematically shows a typical arrangement of these parts.
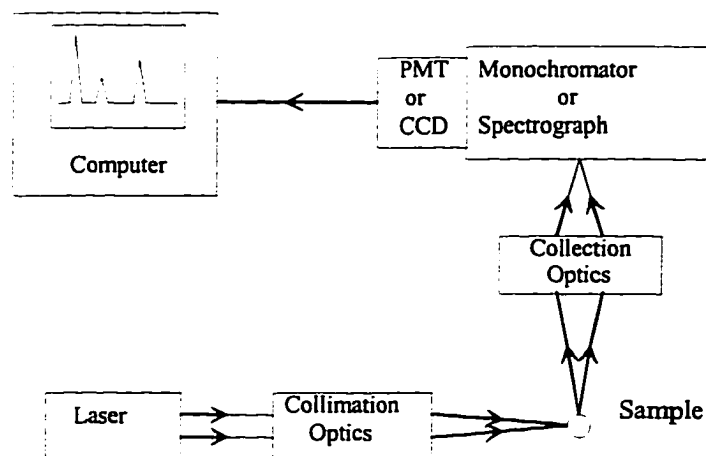
Figure 2.2. The basic setup for Raman spectroscopy

2.2 Resonance and Surface-Enhanced Raman Spectroscopy

The normal Raman effect described above is based on an assumption that no electronic energy is close to the energy of the exciting beam. When the exciting frequency approaches that of electronic transitions, the observed Raman spectrum changes dramatically, showing an enhancement of intensity of certain vibrational modes. This phenomenon is known as resonance-enhanced Raman (RR) scattering. A simplified energy diagram of RR is shown in Fig. 2.3. RR is extremely important in the study of certain biological molecules, where the intensity of Raman bands of a particular chromophoric group in a molecule can be selectively enhanced by a factor of 10^3 to 10^5.

Surface-enhanced Raman spectroscopy (SERS) is another Raman technique that has much higher sensitivity than normal Raman spectroscopy. It was first observed by Fleishmann and co-workers in 1974 [22]. They found strongly enhanced Raman scattering from pyridine molecules adsorbed on silver electrode surfaces that had been roughened
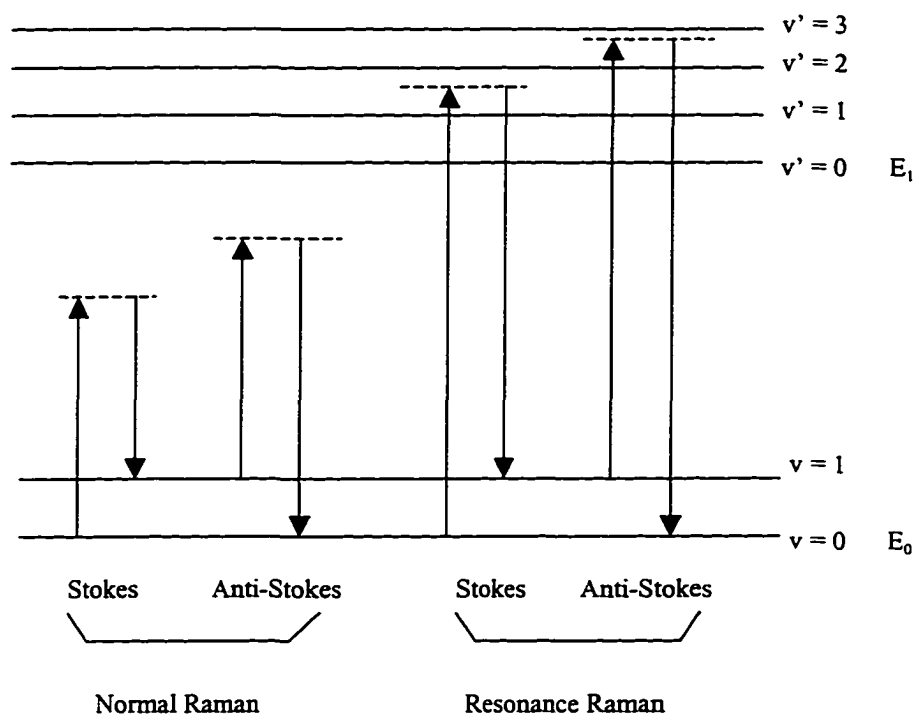
Figure 2.3   Energy level of normal Raman and resonance Raman

electrochemically by oxidation-reduction cycles. In subsequent studies, the observed

Raman scattering signals for the absorbed molecules were identified as from surface-

enhanced effects and estimated to be 3-6 orders of magnitude more intense than those from

non-adsorbed compounds. The theoretical understanding of the mechanisms for surface

enhancement is not yet complete. It can be explained either by the "molecular"

enhancement mechanisms, in which molecular polarizability (α in Eq. 2.1) is perturbed by

interactions of the adsorbate with the surface, or by "field" enhancement mechanisms, in

which the field (E in Eq. 2.1) experienced by the adsorbate molecule is larger than it would

experience far from the surface. Because of the large surface enhancement, SERS is a very sensitive technique; current detection limits are in the picomole-to-femtomole range.

2.3 Applications of Raman spectroscopy

Raman spectroscopy has many applications. A brief overview of applications of Raman spectroscopy in different fields follows.

2.3.1 Applications in Chemistry

Raman spectroscopy is a vibrational spectroscopy, and is most commonly used in structural chemistry. It provides information about molecular symmetry of relatively small molecules and functional groups in large and complex molecules. It also provides a way of studying the structures of electronically excited molecules and unstable species produced by laser photolysis at low temperature.

In structural chemistry, one of the applications of Raman spectroscopy is structure determination by symmetry selection rule or structure-sensitive vibrations. For example, Christe et al. [23] have determined the XeF_5^- ion structure by both x-ray diffraction and Raman spectroscopy. This anion takes a highly unusual $\mathbf{D}_{5h}$ structure, and has 12 normal vibrations. However, only 3 vibrations are Raman active. The observed Raman spectrum clearly shows the presence of three bands at 502, 422 and 377 cm^{-1}, in agreement with the $\mathbf{D}_{5h}$ structure.

Resonance-Enhanced Raman Spectroscopy (RRS) has also been used to study various molecular dynamics, such as photodissociation, photoionization, exciting state dynamics, and oxidation reactions. Zigler and co-workers [24] have studied the short-time gas molecular photodissociation dynamics using RRS. In their work, rotational RRS was used to measure the excited-state lifetime of the gas molecules.

Surface-enhanced Raman has been extensively used to study the structure of a variety of compounds adsorbed at metal surface, which is extremely important in a variety of fields such as adhesion, lubrication, corrosion inhibition, and detergents. For example, Sun *et al.* [25] analyzed the SERS spectra of cetylpyridinium chloride (CPC) and cetyltrimethylammonium bromide adsorbed from solution onto a silver electrode. Comparing the relative intensities of the SERS spectrum and the normal Raman spectrum of CPC, they were able to determine the part of the CRC molecule oriented on the silver surface. Koglin *et al.* [26] used SERS to investigate the adsorption of cytidine-3'-monophosphate on silver electrode as a function of potential. They found that the part of the molecule directly contacts the silver surface changes under different electrode potential.

Raman spectroscopy is also a powerful tool for the study of inorganic species in an aqueous solution. The weak Raman scattering from water makes it more facile than their study by IR spectroscopy. The peak position, intensity, and other band properties provided by the vibrational spectrum allow one to identify the species present and measure the concentration, thus to monitor the chemical reaction process, obtain the equilibrium constants and rate constants, and investigate the effect of temperature and pressure [27].

2.3.2 Biological Applications

Raman spectroscopy is an ideal method for biological studies. This is mostly due to the following reasons. (1) Raman spectroscopy is a nondestructive method; it is suitable for the identification of delicate structures and conformation of molecules in living cells, tissues, and organisms. (2) Raman spectroscopy is able to record molecular

spectra of compounds both in the solid state and in aqueous solution because of the weak Raman scattering of water. This is particularly important in biological systems because most molecules are surrounded by water. (3) Resonance Raman scattering provides the possibility of selectively enhancing particular chromophoric vibrations using a small quantity of biological samples. (4) Raman microscopy offers a high spatial resolution on the order of $1\mu m$; this is suitable for analyzing biological samples in which several constituents can coexist in a small area.

In biological applications, Raman spectroscopy is mostly used for structure analysis, molecular dynamics, and interactions. Such applications include: characterization of liver cells [27], muscles [28], gallstones [29][30], eye lenses [31], proteins [32][33]; determination of the structure and function of rhodopsins [33]; study of the sequence-dependent DNA conformations [34]; study of the interaction between DNA and carcinogenic molecules [35], between DNA and drugs [36]; etc.

2.3.3 Semiconductor Applications

Raman spectroscopy is able to provide unique information relating to semiconductors and to defects in semiconductors [37], either in bulk, thin-film or device form, as well as semiconductor interfaces such as semiconductor/vacuum, Schottky barriers, metal-insulator-semiconductor (MIS), heterojunctions, etc. This technique is probably the most useful method for the study of lattice vibrations and their interactions with other excitations. Since lattice vibrations are very sensitive to local environments, Raman spectroscopy can provide information about material structure and/or quality on the scale of a few lattice constants.

The main application of Raman spectroscopy relating to semiconductors lies in the detection and identification of defects, including strain. Wagner [38] has reviewed the impurity characterization in III-V semiconductors by Raman spectroscopy. Besides that, Raman spectroscopy has been used to monitor the low-dose ion implantation in silicon [39]. Raman microprobe has been used to characterize structural defects in patterned gallium arsenide on silicon [40]. Quantitative measurements of Raman scattering from acceptors in gallium arsenide have been reported [41], and Raman scattering from longitudinal optical phonons in gallium arsenide/ Aluminum arsenide superlattices has been observed [42]. Raman microscopy also has been used to analyze the strain in gallium arsenide/silicon structures [43], in gallium arsenide heteroepitaxial film grown on sapphire, and in silicon-on-sapphire substrate [44].

Raman spectroscopy is also a very powerful tool for characterizing the quality and defects of the chemical vapor deposited (CVD) diamond. This will be further discussed in the following chapters.

2.3.4 Industrial Applications

With the development of the FT-Raman, fiber optic Raman spectroscopy, and new detectors, Raman spectroscopy has been brought from the laboratory to the industry. Now, it is possible to use Raman spectroscopy for *in-situ* measurements. One of the examples is to use Raman spectroscopy in environment analysis. K. I. Mullen and co-workers [45] have used the SERS technique and optical fibers to detect the hazardous metallic ions in aqueous solutions *in situ* and in real time. This was done by monitoring the changes in the Raman spectra of indicators, which form complexes with the metallic ions. With the help of the surface enhanced resonance Raman spectroscopy, Xi *et al.*[46]

were able to determine low concentrations of nitrite in aqueous solutions to monitor the extent of pollution and eutrophication in the water. Other industrial applications include using FT-Raman to study an emulsion polymerization reaction in paint industry [47], to estimate the iodine number of the lipid containing foodstuffs for unsaturation determination in food industry [48], and to identify illicit drugs in the forensic area [49].

2.4 Quantitative Analysis Using Raman Spectroscopy

Raman peak intensity or peak area can be used to measure the species concentrations. However, the variations in the intensity of the exciting light from one scan to the next, variations in the sample, including changes of refractive index and optical absorption, and variations in the orientation of the different samples in the optical path, all cause a lack of reproducibility of the concentration measurement. The way to overcome these problems is either choosing a Raman line in the sample that is unaffected by compositional changes, or to introduce a small quantity of a presumably inert material into the sample as an internal intensity reference. Such a material must not interact chemically with the species of interest; it must be stable; and it must have Raman signals distinct from those of the tested sample [27]. This idea is illustrated in Fig.2.4.

Two lines of the Raman spectrum, one from the standard (ST) and another from the sample (SP), are shown on the left side of the figure. The intensity of these two lines can be expressed as [50]:
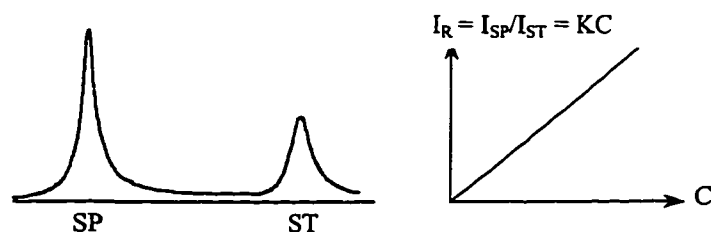
Figure 2.4   Schematic diagram to illustrate the method of measuring relative Raman intensity

$$I_{SP} = R(v)\frac{1}{A(v)}v^4 I_0 J(v) C_{SP}$$

$$I_{ST} = R(v')\frac{1}{A(v')}v'^4 I_0 J(v') C_{ST}$$

where I is the Raman line intensity (either peak height or peak area), C is the concentration. The subscripts SP and ST correspond to the "species of interest" and "standard" respectively. $R(v)$ is the overall spectrometer response, $A(v)$ is the absorption in the optical path, v is the frequency of the scattered light, I_0 is the intensity of the exciting light, and $J(v)$ and is a molar scattering parameter. All the terms involving v' indicate those of the internal standard. The relative intensity, I_R, is defined as

$$I_R = \frac{I_{SP}}{I_{ST}} = \frac{R(v)A(v')v^4 J(v)}{R(v')A(v)v'^4 J(v')C_{ST}}C_{SP}.$$

Although the lead terms do not cancel, they remain constant if C_{ST} is constant. Thus I_R is essentially the intensity from the species per intensity per mole per liter of standard, and is proportional to the concentration of the species of interest C_{SP}:

$$I_R = K \cdot C_{SP}$$

The constant K is designated as the molar intensity, or the molar scattering coefficient. Knowledge of K for a particular species allows one to calculate the concentration C from the measured I_R.

2.5 Referencing Techniques in Quantitative Raman Analysis

To compensate the fluctuation in the exciting light source, optical alignment, and sample absorption in the quantitative Raman measurement, referencing technique is necessary. The existing referencing techniques include (1) using the solvent as the internal standard; (2) selecting a particular Raman band for reference that is unaffected by compositional changes; and (3) adding an ideal internal standard material into the tested sample.

In solution measurements, using solvent as the internal standard is an ideal method if the Raman spectrum of the solvent is suitable for referencing and the concentration of analyte is low. Water, obviously a uniquely important solvent, has been used as internal standard for concentration measurements in aqueous solutions [51][52]. The Raman spectrum of water is shown in Fig. 2.5. In the 1000 to 2000 cm^{-1} range, water has only one band at 1640 cm^{-1}. However, the Raman spectrum of water is very weak, using water as an internal standard is effective only when the intensity of Raman spectrum of the analyte is comparably weak as that of water. On the other hand, the Raman band of water around 1640 cm^{-1} is very unusual in the aspect that it is much broader than typical Raman line due to the hydrogen bonding. Thus the Raman bands of the analyte may be superimposed on that of water. Therefore, even the Raman band of

analyte and water are distinguishable, extra data processing is needed to separate the

analyte Raman spectrum from the water band.
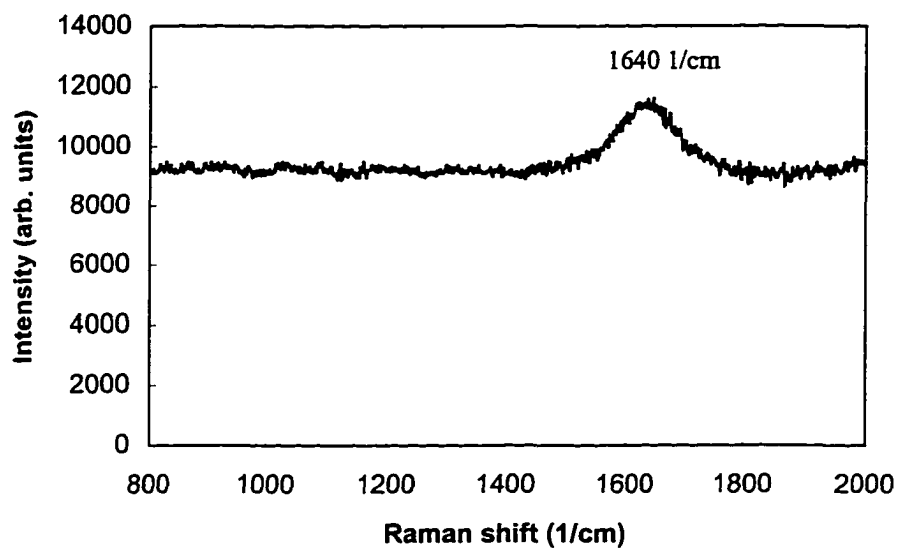
Figure 2.5 A Raman spectrum of water

An example of using water as an internal standard is provided by Shope and co-workers [51]. Quantitative measurement of ethanol, methanol, and acetone in dilute aqueous solution has been done in order to simulate the measurement of by-products for monitoring the course of a fermentation reaction. Least-squares fit has been used to separate the analyte Raman spectra from the water spectrum. The detection limit for ethanol, methanol, and acetone are 0.04%, 0.02%, 0.09%, respectively. Using water as internal standard was also reported by Gilmore *et al.* [52]. In their case, fiber-optic Raman spectroscopy with a diode laser excitation is used to quantitatively measure the concentration of the environmentally important dyes. Both of the applications are for low

concentration measurement, so that the water reference spectrum intensity is almost constant and comparable to that of the analytes.

Organic liquids could be a solvent for some solutions. If the Raman spectrum of the solvent does not interfere with that of the analyte, it can be used as an internal standard. In the research done by Womack et al. [53], the concentration of azo dyes in methanol is determined by resonance-enhanced Raman spectroscopy using 1040 cm^{-1} band from the solvent methanol as an internal standard. The non-linearity due to the huge absorption of the dye was successfully corrected by using the internal standard. Another example of using organic solvent as the internal standard was reported by Lin et al.[54]. They used the 2252 cm^{-1} Raman band from the solvent acetonitrile as an internal standard to quantitatively measure the concentration of anthracene, 9-methylanthracene, and 2-methylanthracene with detection limits of 2.2, 1.2, and 1.0 mg/L, respectively.

In the case when the measurement is applied to composite materials, if one of the components does not change in concentration, the Raman band of this component could be used as a standard. An example is given by Mann et al. [55]. In their experiment, quantitative Raman spectroscopy is used to determine the impurities in solid materials. Samples of sulfamethoxazole spiked with 0.5% to 5% of sulfanilamide and sulfanilic acid as impurities were used as test materials. Because the impurity concentration is kept at a low level, the Raman intensity of the host material is used as an internal standard. The detection limit is about 0.5%.

If none of the Raman bands in the original testing material can be used as an internal standard, a material with known characteristics has to be added as the standard to perform the quantitative measurement. This material should be chemically inert and have

a distinguishable Raman band, which does not disturb the Raman spectrum of the analyte. ClO_4^- is a convenient choice for aqueous solutions, because it is chemically inert and has a strong Raman band at 928 cm^{-1} as shown in Fig. 2.6 [50]. However, this invasive measurement will contaminate the test sample, and is not acceptable for most industrial process monitoring.
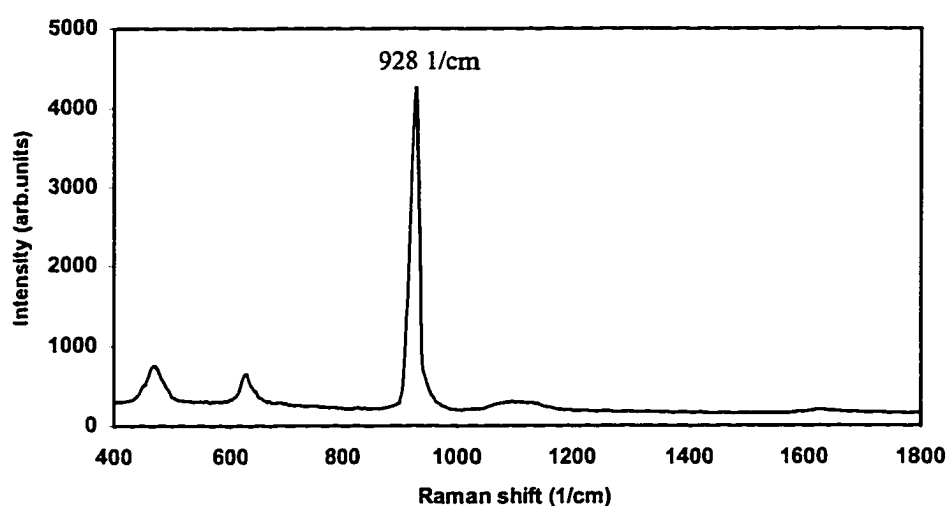
Figure 2.6 A Raman spectrum of $KClO_4$

In summary, the existing referencing methods discussed above are only suitable for special cases. Their effectiveness strongly depends on the sample type, the solvent type, and the measurement conditions. To date, there is still no universal referencing technique, which can be used for quantitative Raman spectroscopy.

2.6 Why Diamond?

The concept of using a solid material as an internal standard has rarely been reported. The major reason is that the solid material can not be mixed thoroughly with

the sample, and it is hard to keep the relative position between the standard material and the sample. But this can be changed when a fiber-optic Raman probe is employed. The solid standard material can be attached to the fiber probe, thus the relative positions between the standard material and the fiber-optic Raman probe can always be kept the same. The advantage of this innovative approach is that the internal standard is no longer dependent on the analyte. The probe becomes self-referenced, and can be used for general-purpose measurement without contaminating the analyte.

Among various solid materials, diamond is a suitable material to be used as a standard. Diamond has long been renowned for its unique properties. Table 2.1 provides a list of the principal properties of diamond. Diamond is the hardest material, has the highest thermal conductivity, and high electrical resistance. In addition, diamond is transparent over a wide wavelength range, can withstand high electromagnetic radiation power fluxes from laser beams and x-ray source, and can be subjected to high pressure and high temperature. However, the most interesting property of diamond applicable here is its chemical inertness and its "single-line" Raman spectrum.

Diamond is chemically stable at room temperature. It does not react to common acids even at elevated temperature [56]. All forms of diamond have practical use in corrosive environments. The corrosive resistance of bulk natural diamond is the highest yet recorded [57]. As a result, diamond can be put into to various chemical samples as a standard without being etched or chemically altering the analytes.

The second interesting aspect of using diamond as a standard is its unique "single-line" Raman spectrum. The Raman spectrum of natural diamond was first measured by

Ramaswamy [58], and Robertson and Fox [59], within two years of the discovery of the

Raman effect. Further investigations were done by Solin and Ramdas [60], and

Table 2.1 Principal properties of diamond

Hardness	1.0×10^4	kg/mm
Coefficient of friction (Dynamic)	0.03	
Sound velocity	1.8×10^4	m/s
Density	3.52	g/cm^3
Young's modulus	1.22	GPa
Poisson's ratio	0.2	
Thermal expansion coefficient	1.1×10^{-6}	K^{-1}
Thermal conductivity	20.0	W/cm-K
Optical index of refraction (at 591 nm)	2.41	
Dielectric constant	5.7	
Electron mobility	2200	cm^2/V-s
Hole mobility	1600	cm^2/V-s
Work function	Negative on [1 1 1] surface	
Bandgap	5.45	eV
Resistivity	10^{13}-10^{16}	Ω-cm

Dennison *et al.*[61]. Diamond belongs to the space group *Fd3m* with two atoms per

Bravais unit cell. It possesses one triply degenerate first order lattice phonon with F_{2g}

symmetry. This is the only mode, which is Raman active in the first order. The

corresponding first order Raman spectrum of diamond has a single line at 1332 cm^{-1} as

shown in Fig. 2.7. This peak has an extremely narrow natural line width, which is around

2 cm^{-1}. For smaller crystallites found in natural diamonds, synthetic diamonds,
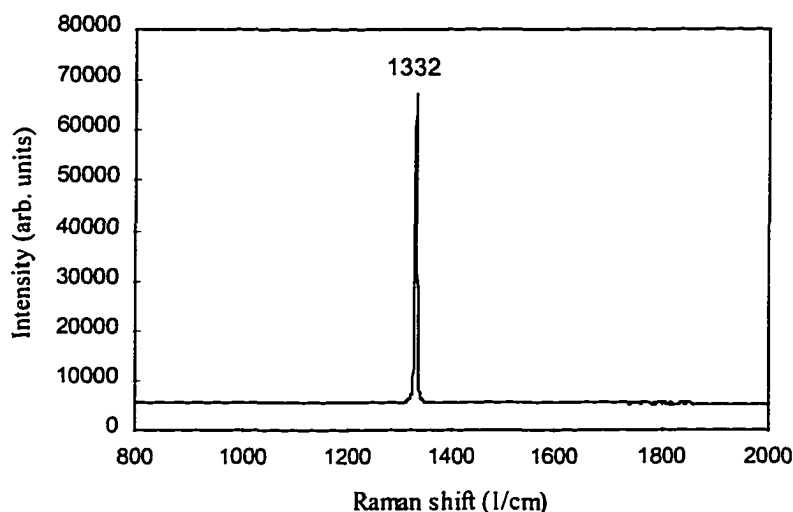
Figure 2.7   Raman spectrum of natural diamond

and diamond films, this line broadens, but does not shift appreciably. The intensity of

this line increases with the excitation energy, which is attributed to resonance effect [62].

The second order Raman spectrum of diamond appears in the range of 2050-2770

cm^{-1}. However, the largest peak at 2458 cm^{-1} in this region is ~250 times weaker than the

intensity of the 1332 cm^{-1} line. Thus within 2000 cm^{-1} range, where many useful

vibration spectra occur for organic compounds, diamond has only one Raman band which

is very strong, sharp, and narrow. If diamond is used as an internal standard, the separation between diamond Raman band and that of analyte can be easily done without extra data processing if there is no overlap. Even if the diamond Raman band is superimposed on top of the analyte Raman band, spectra separation still can be done because of the narrow feature of the diamond Raman band. This property makes diamond a perfect solid material to be used as an intensity standard in quantitative Raman spectroscopy. The implementation of diamond as an intensity standard will be the focus of the rest of this dissertation.

2.7 Summary

Raman effect is an in-elastic scattering phenomenon; it can be used to discriminate among a large number of analytes, allowing molecules to be identified and concentrations to be determined. Its application covers many areas. However, Raman spectroscopy is a single beam technology. To use it as a quantitative tool for measuring the concentration of the species, an internal intensity standard is necessary to correct the variation in exciting source, optical alignment, and sample properties. The existing referencing methods can not provide a universal standard that can be used for *in situ* measurement. A new concept of using diamond as an internal standard is proposed here. The chemical inertness and the unique Raman spectrum of diamond make it a perfect internal standard. Combining diamond with fiber optics, it is possible to develop a general-purpose probe for *in situ* concentration monitoring.

CHAPTER III

EXPERIMENTAL RESULTS

Details of four different structures for Raman excitation and signal collection using fiber-optic probes are presented first in this chapter, followed by four specific designs incorporating natural or synthetic diamond. Experiments are conducted to verify the effectiveness of diamond as an internal standard in quantitative fiber-optic Raman spectroscopy. Concentrations of organic species are measured with these probes and results are presented along with probe calibration and error analysis. Further, effects of varying the power of excitation source, refractive index of the tested media, and the optical alignment are discussed.

3.1 Probe Design

Optical fiber has been widely used in Raman spectroscopy [8-19][64-73]. The advantages of using optical fiber to guide the excitation source and collect Raman signal have been stated in Chapter I. The performance of fiber optic Raman spectroscopy is highly dependent on the structure of the sampling probe. Two major aspects of the probe design should be considered, which are the collection efficiency and the elimination of the glass Raman signal generated inside the fiber. Different fiber-optic probes have been presented to optimize the performance by many researchers [8][16][18].

The simplest design is the single fiber probe. The typical set up for single fiber system is shown in Fig. 3.1. The excitation laser is coupled to the fiber through an objective lens. The Raman scattered light is received by the same fiber and then
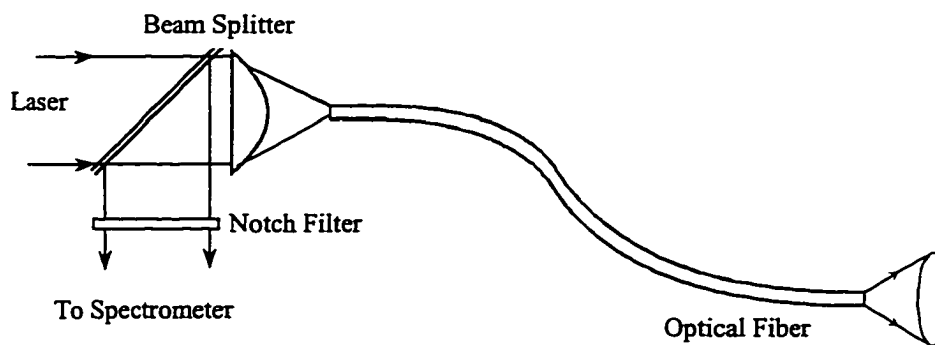
Figure 3.1   Single optical fiber Raman probe

redirected to the spectrometer by a beam splitter. The advantages of this single fiber

probe are small size, compact structure, and the high collection efficiency due to the

100% overlap of the excitation and collection cones at all distances from the fiber end-

face. However the glass Raman background for the single fiber probe is huge because of

the back propagation of the glass Raman signal inside the fiber. Although background

subtraction can be done to remove the glass Raman background, it is not effective when

the analyte signal is weak or the fiber is very long.

Dual fiber structure can be used to reduce the glass Raman background. A simple

design of dual fiber probe is shown in Fig.3.2 (a), with an excitation fiber and a collection

fiber arranged parallel to each other. The dark areas shown in Fig. 3.2 indicate the

overlap between the excitation and collection volume. This probe has decreased

sensitivity compared to that for the ideal single fiber probe, because overlap of the

excitation and collection volume is reduced. Sensitivity can often be improved by tilting

both fibers by a small angle as in Fig.3.2 (b), or by arranging them orthogonal as in

Fig.3.2 (c). For many applications, the latter gives the best results. The performance of

this probe can be improved further by using two gradient index (GRIN) lenses in front of
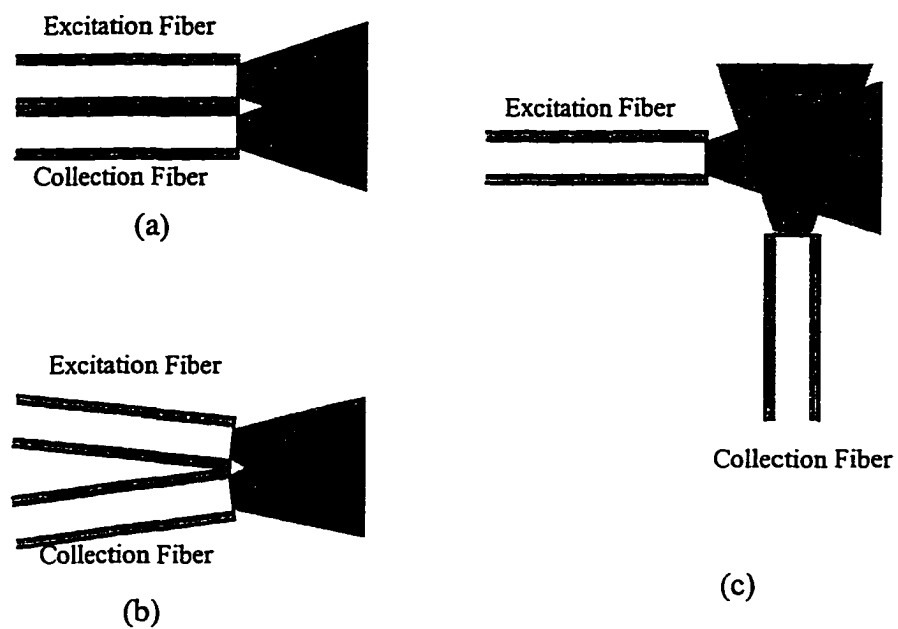
Figure 3.2 Dual optical fiber Raman probe
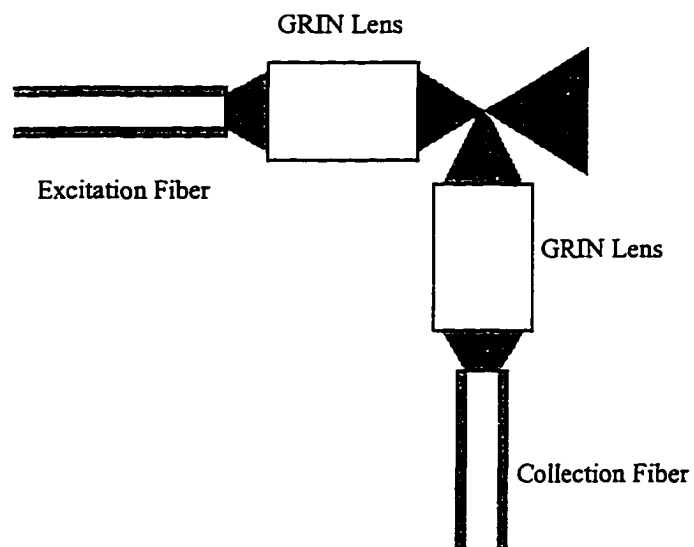
Figure 3.3 Perpendicular dual fiber Raman probe with GRIN lenses

both fibers (see Fig. 3.3). This probe remains low-cost and is very efficient in

suppressing the fiber Raman background [69]. The disadvantage of this probe is that it

looses the compact structure and becomes difficult to handle.

One of the elegant solutions of suppressing the glass Raman background while

maintaining high collection efficiency is to use a double-core optical fiber shown in

Fig. 3.4. The performance of the probe can be optimized by calculations of the fiber

Excitation Fiber Core

Collection Fiber Core
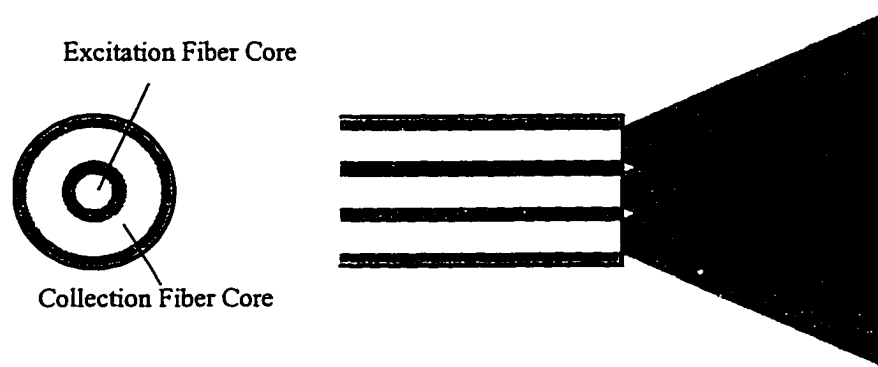
Figure 3.4   Double-core fiber optic Raman probe

dimensions [74]. Unfortunately, the double-core fiber is not commercially available. An

alternative of the double-core fiber-optic probe can be a fiber-optic bundle with one

excitation fiber in the middle and six collection fibers surrounded (see Fig. 3.5).

However, this design is only suitable for short distance application since the bundle is

expensive.

For long-distance remote measurement, dual fiber probe is still the practical

choice. When total elimination of glass Raman background is necessary, optical filters

can be used to improve the performance of the probe. Figure.3.6 shows the structure

Figure 3.5   Fiber-optic bundle Raman probe

(a) For solution
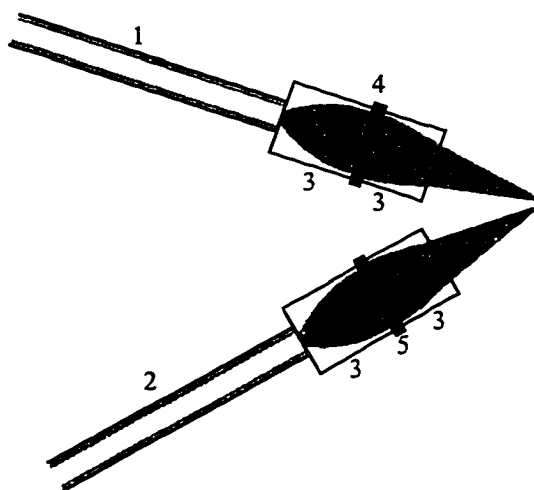
(b) For solid Sample

Figure 3.6   Two fiber Raman probe with filters for long-distance remote applications

1 -- Excitation fiber, 2 -- Collection fiber, 3 -- GRIN lens, 4 – Band pass filter, 5 -- Notch filter

of such a probe. A GRIN lens and a band pass interference filter is placed in front of the excitation fiber, so that only the excitation laser can go through the filter and the glass Raman background can be eliminated. Another GRIN lens and a notch filter are placed in front of the collection fiber to filter out the excitation laser. The purpose of the GRIN lenses is to improve the collection efficiency and make the light go through the filter collimated. For collecting the Raman signal from solid materials, the probe can be modified as Fig. 3.6(b).

In this work, the first probe design is to verify the effectiveness of the diamond as a referencing standard. Thus, a fiber-optic bundle probe as shown in the Fig. 3.5 is chosen to get high collection efficiency for the laboratory experiments. The probe is made by sealing seven quartz optical fibers in a stainless steal tube with epoxy and then optically polishing. The fibers have 200/220 μm core/cladding diameter and 0.22 NA (Polymicro). The center fiber is used for excitation, while the other six are used as collection fibers for Raman signal. These collection fibers are arranged in a linear array and sealed in a stainless steal tube on the other end, such that the output light shape matches the slit in the spectrograph. The total length of the probe is about 2.5 meters.

Now a diamond sample needs to be incorporated with the fiber optic probe to provide a standard. The first attempt is to attach a diamond window directly to the fiber probe (Probe D1). As shown in Fig. 3.7, a type IIA natural diamond window (Harris Diamond Corporation) of 2.0-mm diameter and 0.25-mm thickness is attached to the fiber probe using Raman free epoxy. This design is simple and compact, however, due
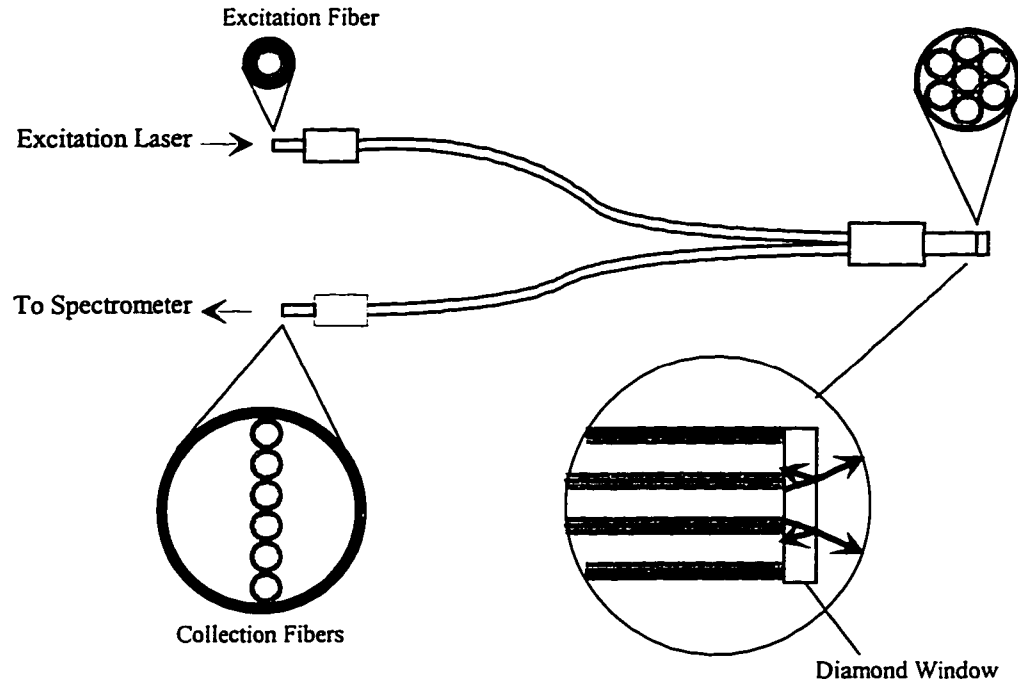
Figure 3.7 An optical fiber bundle Raman probe with a diamond window attached on the end-face

to the larger difference between the refractive index of diamond ($n_{diamond}$ = 2.4) and that of

air (n_{air} = 1.0), a large amount of glass Raman signal produced inside the exciting fiber is

reflected back to the collecting fiber at the outer-interface of diamond and air. For a

normal incidence, the reflection at an interface of two materials is given as:

$$R = \left(\frac{n_1 - n_2}{n_1 + n_2} \right)^2$$

(3.1)

where n_1 and n_2 are the indices of the two material. Thus, for diamond-air interface, the

reflection is calculated as 17.1%. This reflection not only reflects the glass Raman signal

back to the collection fiber, but also reduces the output of the excitation laser intensity.

Moreover, when the probe is inserted in different solutions, the intensity of the reflected

glass Raman signal will change with different indices of the solutions, making the

background subtraction difficult. Figure. 3.8 shows a Raman spectrum of this probe

when placed in air (the experimental setup will be discussed in the next section). A large

glass background is seen in the spectrum especially in the 700-1250 cm^{-1} range. Another

Raman spectrum is acquired by dipping the probe into the solution with 15% ethanol in

water, which is shown in Fig. 3.9. Due to the presence of the glass Raman signal, the

ethanol spectrum is distorted. The intensity of glass background is also changed in

comparison to the spectrum in air because of the difference in indices of air and solution.
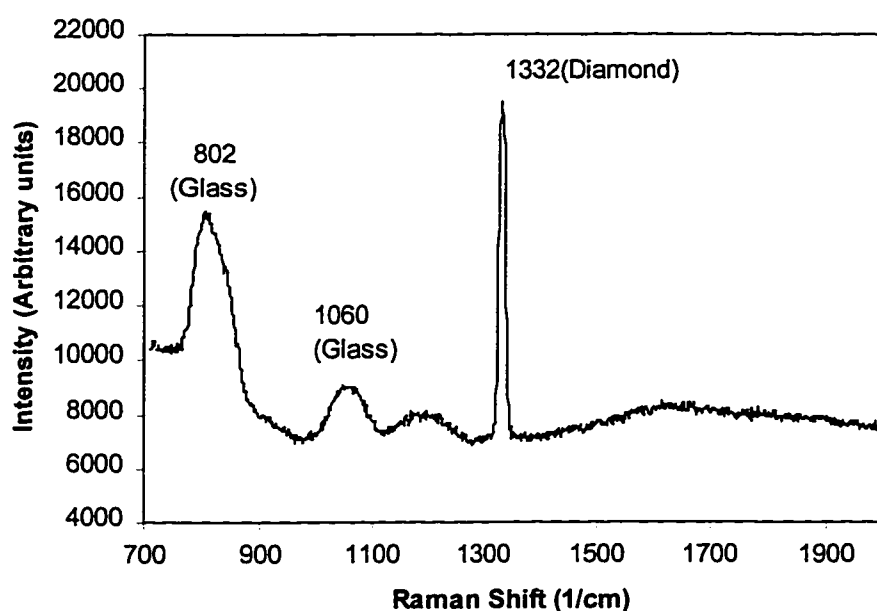
Figure 3.8 A Raman spectrum of the Probe D1 in air
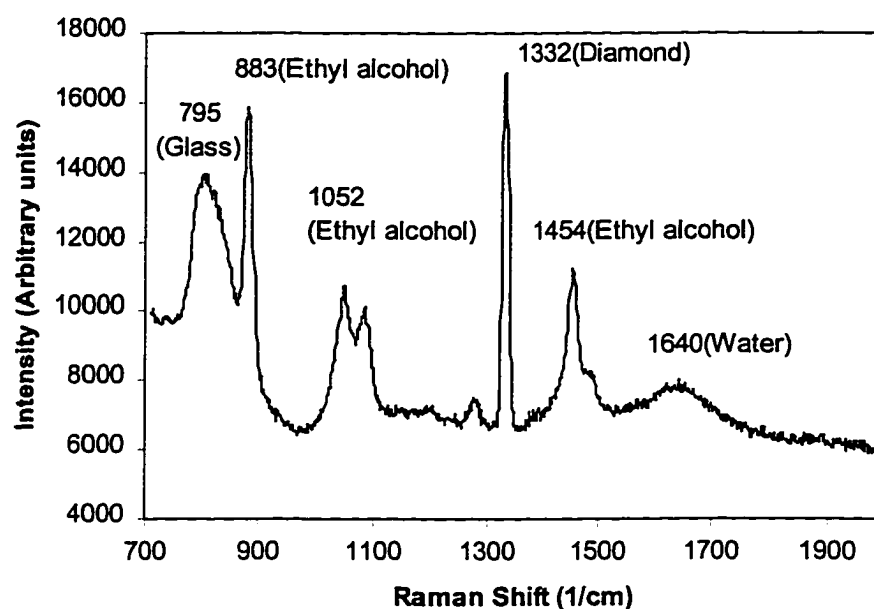
Figure 3.9   A Raman spectrum of 15% ethyl alcohol in water acquired with the Probe D1

Another disadvantage of this design is that the performance of the probe highly depends on the index of refraction of the tested material. The closer the refractive indices between the tested material and diamond, the smaller the reflection of the excitation laser at the interface, which reduces the Raman intensity of diamond and increases the Raman intensity of the analyte.

In order to reduce the glass Raman background and the refractive index dependence, a new structure is designed (Probe D2). As shown in Fig. 3.10, a 500-μm synthetic diamond particle (General Electric) is put inside a glass tube, which is then heated to the glass melting point. The surface tension of the melted glass will automatically form a spherical surface and seal the diamond particle inside the glass. Then the other side of the glass is optically polished and attached with Raman free epoxy

onto the end-face of the fiber optic Raman probe. The diamond particle is intentionally positioned off-center so that most of the exciting light is transmitted to the sample. The polishing step is controlled such that the center of curvature of the lens
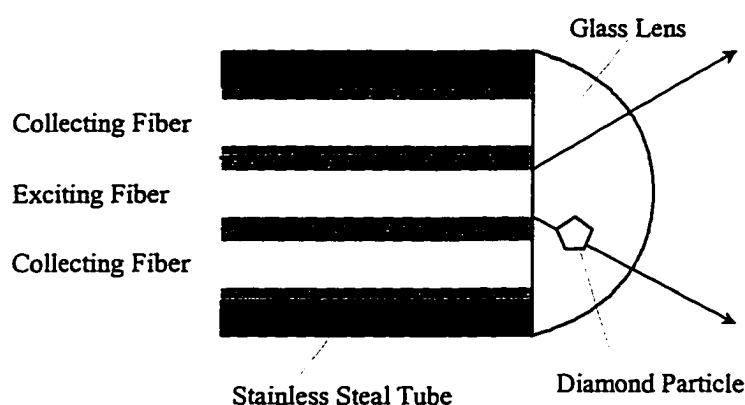
Figure 3.10   A fiber-optic bundle Raman probe with a diamond particle sealed in a convex glass lens

coincides with the virtual apex of the excitation light cone. Thus the incident excitation light will be normal to the outer spherical surface. This design has the advantage that the glass Raman signal reflected by the outer surface is directed back to the exciting fiber instead of the collection fiber. Another advantage is that exciting light cone-shape is independent of the refractive index of the sample because of the normal incidence.

3.2 Experimental Setup

A schematic diagram of the experimental setup available in the Photonics Research Laboratory for fiber-optic Raman spectroscopy is shown in Fig. 3.11. The 514.5 line of an argon ion laser (Spectra Physics) is used as the exciting source. A 20X
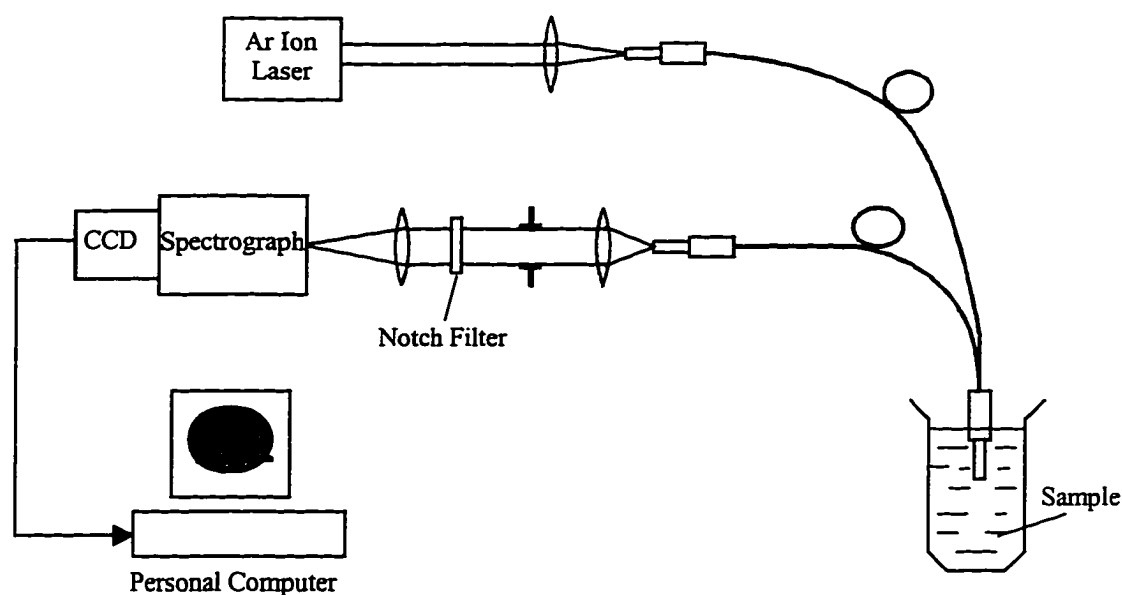
Figure 3.11   Schematic diagram of experimental set up for fiber optic Raman system

objective lens is used to couple the laser to the excitation fiber. A 3-D adjustable stage is

used to align the excitation fiber at the focal spot of the laser. The fiber optic Raman

probe with a diamond particle attached on the top is immersed into the sample. The

collection fiber is adjusted such that the direction of the collection array matches the

direction of the spectrograph slit. Light from the collection fiber is collimated with an $f/2$

convex lens and then filtered with a 514.5 nm holographic notch filter (Kaiser Optical) to

remove the Rayleigh scattered laser light. A variable aperture is put between the $f/2$ lens

and the notch filter to eliminate the uncollimated light, thus improving the efficiency of

the notch filter. Raman signal after the notch filter is then focused with an $f/4$ convex

lens onto the slit (50-μm width) of an image-corrected $\frac{1}{4}$ m spectrograph (Chromex).

The Raman signal is dispersed with a 600-groove/mm grating blazed at 0.5 μm, and then

detected by an ST6-UV silicon CCD detector (Santa Barbara Instruments Group). The

CCD detector consists of 750 horizontal pixels and 350 vertical pixels of 12 μm width. It is thermoelectrically cooled to -35 °C to reduce thermal noise. The output of the CCD detector is interfaced with a computer to collect, process and display the spectral data. The output frame from the CCD can be accumulated to increase the signal-to-noise ratio. The number of the frames accumulated is determined by the integration time, which can be set through the computer software.

The initial visual alignment between the collection fiber and the spectrometer can be done by sending white light through the probe. The transmitted light is imaged onto the slit of the spectrometer. A fine adjustment can be done by setting the system in the "focus" mode, and the image of the collection fiber is viewed at the computer screen and centered at the slit. An example of a focused image of the collection fiber after fine adjustment is shown in Fig. 3.2.
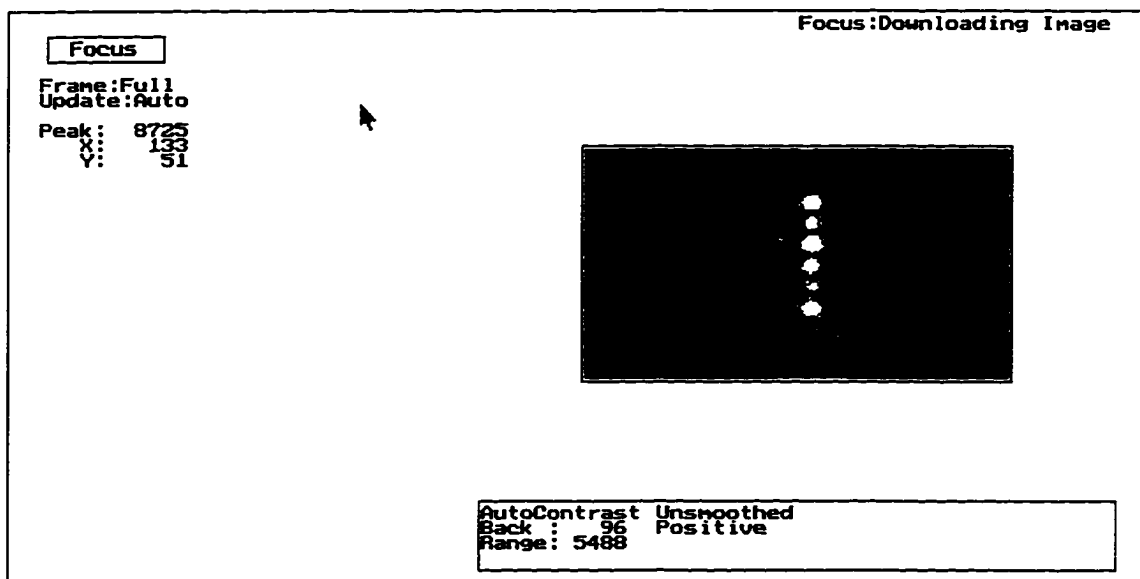
Figure 3.12   The focused image of the collection fiber captured from the computer screen

Raman spectra of the probe placed in air and water are acquired with this setup

and shown in Fig. 3.13 (a) and (b) respectively. The integration time is 60 seconds. A
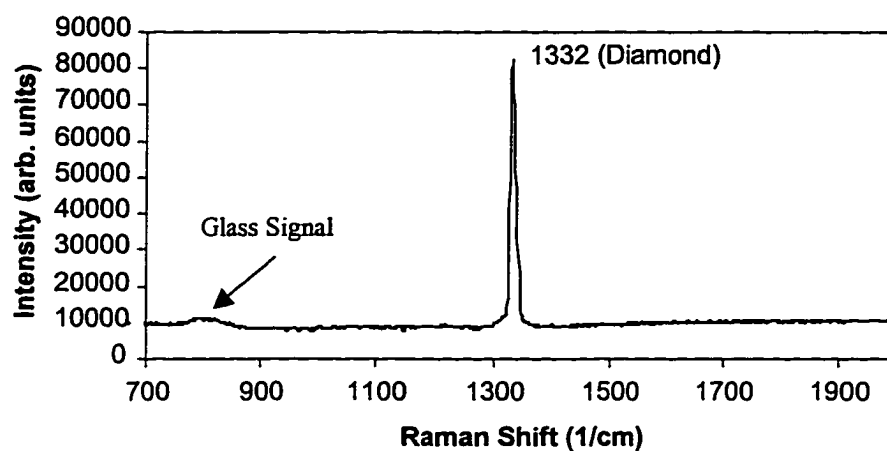
(a)
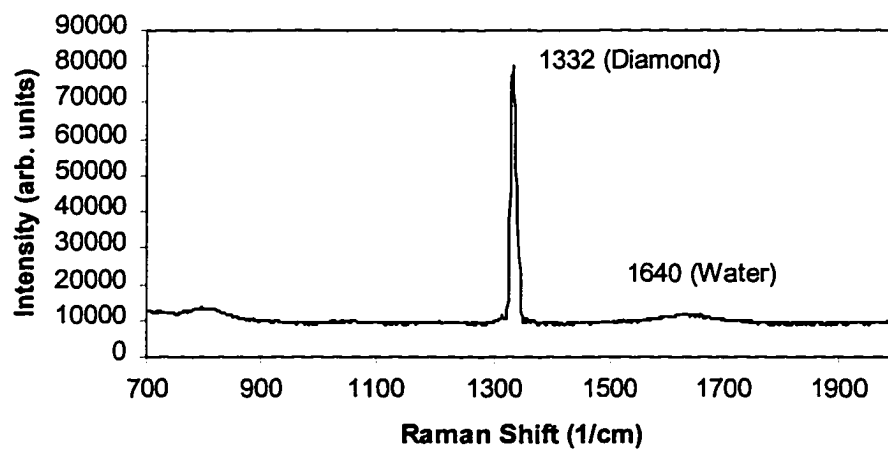
(b)

Figure 3.13 Raman spectra of the Probe D2 in (a) air and (b) water

small portion of glass Raman signal still visible around 800 cm^{-1}, but it is relatively small

compared to the diamond signal. The intensity of the diamond peak is almost the same in

both cases even though a large difference in refractive indices exists between water

(1.333) and air (1.000). Hence we conclude that the intensity of the diamond Raman

peak is insensitive to the refractive index of the external media.

3.3 Experimental Results and Data Processing

3.3.1 Experimental Data

A series of experiments is performed using Probe D2 shown in Fig.3.10. A

mixture of ethanol and water solution is used in the experiment. The sample solutions

used for testing are listed in Table 3.1. Fig. 3.14 shows the Raman spectra of the

solutions with different ethanol concentrations. The integration time is 60 seconds.

3.3.2 Quantification of Raman spectrum

The quantification of the Raman intensity is an important aspect of the analysis.

A quantitative spectral analysis is usually done by two steps. The first step is to build a

linear relationship (a model) between the concentration of the sample and the

corresponding spectral information. The second step is to use the model to deduce the

concentrations of 'unknown' samples from their spectra. A variety of techniques is

available for quantifying the Raman spectrum. Following is a brief description of the

popular methods.

(1) Simple Linear Regression (SLR). SLR is the simplest quantitative spectral

analysis method, which includes peak height method or peak area method. In the peak

height method, a simple linear regression generates the model or linear equation that best

Table 3.1 Concentration of the tested samples

Sample number	Ethanol (g)	Water (g)	Ethanol Weight Percentage (W/W %)	Ethanol Concentration* (g/l)	Ethanol Volume Percentage** (V/V %)
1	0.0000	4.6551	0	0	0
2	0.0539	4.4831	1.188	11.84	1.50
3	0.1315	4.3525	2.933	29.13	3.69
4	0.2315	4.3398	5.064	50.13	6.35
5	0.5253	4.1600	11.212	109.94	13.93
6	0.9850	3.5705	21.622	208.95	26.47
7	1.6984	2.4779	40.668	379.78	48.12
8	2.5941	1.7245	60.068	535.21	67.81
9	3.0888	0.7694	80.058	675.27	85.55
10	3.8215	0	100	789.3	100

* Here the concentration is defined as the weight of ethanol in the unit volume of the mixture.

** This volume percentage is defined as the ratio of ethanol volume to the total volume of the mixture.

Note that the total volume of the mixture is not equal to the sum of the individual volume of ethanol and water.
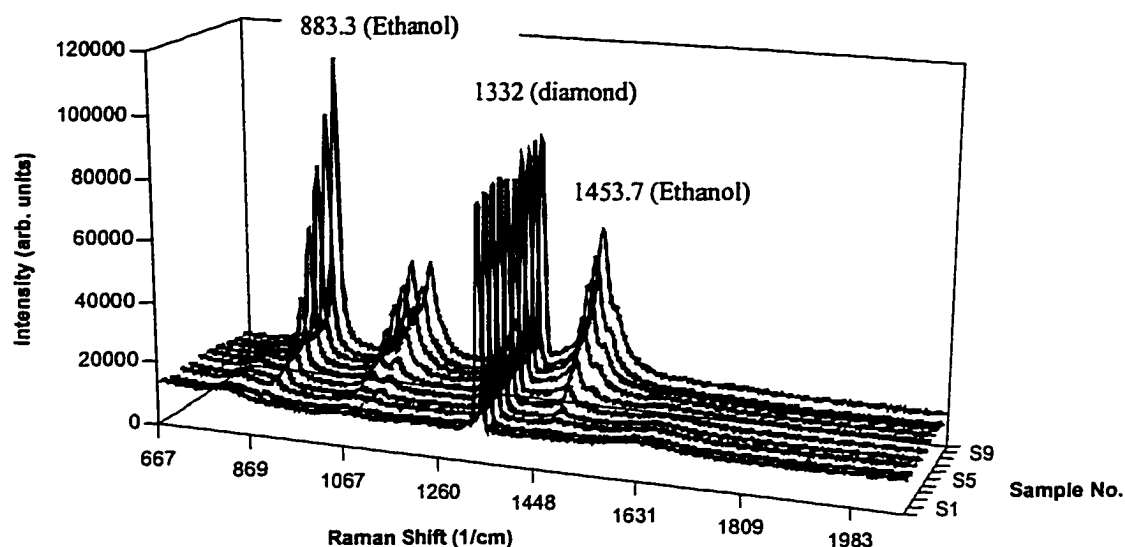
Figure 3.14   Raman spectrum of ethanol in water with different concentrations
acquired with the Probe D2

describes the relationship between the concentration of the analyte and the peak height.

This method is preferable in most simple cases, since the measurement is made at the

peak maximum, where the S/N is optimum. However, the peak height measurement

requires an explicit baseline location, and it may be difficult to use when the spectra show

overlapped peaks. In addition, a value based upon a single point in a set is especially

vulnerable to high-frequency noise. It is desirable to filter the signal before a peak height

is measured. Digital filtering methods can be used to eliminate the high frequency noise.

Peak area method measures the area of a particular peak of a component to

perform the quantification. The integration process involved in the area calculation can

smooth the data and reduce the high frequency noise. As in peak height method, a well-defined base line is also needed for the peak area calculation. This method is not preferable when signal to noise ratio (S/N) is low; in this case small errors have a disproportional effect on the final result because all points in the spectrum are given equal weight in the calculation.

(2) Correlation. Quantification by correlation of the sample spectrum with a reference spectrum usually gives better results than the SLR methods. Correlation is defined by Eq.(3.2):

$$x(t) = \int_{-\infty}^{+\infty} r(t + \tau) \cdot s(\tau) d\tau \ . \tag{3.2}$$

Here $r(t)$ and $s(t)$ are the reference and sample spectra respectively, $x(t)$ is the correlation result, and τ is a variable that describes the position of $r(t)$ along the abscissa. This process can be carried out efficiently by using the Fourier transform, because the correlation in time domain corresponds to the multiplication in frequency domain. As a technique of quantification, the correlation value has the same properties as absorbance in a peak measurement [75][76]. Better results are generally expected because the whole data set can be used, rather than just one point. The multiplication indicated in Eq. (3.2) causes the data points of the sample set to be weighted in proportion to the intensity of the corresponding point in the reference set. This is usually proportional to S/N. Also, the high frequency noise is rejected by the integration in Eq. (3.2). In those cases in which the background features remain constant from one measurement to the next, a calibration curve can be established by correlation. If a major sample constituent

produces a spectral peak interfering with that of the analyte, correlation procedure will eliminate the effects of interference.

(3) Least Square Fit. The least square fit is an alternative method that is preferable under certain circumstances. The operation is based on the idea that a spectrum can be considered to be a vector that can efficiently be manipulated by the techniques of matrix algebra. If a 128-point spectrum is taken as a vector in 128 space, scaling the spectrum to reflect a change in concentration is a manipulation on 128 simultaneous equations. If the data are experimental, evidently there is error in each measurement and the equations are inconsistent. A least square operation allows resolution of these inconsistencies and makes it possible to use matrix operations. Consider the following equation

$$\mathbf{X} = \mathbf{RC} + \mathbf{E}, \tag{3.3}$$

where $\mathbf{X}$ represents a spectrum ($1 \times n$ matrix, with n the number of data points), $\mathbf{R}$ ($m \times n$) is a set of reference spectra, one for each of the m components in the sample, $\mathbf{C}$ ($1 \times m$) is the predicted concentration matrix, which is the scale factor by which $\mathbf{R}$ is fitted to $\mathbf{X}$, and $\mathbf{E}$ ($1 \times n$) represents the error associated with each measurement. The least square solution is shown in Eq.(3.4) as

$$\mathbf{C} = (\mathbf{R}^T \mathbf{R})^{-1} \mathbf{R}^T \mathbf{X}. \tag{3.4}$$

Here the superscript T denotes a transpose and -1 an inverse.

The major restriction in the least square procedure is that there must be a component in the reference matrix for each significant component in the sample set. This restriction can be circumvented to some extent by including simulations of components

in the reference matrix. For example a DC part can be accounted for by for by including a ramp as a component.

This method is also called multiple linear regression (MLR). It generally runs faster than correlation, provided it does not include a filtering step. It is the best method when the analyte is dealing with well-behaved systems (i.e., linear response, no interfering signals, no analyte-solvent interactions, low noise, and no collinearities). However, it may have problems when the real data includes a lot of noise. MLR attempts to use all of the variance in the **R** matrix, including any irrelevant information, to model **C**. Thus a very high probability exists for including noise in order to build the model.

Recently, more powerful quantitative spectrum analysis methods such as principal component regression (PCR) and partial least-squares regression (PLS) [77-79] have been introduced. These methods use factor analysis to extract information from the spectra for building the model. Computer software for implementing these methods is now commercially available. The details of this method are beyond the scope of this research and will not be discussed.

3.3.3 Probe Calibration

Calibration of the probe should be done carefully with a proper definition of concentration. Different definition, such as weight/weight percentage [73,80], molarity (mole solute per kilogram solvent) [55], ratio of molecular numbers (ppm)[53, 81], and mole concentration (mole per liter of solvent) [65] have been used in quantitative Raman analysis. The first three concentration units are assumed to be "temperature independent" as stated in the references. However, strictly, none of the concentration units listed above is linearly proportional to the intensity of the Raman signal. If the excitation volume and

collection volume are fixed for a particular Raman system, Raman intensity of the analyte is determined by the amount of species (mole or weight) per volume of the mixture [8].

Unfortunately, the volume of the mixture is usually temperature dependent because density is temperature dependent. This makes the calibration difficult. If both solute and solvent are liquids, by neglecting the thermal expansion of the mixture, volume percentage or weight per volume of mixture can be used for calibration if a linear model is used. However, it must be noted that the denominator in this ratio is the volume of the mixture, rather than the sum of the volume of the two individual materials. Weight percentage, molarity, or mole concentration can be used only if the addition of the solute does not change the total volume of the mixture or the change is negligible. This is true for solutions with very low concentrations or if the solute is a solid. In this work, the concentration of the ethanol in water varies from 0% to 100%. Thus, volume percentage is used for calibration.

As for the quantification of the Raman intensity, the tested solution is known as the mixture of ethanol and water, and the concentration of ethanol is of interest. With long integration time, a high signal to noise ratio can be obtained. Thus either peak area or least squares fit will be used for calibration. The advantage of the peak area method is that no reference spectrum is needed when the normalization with diamond is done. For least squares fit, only one major Raman band of the analyte is used for calculation and irrelevant portion of the spectrum is avoided. When the major Raman band interferes with other Raman signals, a spectra separation will be done using a least squares fit algorithm.

The ethanol Raman peak at 883.3 cm⁻¹ (861-907 cm⁻¹) is used for both peak area and least square fit calculation. A base line subtraction is done by drawing a straight line between the starting point and end point of the selected band, and the amount of data below this line is subtracted for the original band. This is based on the assumption that the selected peak has a fairly flat background and does not interfere with other Raman peaks. Figure 3.15 shows the selected ethanol peak from Fig. 3.13 after base line subtraction is done.
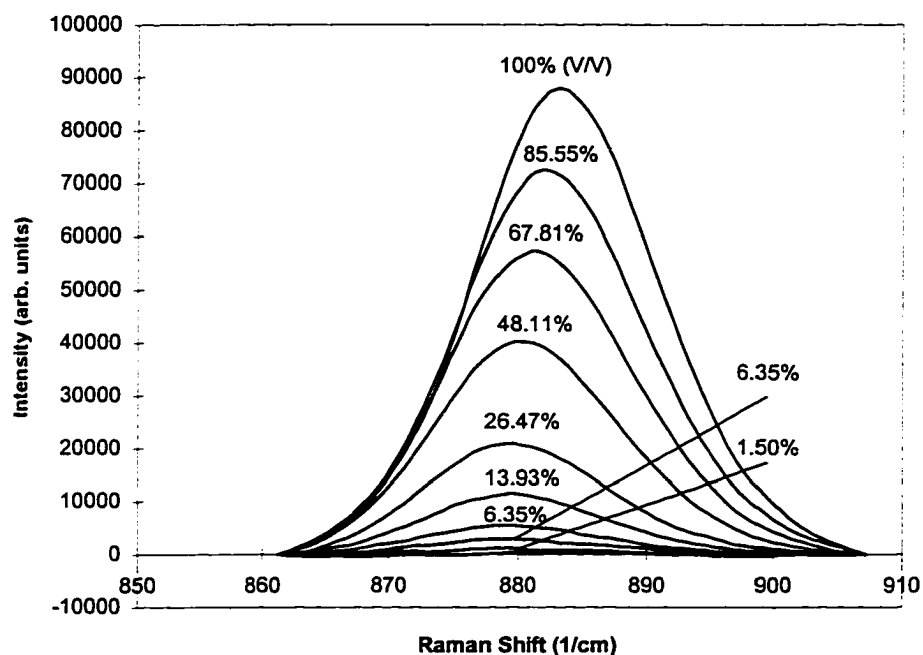
Figure 3.15   The selected ethanol band after base line subtraction

Peak areas are calculated based on these spectra. The results are shown in Table 3.2 and plotted in Fig. 3.16. A linear equation is obtained through regression to build a model between concentration and peak area, which is expressed as:

$$C_p = 1.2281 \times 10^{-4} A + 0.043822 \qquad (3.5)$$

where C_p is the predicted concentration and A is the peak area. The errors seen in the

predicted concentration are due to the noise in the system, the inaccuracy in the baseline

subtraction, and the fluctuation in the excitation source.

Table 3.2 Predicted ethanol volume percentage based on peak area method

Sample Number	Measured Percentage (%)	Peak Area (arb. units)	Predicted Percentage(%) (by linear regression)	Error (%)
1	0	998	0.17	0.17
2	1.50	10785	1.37	-0.13
3	3.69	28723	3.57	-0.12
4	6.35	54972	6.79	0.44
5	13.93	111069	13.68	-0.25
6	26.47	206292	25.38	-1.09
7	48.12	398242	48.95	0.83
8	67.81	560138	68.83	1.02
9	85.55	693431	85.20	-0.35
10	100	809553	99.47	-0.53
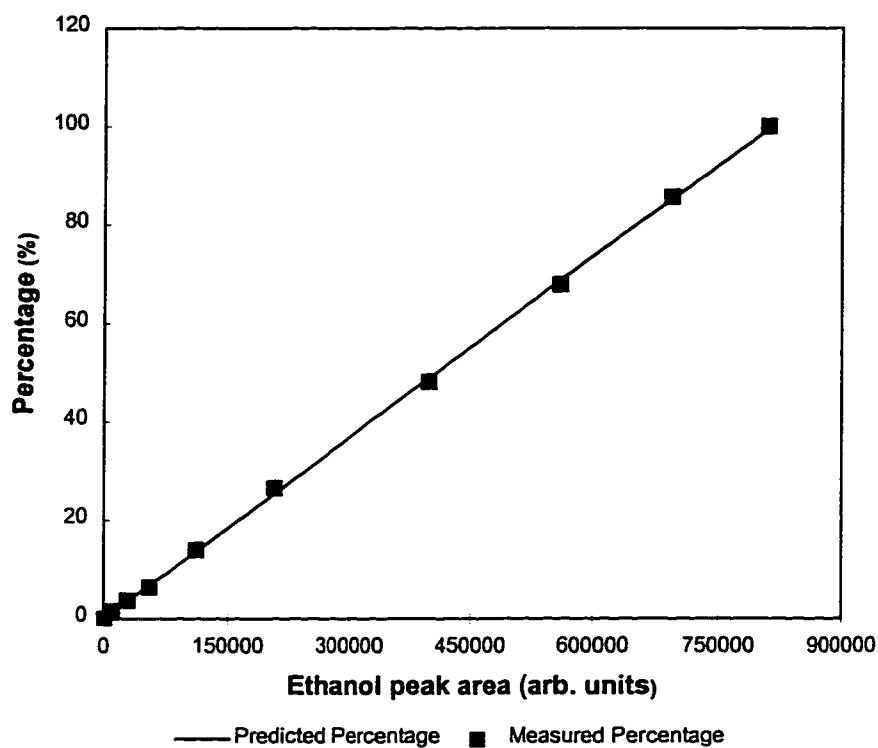
Figure 3.16 Predicted and measured ethanol percentages vs. peak area

To eliminate the error due to the variations in the laser intensity, the spectra are normalized by the diamond signal. The peak area of diamond band (1318-1352 cm^{-1}) is measured. Normalization is done by dividing each ethanol Raman spectrum by the diamond peak area. The Raman spectra after normalization are shown in Fig. 3.17. The peak areas of ethanol at 883.3 cm^{-1} after normalization are recalculated. Again, a model is built using linear regression, which is given as:

$$C_p = 57.73176 A_n - 0.19732 \qquad (3.6)$$

where A_n is the normalized ethanol peak area.
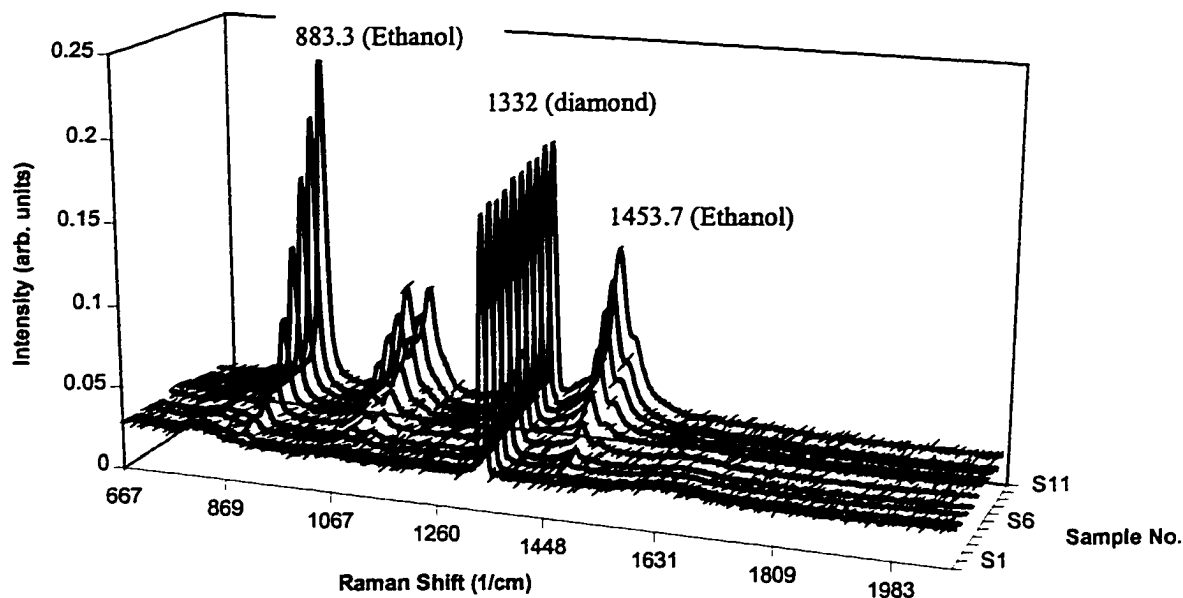
Figure 3.17   Normalized Raman spectra of ethanol in water acquired by the Probe D2

The concentration prediction based on normalized ethanol peak area is shown in Table

3.3 and Fig. 3.18. Note that the maximum error of the normalized result is 0.58%, which

is less than the maximum error, -1.09%, before normalization.

The calibration procedure is repeated using least-square fit method. Here, since

only the concentration of one Raman band is of interest, Eq. (3.3) can be simplified as

$$X = R\,c. \tag{3.7}$$

Here both X and R are vectors, and c is the factor which brings the reference spectrum R

to fit the sample spectrum X. In this calibration, only the 883.3 cm^{-1} ethanol peak is used

in the least square fit process, and the 100% ethanol spectrum is used as a reference

Table 3.3 Predicted ethanol volume percentage based on peak area method after normalization with

diamond band

Sample Number	Measured Percentage (%)	Diamond Peak Area (arb. units)	Normalized Ethanol Peak Area	Predicted Percentage (%)	error (%)
1	0	465108	0.00214	-0.07	-0.07
2	1.50	465512	0.02316	1.14	-0.36
3	3.69	477688	0.06012	3.27	-0.42
4	6.35	473225	0.11616	6.51	0.16
5	13.93	451178	0.24617	14.01	0.08
6	26.47	442151	0.46656	26.74	0.27
7	48.12	470333	0.84672	48.69	0.57
8	67.81	471512	1.18796	68.39	0.58
9	85.55	468896	1.47886	85.18	-0.37
10	100	468467	1.72809	99.57	-0.43
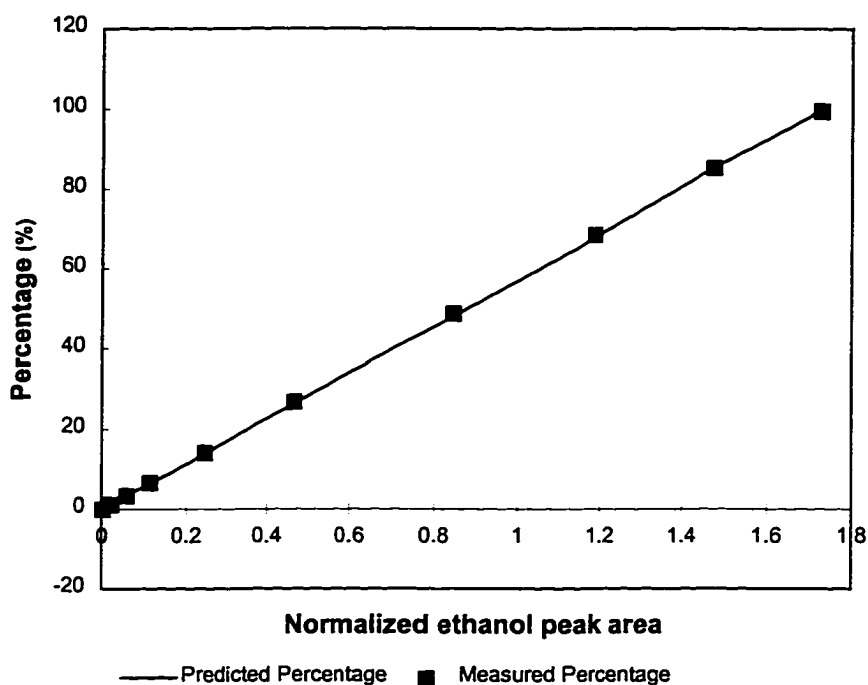
Figure 3.18   Predicted and measured ethanol percentages vs. normalized peak area

spectrum. The same process is also applied to the diamond peak to get the normalization

factors. Normalization is done by taking the ratio of the ethanol fit factor c_e and the

diamond fit factor c_d. The result is shown in Table 3.4. No significant difference is seen

between the results from peak area method and least square fit method. This is mostly

due to the high S/N ratio in the spectra. To simplify the calculation, the peak area method

will be followed in the remaining experimental analysis.

The detection limit for the system is defined as the concentration when the root-

mean-square (*rms*) S/N equals 2 on the strongest Raman band [52]. For this experiment,

the laser power coupled to the excitation fiber was measured as 5 mW, and 60 second

CCD integration time was used. The *rms* noise is calculated as 131. The peak intensity

Table 3.4   Predicted ethanol volume percentage based on least square fit method

after normalization with diamond band

Sample Number	Measured Percentage (%)	Normalized Fit Factors (c_e/c_d)	Predicted Percentage (%)	Error (%)
1	0	0.0031	0.45	0.45
2	1.50	0.0163	1.77	0.27
3	3.69	0.0333	3.46	-0.23
4	6.35	0.0589	6.01	-0.34
5	13.93	0.1435	14.45	0.52
6	26.47	0.2597	26.03	-0.44
7	48.12	0.4744	47.43	-0.69
8	67.81	0.6780	67.73	-0.08
9	85.55	0.8639	86.26	0.71
10	100	1	99.83	-0.17

of the 883.3 cm^{-1} ethanol band for 100% concentration is 97437 (arb. units). Thus the

detection limit is calculated as 0.27%.

3.3.4   The repeatability of the normalized model

Ideally, the calibration of the probe for ethanol concentration measurement needs

be done only once if normalization has been done. The probe can be used for subsequent

experiments without recalibration. To check the performance of the probe, the

experiment is repeated by redoing the optical alignment and reducing the laser power by 20 %. The ethanol peak is measured and normalized by the diamond peak area. The same model as Eq. (3.6) is used to predict the percentage of the ethanol. The result is listed in Table 3.5. The predicted errors shift mostly to the positive and with a maximum of 1.1%. The increased error can be due to the change of the optical alignment, because different alignment may change the mode distribution inside the excitation fiber, thus changing the intensity distribution in the output light. The relative Raman intensity

Table 3.5 Predicted ethanol volume percentage after normalization with reduced
excitation laser power

Sample Number	Measured Percentage (%)	Normalized Ethanol Peak Area	Predicted Percentage using Eq.3.6 (%)	error (%)
1	0	0.00435	0.05	0.05
2	1.50	0.02911	1.48	-0.02
3	3.69	0.07423	4.09	0.40
4	6.35	0.12091	6.78	0.43
5	13.93	0.25750	14.66	0.73
6	26.47	0.47799	27.39	0.92
7	48.12	0.85212	49.00	0.88
8	67.81	1.19688	68.90	1.09
9	85.55	1.5043	86.65	1.10
10	100	1.75419	101.08	1.08

between diamond particle and the sample may change due to the change in the intensity distribution. However the error is fairly small compared to the 20% change in excitation laser power.

To further investigate the effect of fluctuation in excitation laser power, the experiment is repeated using a fixed concentration of the ethanol in water and varying the excitation laser intensity. The laser power coupled into the excitation fiber is monitored with an optical power meter, and a series of spectra is taken by varying the laser power from 1.75 to 7 mW. Figure 3.19 (a) shows the Raman spectra of 67.81 % ethanol-water solution under different excitation laser power. The 883.3 cm^{-1} ethanol peak area is calculated and plotted against the excitation power, which is shown in Fig. 3.19 (b). As expected, the ethanol peak area is proportional to the excitation power. However after normalization with the 1332 cm^{-1} diamond peak area, a fairly constant result is obtained as shown in Fig. 3.20. The normalized peak area of the 883.8 cm^{-1} ethanol band is calculated and used in Eq. (3.6) to predict the percentage of the ethanol. The result is listed in Table 3.6. The average predicted percentage is deviated from the measured percentage by 2.03 %. Again this may be due to the optical alignment change. However the standard deviation is only 0.47% for a 75% variation in excitation power.

To investigate the effect of optical alignment on the measurement, spectra are collected for the 67.81% ethanol-water solution after six optical realignments. The standard deviation of the predicted percentage is calculated as 4.6% after normalization, which is much lager than the standard deviation when only the excitation power is changed. This means the probe is quite insensitive to the excitation laser power but the sensitivity depends slightly on the optical alignment.

(a)

(b)
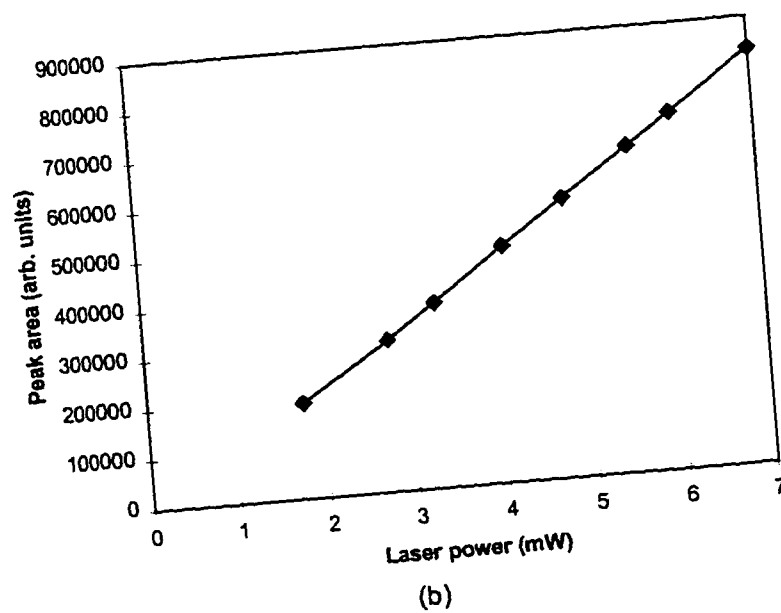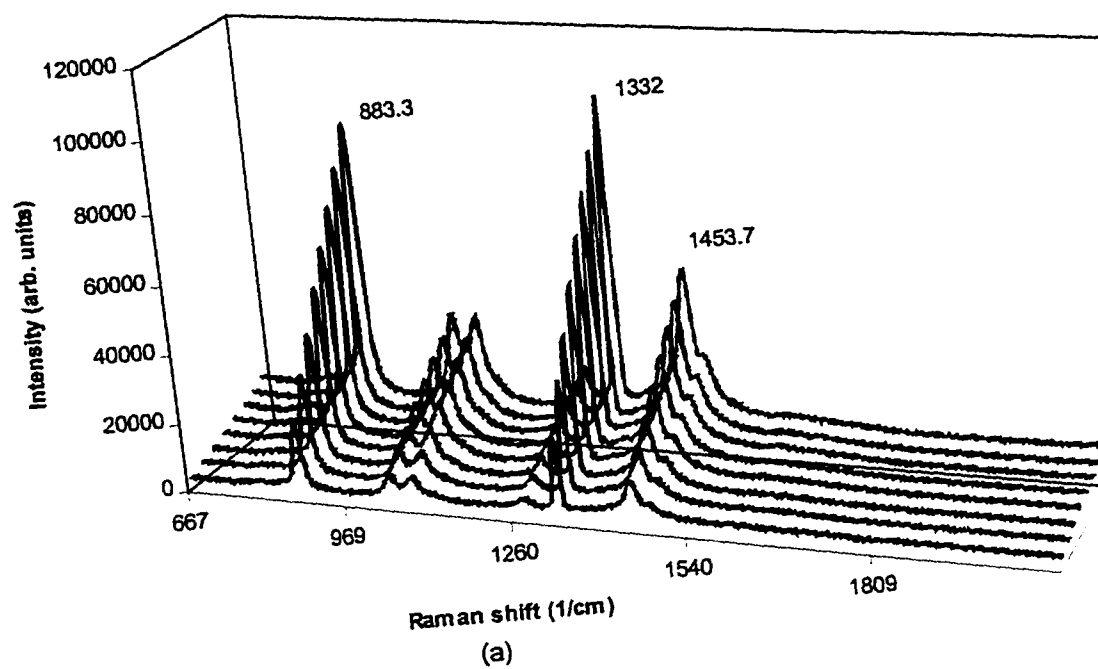
Figure 3.19 (a) Raman spectra of 67.81% ethanol-water solution under different excitation laser power;

(b) 883.3 cm^{-1} ethanol peak area vs. excitation laser power.
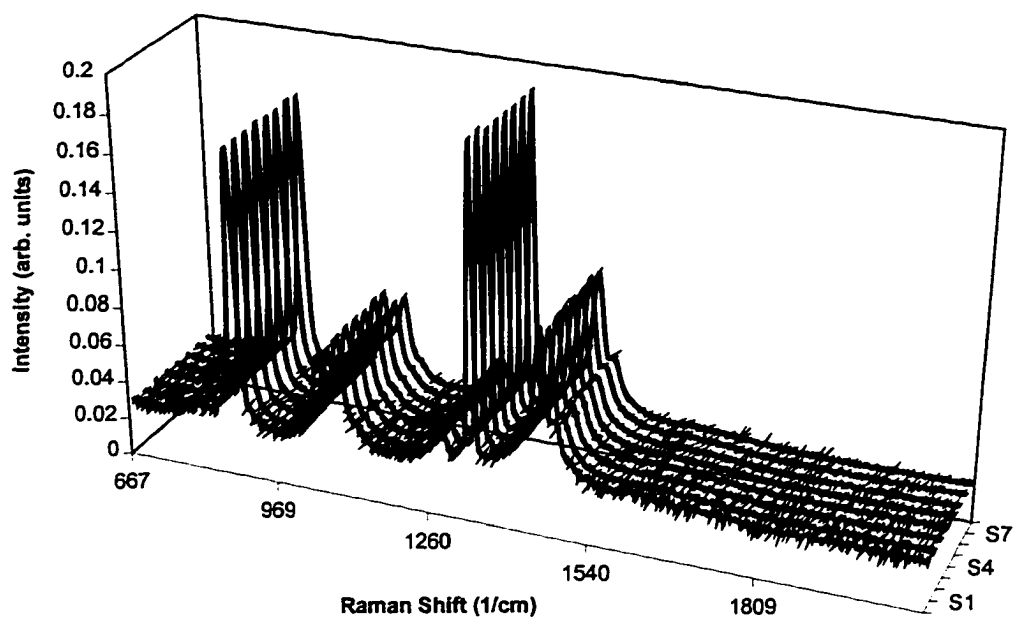
(a)
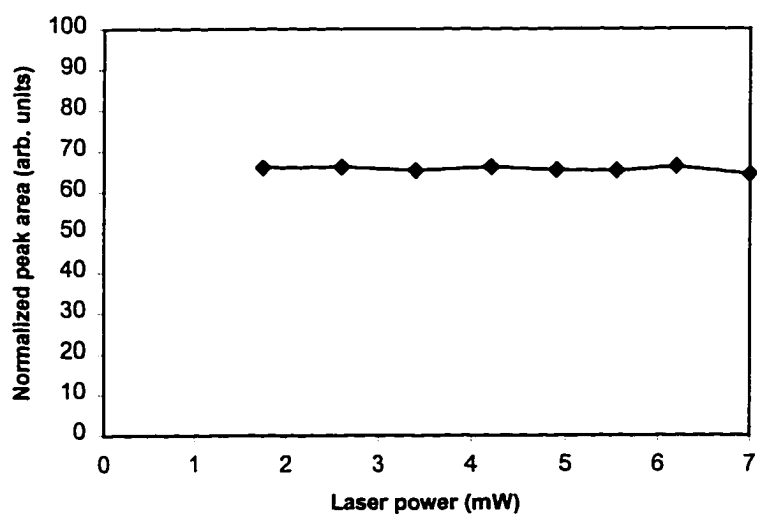
(b)

Figure 3.20 (a) Normalized Raman spectra of 67.81% ethanol-water solution under different excitation

laser power; (b)Normalized 883.3 cm⁻¹ ethanol peak area vs. excitation laser power.

Table 3.6   Predicted ethanol percentage for 67.81% ethanol-water solution

under different excitation laser power

Sample Number	1	2	3	4	5	6	7	8
Normalized Ethanol Peak Area (arb. units)	1.14823	1.15053	1.13567	0.15071	1.13771	1.13371	1.15155	1.13425
Predicted Percentage using Eq.(3.6) (%)	66.09	66.23	65.37	66.24	65.48	65.25	66.28	65.28

3.3.5   The Effect of Refractive Index

Usually the index of refraction varies with the concentration of the solution. Ideally, the measurement result should not depend on the refractive index of the solution. However, in fiber optic Raman spectroscopy, the refractive index of the solution may affect the result in two ways: (1) change in the numerical aperture of both excitation fiber and collection fibers, thus affecting excitation cone shape and collection efficiency, and (2) change in the reflectivity at the glass-solution interface.   For the current design of Probe D2, the diamond particle is sealed by glass with a spherical surface. Thus the excitation light is expected to hit the outer surface at normal angle and the direction of excitation laser is independent on the refractive index of the solution. For the second effect, the reflectivity for normal incidence at an interface with different refractive indices is given by Eq. (3.1). As $n_1 = 1.46$ is the refractive index of glass, n_2 may vary from

1.33 to 1.5 for most aqueous or organic solutions, the reflectivity change varies from 0 to 0.21 %. This effect is very small; thus the probe design should not be sensitive to the refractive index of the solution. Experimental results on ethanol-water solution show a linear relationship between the Raman intensity and the measured ethanol percentage, which is further proof that the probe is insensitive to the index change of the solution.

However, for the ethanol-water experiment, the refractive indices of ethanol ($n_e = 1.3611$) and water ($n_w = 1.3333$) are very close, the change in refractive index is small for different concentrations. To further investigate the effect of the refractive index, the concentrations of ethanol in dimethyl sulfoxide (DMSO) are measured using the same probe. The refractive index of DMSO is 1.4780. A significant change in refractive index of the solution will occur when the ethanol percentage varies from 0% to 100%. Fig. 3.21 shows the Raman spectra of the ethanol-DMSO solutions with different ethanol concentrations. The 883.3 cm^{-1} ethanol peak area is again used for calculation since there is no interference between ethanol and DMSO at this region. After normalized with the diamond peak area, a linear regression is still used to predict the ethanol percentage. The result is shown in Fig. 3.22. The maximum prediction error is 0.8%, which is comparable to the 0.58% maximum prediction error in the ethanol-water experiment. There is no obvious non-linearity in the experimental data, which again confirms that the probe is insensitive to index change of the solution.
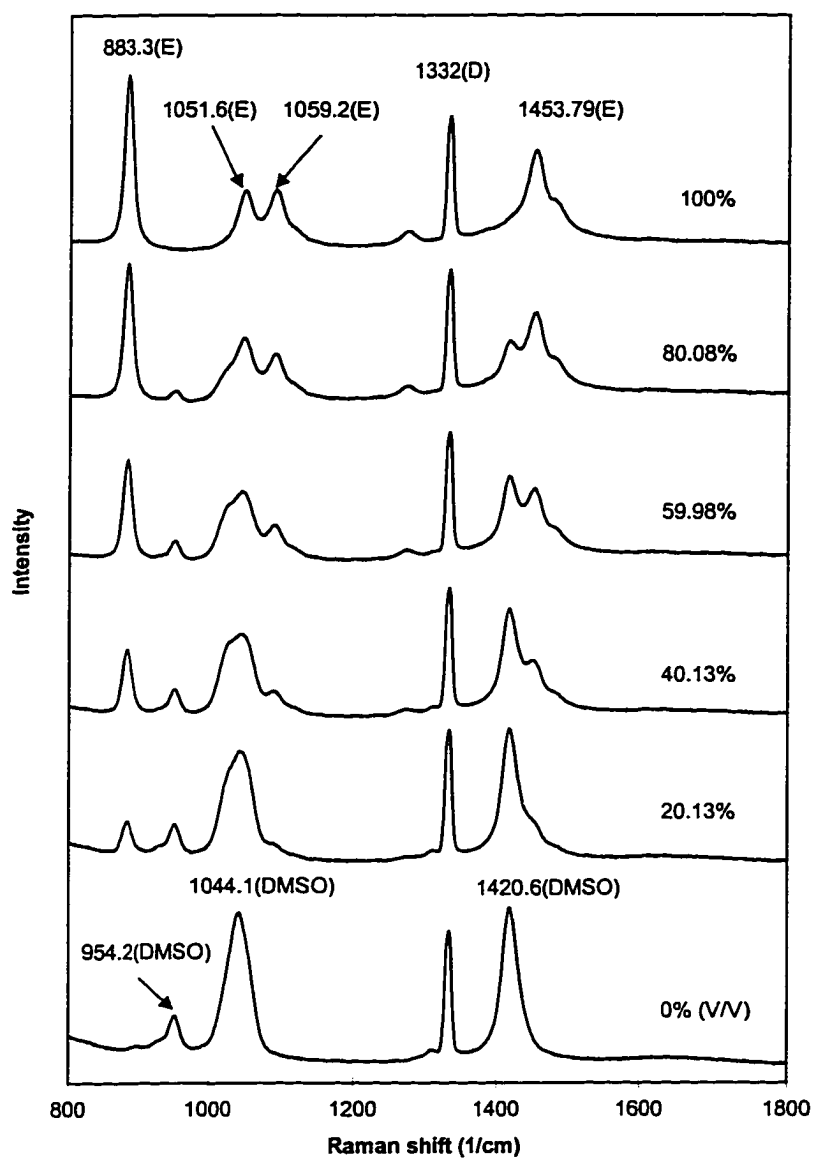
Figure 3.21 Raman spectra of ethanol-DMSO solution with different % ethanol concentrations
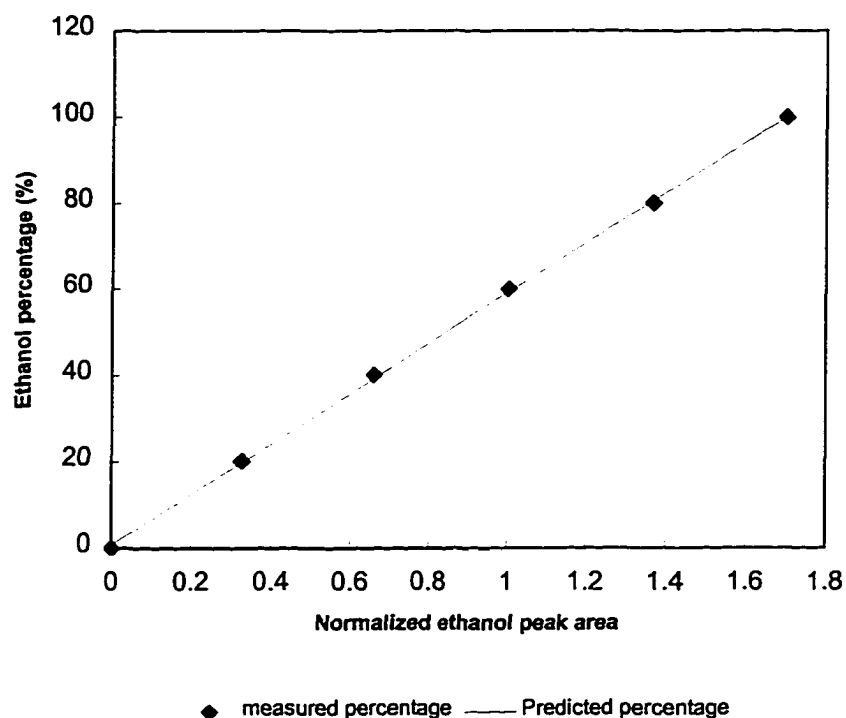
Figure 3.22   Measured and predicted ethanol percentage vs. normalized ethanol peak area

4.4 Modified Probe Design

The Probe D2 performs well to compensate for power fluctuations in excitation

laser. It also gives Raman signals independent of refractive index of the measured

solution. However, there are two drawbacks for this design: One is that it can not totally

compensate for the variations in the optical alignment in launching the excitation laser.

The other is that the referencing diamond Raman peak intensity is fixed for a particular

probe, which may not be desirable when the Raman intensity of the analyte is too strong

or weak compared to the diamond peak intensity.

A modified probe design is shown in Fig. 3.23 (Probe D3). A bulk diamond sample is attached on a stainless steal frame and positioned away from the fiber. The analyte will be between the fiber and the diamond reference sample when the probe is immersed in it. Instead of a small diamond particle, a big diamond window is needed to
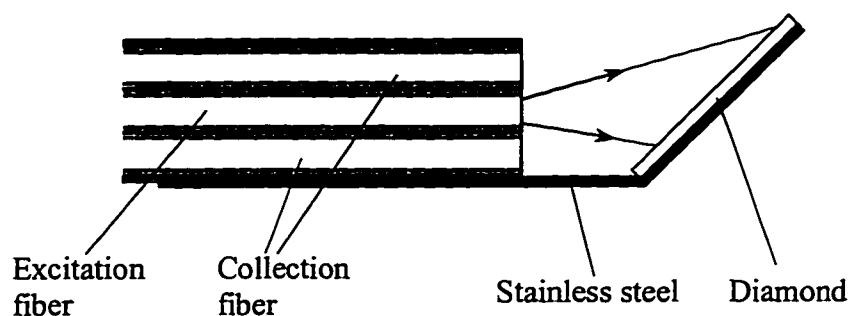
Figure 3.23   fiber optic Raman probe with a bulk diamond placed in front of it

cover the entire excitation light cone. The diamond window is placed at an angle of 45° to eliminate the reflection of glass Raman signal into the collection fiber. This design has several advantages. Since the diamond covers the whole excitation light cone, even if the intensity distribution within the cone changes due to different optical alignment, the diamond will experience the same effect as the analyte solution. Thus the normalized result will be independent of the optical alignment. Secondly, adjusting the spacing between the diamond and the fiber can easily change the intensity of the diamond Raman band.

To test the performance of this probe, experiments are repeated using the ethanol-water solution. The experimental set up is the same as before. A 4×4 mm² synthetic bulk

diamond (Sumitomo) is placed in front of the fiber with a spacing of 4 mm. A series of

Raman spectra are acquired with this probe. The 883.3 cm^{-1} ethanol Raman peak is

measured and then normalized by the diamond peak area. The result is listed in Table 3.7

and Fig. 3.24.

Table 3.7 Experimental results for ethanol-water solution using bulk diamond probe

Sample Number	1	2	3	4	5	6
Normalized diamond peak area	-0.00159	0.08684	0.18994	0.29140	0.39150	0.47756
Measured percentage (%)	0	18.43	40.09	61.33	81.92	100
Predicted percentage (%)	0.04	18.49	40.00	61.17	82.06	100.01
Error (%)	0.04	0.06	-0.09	-0.16	0.14	0.01
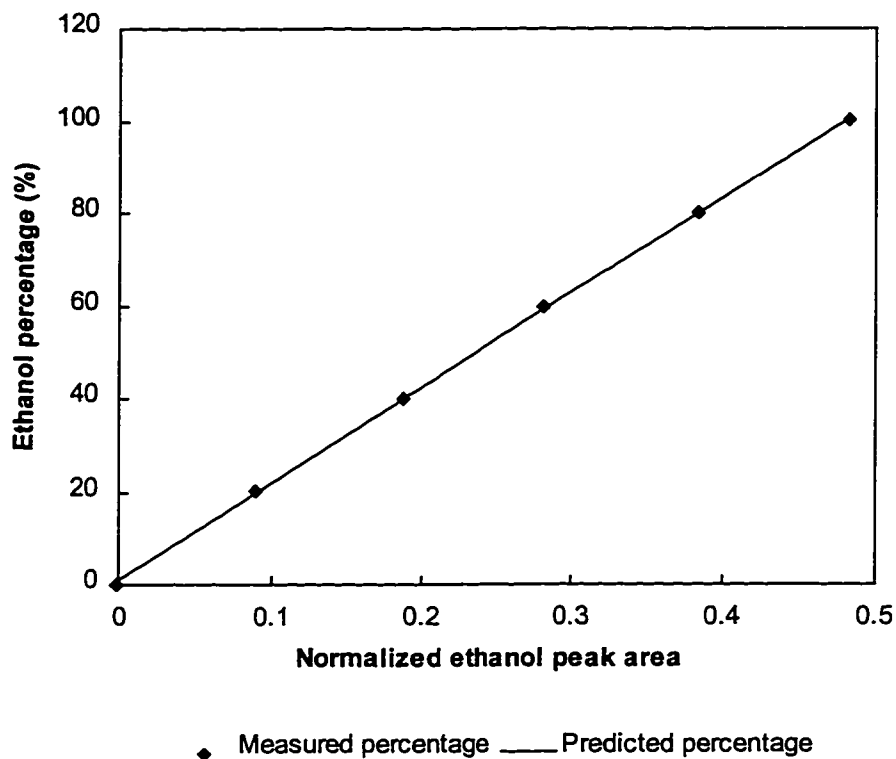
Figure 3.24 Predicted and measured ethanol percentages *vs.* peak area for the bulk diamond probe

The prediction model is built through a linear regression, which is given as

$$C_p = 208.6384 \times A_n + 0.373379, \tag{3.8}$$

where C_p is the predicted ethanol percentage and A_n is the normalized ethanol peak area. A very linear relationship between the normalized ethanol peak area and the measured. ethanol percentage is observed, and the small prediction error shows the good performance of the probe.

The effect of optical alignment on the probe performance is also investigated. The signal from the 82.06% ethanol solution is acquired for six alignment procedures. The normalized ethanol peak area is measured and used in Eq. (3.8). The standard

deviation observed is ±0.31%, which is less than standard deviation (±4.7%) for the Probe D2.

However, this design has a dependence on the refractive index of the analyte. When the excitation laser hits the diamond surface, the amount of light transmitted into the diamond and reflected by the diamond surface depends on the difference of the refractive index between the diamond and the tested media. The smaller the difference in refractive index, the larger the amount of light transmitted into the diamond, leading to an increase in the Raman intensity of the referencing diamond peak. This effect will cause a non-linearity between the Raman peak area and the concentration (or percentage) of the analyte. Larger error is expected if the same linear model is used to predict the concentrations of the analyte. To investigate the effect of refractive index on the probe performance, the ethanol-DMSO solution experiment is repeated using this probe. The area of ethanol peak at 883.3 cm^{-1} is measured and then normalized by the diamond peak at 1332 cm^{-1}. The same model (Eq. 3.8) is used to predict the ethanol percentage. The result is shown in Table 3.8 and Fig. 3.25.

An obvious non-linearity is observed between the normalized ethanol peak areas and the measured ethanol percentages. This is an indication of refractive index dependence of the probe. A larger error occurs when the previous model based on linear regression is still used for prediction. As expected, a decrease in diamond Raman intensity is observed when ethanol percentage becomes higher as shown in Table 3.8. This is because the difference between refractive index of ethanol (1.3611) and diamond (2.4173) is lager than that between DMSO (1.4780) and diamond.

Table 3.8   Experimental results for ethanol-DMSO solution using bulk diamond probe

Sample No.	1	2	3	4	5	6
Diamond Peak area (arb. units)	5189963	5188354	5015521	4942209	4844316	4726328
Normalized ethanol peak area	-0.0007	0.08994	0.18817	0.28198	0.38280	0.48280
Measured percentage(%)	0	20.13	40.13	59.98	80.08	100
Predicted percentage(%)	0.23	19.14	39.63	59.21	80.24	101.10
Error (%)	0.23	-0.99	-0.50	-0.77	0.16	1.10
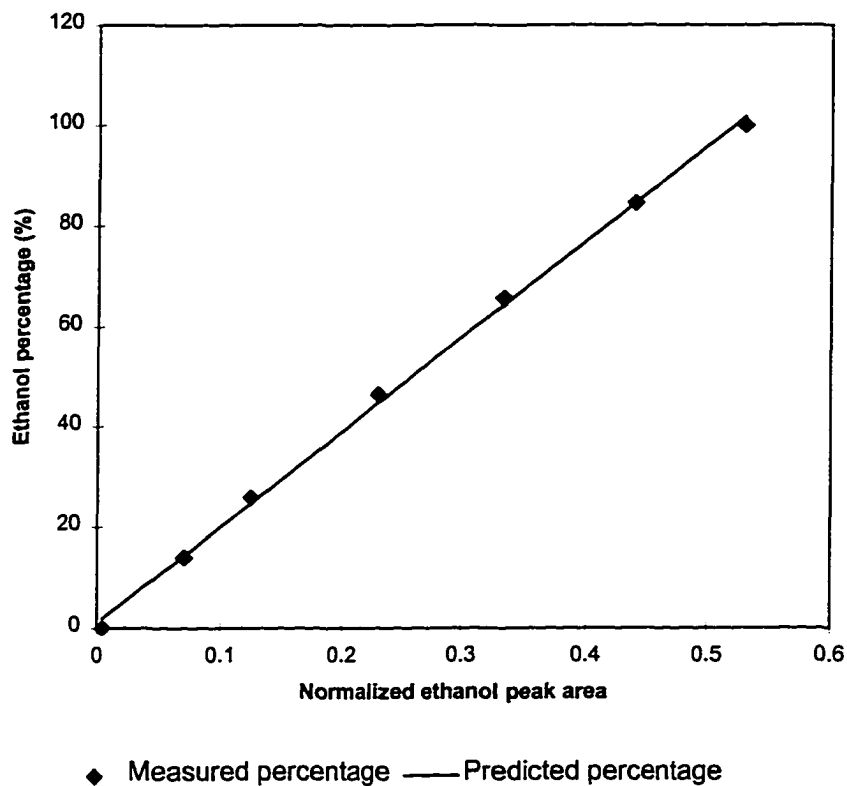
Figure 3.25   Predicted and measured ethanol percentages in DMSO *vs.* peak area

for the bulk diamond probe

3.5 Remote Sensing

The unique feature of optical fibers in guiding the excitation light and Raman

signal can be effectively utilized for long-distance remote sensing applications.

However, the former creates a huge glass Raman signal from the long fiber; therefore, a

filtering mechanism is necessary to eliminate it. A remote sensing experiment is

performed with a 500-foot long fiber probe (Probe D4). A diamond window acts as a

referencing standard and is attached to an existing 500-foot fiber optic probe made by

Detection Limit. To eliminate any fluorescent background, an infra red diode laser at 852

nm is used as the excitation source. The probe structure is shown in Fig. 3.26. The

excitation laser is guided by the excitation fiber and then collimated with a convex lens
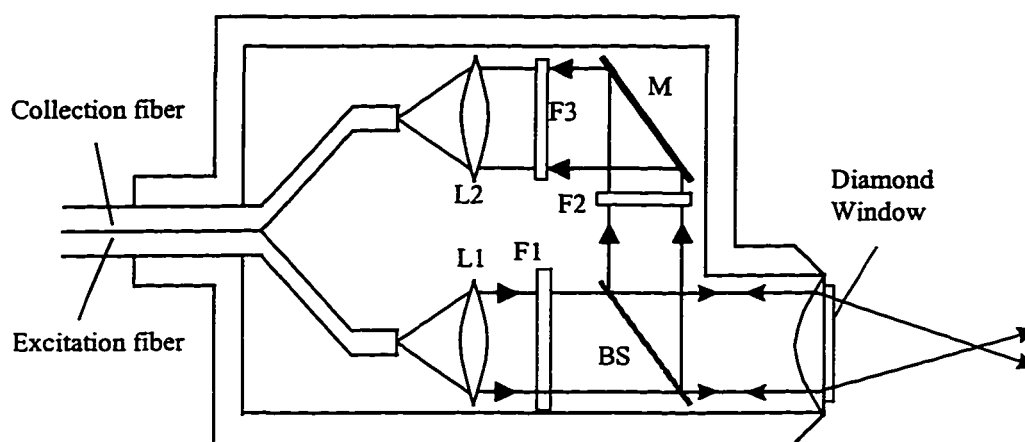
L1, L2 – Lens, M — Mirror, F1 – Band pass filter, F2, F3 – High pass filter, BS – Dichroic beam splitter

Figure 3.26   Probe structure for remote sensing

L_1. A Band pass filter F1 is used to eliminate glass Raman signal. The excitation laser

then passes through a dichroic beam splitter BS and focused by a 10X objective to the

outside. A 4×4x1 mm³ bulk diamond (Sumitomo) is attached to the objective as a

referencing standard. The Raman signal is reflected at the beam splitter and redirected by

a mirror M, then coupled to the collection fiber through another convex lens L_2. The two

high pass dielectric filter F2 and F3 are used to remove the Rayleigh scattered laser light.

The collection fiber is connected to a spectrograph, which is interfaced to a desktop

computer.

A benzene-pentane solution is used as the test material to measure the percentage

of the benzene. The probe is dipped into the solution during the measurement. For each

sample solution, the Raman spectrum is acquired three times by repositioning the probe each time, so that the standard deviation can be calculated. The integration time for high benzene percentage solutions is 8 seconds, and for low benzene percentage solutions is 40 seconds. Peak area of benzene is used to predict the percentage. Since the major peak of benzene at 992.5 cm^{-1} overlaps with pentane spectrum, a spectra separation is necessary before the peak area can be calculated. The Raman spectral separation of benzene and pentane can be done through a least squares fit algorithm. A pure pentane spectrum is used as a reference spectrum. The factor, which is needed to bring the reference pentane spectrum to fit the pentane spectrum in the mixed spectra, can be obtained through least square fit process. Once the fitting factor is available, the pentane spectrum can be easily subtracted from the mixed spectra. The 1450.7 cm^{-1} pentane band is used to perform the least square fit process, since there is no spectral overlap between pentane and benzene at this region. Figure. 3.27 shows one example of spectra separation for 10.25% benzene in pentane solution.

After spectra separations are done for all collected spectra with different benzene percentage, the spectra are normalized with the diamond peak areas. Figure 3.28 shows the benzene spectra after pentane spectra subtraction and diamond normalization. Note that the normalization can also eliminate the effect of using different integration time. The peak area of benzene at 992.5 cm^{-1} (974-1010 cm^{-1}) is then measured, and a linear model is built based on regression to predict the percentage of benzene. The results are
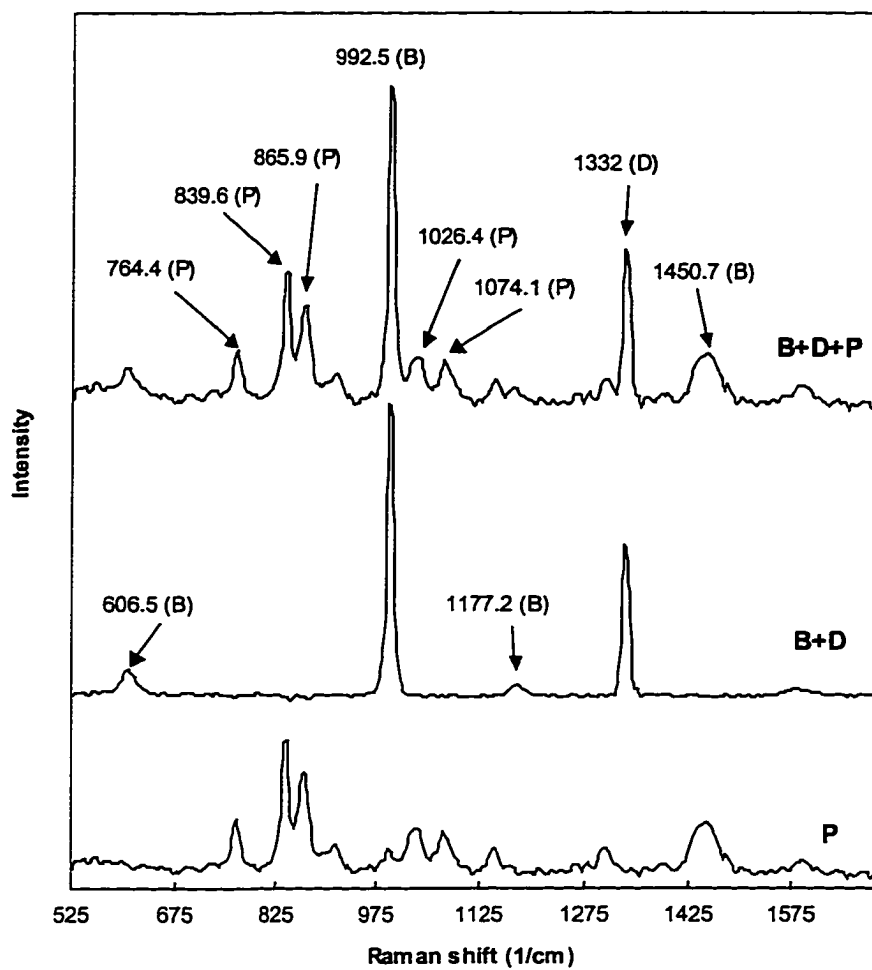
B — Benzene, **D** — Diamond, **P** — Pentane

Figure 3.27   Spectra separation for 10% benzene in pentane using least square fit
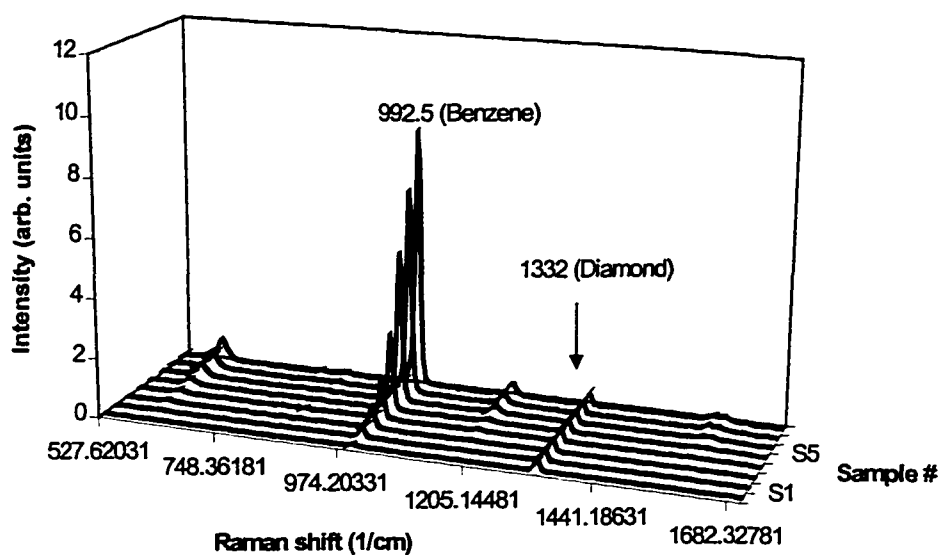
Figure 3.28 Benzene spectra after separation and normalization

listed in Table 3.9 and shown in Fig. 3.29. A non-linear relationship between normalized

benzene peak area and measured percentage is observed in the graph, which is the major

reason of the prediction errors. This non-linearity is due to change in Fresnel reflection at

the diamond-solution interface. The indices of refraction of pentane and benzene are

1.3575 and 1.5011, respectively. Using diamond refractive index of 2.4173, a reflectivity

change of 2.4% is estimated based on normal incidence condition from pure pentane to

pure benzene solution. Thus when benzene percentage becomes high, less reflection

occurs at diamond-solution interface, leading to an increase in Raman intensity of the

solution and a decrease in Raman intensity of diamond. This index of refraction

dependence of the probe can be improved by coating the diamond with a layer of dielectric material with index of refraction close to that of the solution.

Table 3.9 Experimental results for benzene-pentane solution

Sample Number	Measured percentage (%)	Integration time (s)	Benzene peak area (arb. units)	Normalized benzene peak area	Predicted percentage (%)	Error (%)
1	0	40	53	0.002	1.38	1.38
2	1.11	40	5713	0.210	2.16	1.05
3	4.51	40	26227	0.949	4.93	0.41
4	9.76	40	60007	2.145	9.41	-0.35
5	16.45	8	19720	3.831	15.72	-0.73
6	32.01	8	40350	7.710	30.25	-1.77
7	59.65	8	81409	15.209	58.33	-1.32
8	80.73	8	110677	21.123	80.48	-0.25
9	100	8	143029	26.755	101.57	1.56
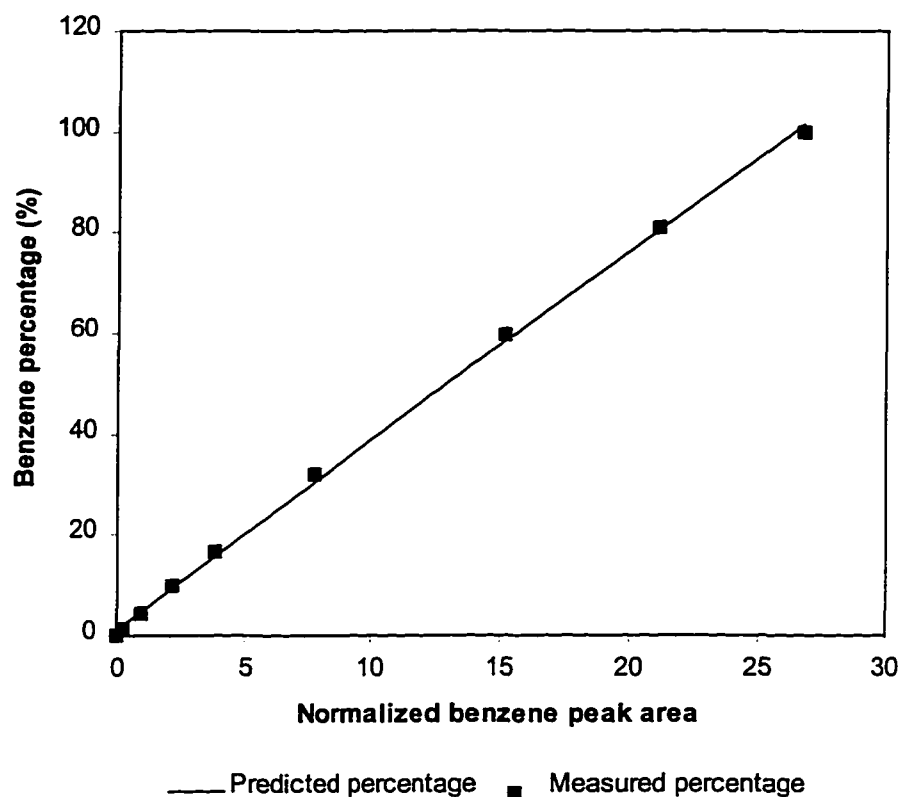
Figure 3.29   Predicted and measured benzene percentages in pentane *vs.* normalized benzene peak area

The detection limit for the system is determined by setting the root-mean-square

(*rms*) S/N equal to 2 on the strongest benzene Raman band. For 40 seconds integration

time, the detection limit is calculated as 0.141%. The maximum standard deviation for

the three different measurements for the same solution is 0.48%, which is larger than the

detection limit. This is probably due to the small amount of sample solution used.

3.6 Summary

The concept of using diamond as a referencing standard for quantitative Raman

analysis is implemented with different probe designs. All designs can successfully

eliminate the effect of variation in the excitation laser intensity. Probe D1 is simple, but

has large glass Raman background, and highly depends on the refractive index of the testing media. Probe D2 has the advantages of being cheap, compact, and less dependent on index of refraction, but it can not totally cancel the effect due to different optical alignment. The Probe D3 has the advantages of less dependence on optical alignment and adjustable diamond Raman intensity. However, this design is expensive because a large bulk diamond is needed to cover the excitation light cone. The probe is also more sensitive to refractive index. An alternative is to replace the expensive bulk diamond with a CVD diamond film. The investigation of CVD diamond will be given in the next chapter.

An example of remote Raman sensing is also presented. The notch filters are used to eliminate the glass Raman signal. With the help of a diamond referencing standard, the results show a good accuracy for predicting the percentage of benzene. The design can compensate the fluctuations in excitation laser. The detection limit is found to be 0.141% for 40 seconds integration time.

CHAPTER IV

EXPERIMENTS ON CVD DIAMOND

In this chapter, CVD diamond is investigated as a standard for quantitative Raman analysis to replace natural diamond. The substrate temperature, total pressure, gas flow rate, and gas composition for the microwave plasma enhanced CVD (MPECVD) diamond deposition system are studied in detail to get high quality CVD diamond. Experimental results based on a CVD-diamond-referenced fiber optic Raman probe are also presented.

4.1 Choice of CVD Diamond

The experimental results presented in Chapter III confirmed unequivocally that diamond could be used as a standard in quantitative Raman analysis. The normalization with the diamond Raman band can effectively eliminate the variation due to power fluctuation in the excitation source and optical alignment. Probe calibration for a particular analyte needs to be done only once for the normalized results. However, the barrier for the commercialization of such a probe is the high price of the bulk diamond, especially for the Probe D3 discussed in Chapter III. A possible solution to this problem is using CVD diamond as a replacement for the natural bulk diamond.

CVD diamond has several advantages for this application. Unlike bulk diamond, large area CVD diamond film can be obtained without increasing the cost. Also, for the structure of Probe D3 shown in Fig. 3.23, if CVD diamond is used, the rough surface and small thickness of CVD diamond film can reduce the dependence of the probe on the refractive index, since scattering rather than reflection will dominate at the diamond and

analyte interface. CVD diamond also provides the possibility of performing SERS. If

coated with silver or gold, the rough surface of CVD diamond film will enhance the

Raman signal in addition to providing an intensity standard. The surface grain size can

be easily controlled by changing the nucleation method or varying the growth time.

However, the Raman spectrum of the typical CVD diamond is not as ideal as that of the

natural diamond to be used as a standard. As shown in Fig. 4.1, the width of CVD
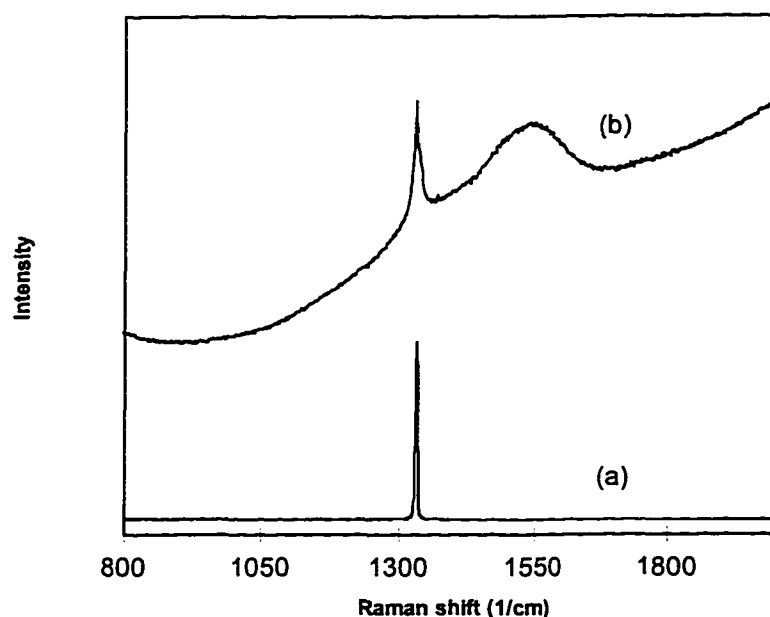
Figure 4.1   A comparison between Raman spectra of natural diamond and CVD diamond

diamond Raman band is usually wider than that of natural diamond, and the background

is not so flat due to the impurity and sp^2 carbon contamination. A broad band peak near

1540 cm^{-1} is an indication of the presence of sp^2 bonding in the CVD diamond film [82].

The intensity ratio of the 1332 cm^{-1} to the 1540 cm^{-1} can be used to quantify the quality of

the CVD diamond [83]. Quality of CVD diamond depends strongly on the deposition parameters and gas compositions. High quality CVD diamond with Raman spectrum close to that of natural diamond is achievable if the deposition parameters and gas composition are optimized [84].

4.2 CVD Diamond Growth

The efforts to grow diamond from gas phase started from the early 20th century. However, the first successful diamond synthesis using low-pressure chemical vapor deposition was achieved by William G. Eversol at the Linde Division of Union Carbide Corporation in 1952. In the early research, gases such as carbon monoxide, carbon tetraiodide, or methane were decomposed to provide source species. The growth rate of these thermal CVD processes was very slow (<0.01μm/h), since the co-deposition of graphite carbon prevented the further growth of diamond. Growth rate has been significantly improved since hydrogen was introduced in the diamond growth process. Chauhan et al. [85] have proved that the hydrogen reacts with graphitic carbon faster than with diamond, leaving the diamond crystals free of graphite and ready for further diamond growth. Now, the mixture of methane and hydrogen has become the typical gas compositions for low-pressure CVD diamond growth.

4.2.1 Diamond Growth Methods

CVD diamond growth methods include hot filament assisted CVD system, RF assisted CVD system, laser assisted CVD system, and MPECVD system [86]. MPECVD methods have been used more extensively than any other diamond growth methods [87-89]. The advantages of microwave assisted CVD method have been well stated by Sato

and Kamp [90] in a review of different diamond growth methods. MPECVD method is an electrodeless process, which avoids contamination of the diamond films due to electrode erosion. The microwave discharges at 2.45 GHz produces higher plasma density than RF discharge, leading to a higher growth rate. Furthermore, the plasma is confined in the center of the chamber in the form of a ball, which prevents carbon deposition occurring on the chamber wall.

In this research, all diamond growth experiments were done with the MPECVD system (ASTeX) in the Microelectronics Laboratory. Fig. 4.2 shows a schematic
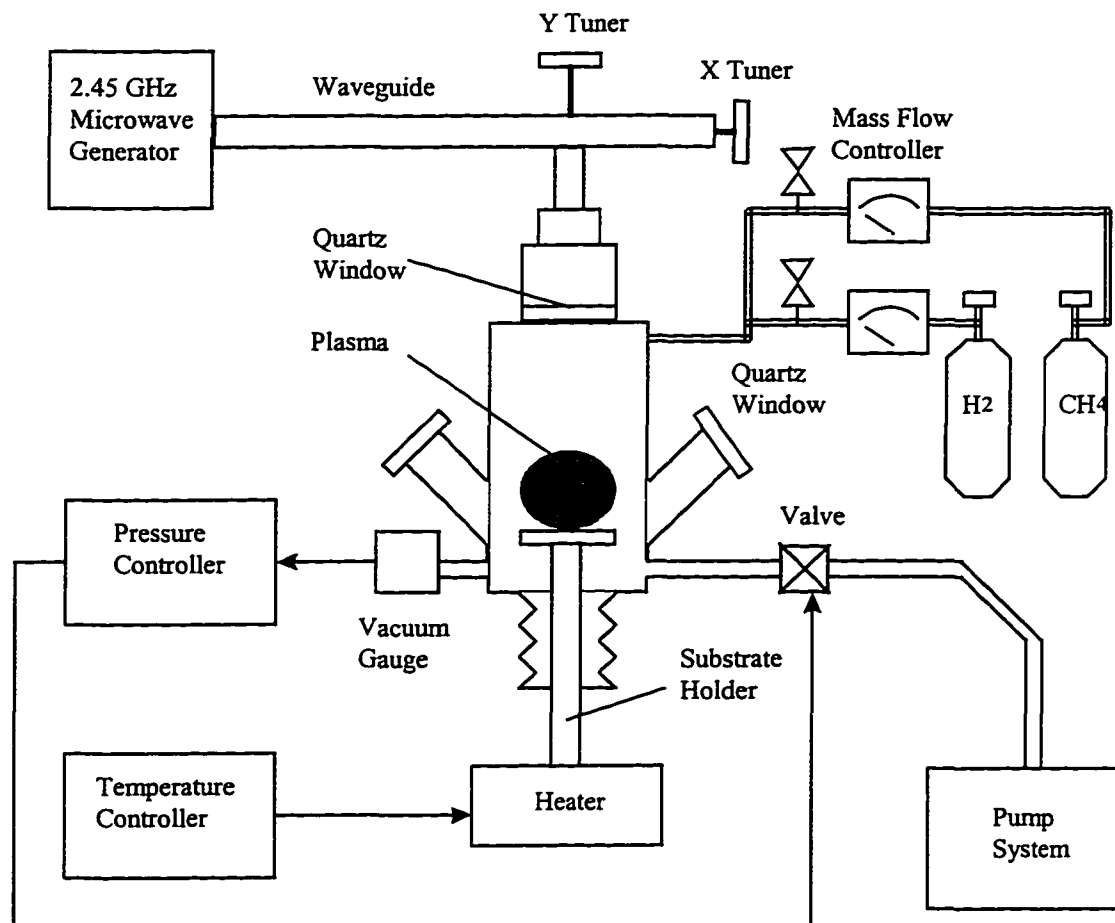
Figure 4.2   A schematic draw of MPECVD diamond growth system

drawing of the diamond growth system. Microwave power at 2.45 GHz is guided by a rectangular waveguide, and then coupled into the growth chamber through a quartz-sealing window. Prior to diamond growth, the chamber is pumped to high vacuum through a mechanical pump and a turbo-molecular pump. During the diamond growth, the chamber pressure is measured by a pressure gauge and automatically controlled through a butterfly valve. The substrate temperature is measured by a thermocouple, and is controlled through a heater. Minimum reflected power could be achieved by adjusting the substrate position and waveguide tuner. The flow rates of gas species used for diamond growth are controlled through the mass flow controllers.

4.2.2 Substrate Preparation

Fused silica is chosen as the substrate to grow diamond. The major reason is that fused silica is transparent, the diamond film quality can be quickly checked by observing the color of the film. Darker color usually indicates high graphite contamination. Another reason is that fused silica is compatible with the fiber-optic material to give more flexibility for probe design.

Substrate nucleation is necessary prior to the diamond growth. It has been found that surface abrasion with hard material such as diamond [91], cubic born nitride [92], silicon carbide powder [93], or stainless steal [94] is effective to create the nucleation sites on the substrate. When diamond powder is used, the enhanced nucleation sites is believed to be due to residual diamond particles left on the surface from the scratching medium and acted as diamond nucleation sites [95]. This has been further proved by Iijima *et al.* [91][96] with the observation by high-resolution transmission electron

microscopy (HRTEM) of diamond nucleation on "diamond seeds" left from the scratch process. However, the reason of the nucleation enhancement by non-diamond power scratching is still unknown. The possible explanation is that the defects on the scratched surface tend to capture the carbon species due to a low surface energy.

For fused silica used as the substrate in our experiments, we have found that abrasion by diamond paste is a very effective method to create the nucleation sites. Nucleation can be done by placing 0.25 μm diamond paste (ENGIS) on ordinary paper, hand-pushing the sample and abrading the surface. High nucleation density could easily be obtained by abrasion for about 10 times or more. Most of the substrates were intentionally treated differently on the two sides. Half area of a sample had a few abrasions (less than 4 times), resulting in low nucleation density such that scattered diamond particles would grow during the deposition. Crystal structure and growth rate were examined in this area under the scanning electron microscope (SEM). The other half area of the sample was heavily abraded (more than 10 times), so that continuous film was grown, and the diamond quality could be roughly estimated by eye-checking of the film color.

4.2.3 Diamond Deposition

After nucleation was done, the substrate was ultrasonically cleaned by acetone and then rinsed with de-ionized water. A test growth run was executed with the parameters listed in Table 4.1 using a gas mixture of methane and hydrogen. The diamond growth lasted for 6 hours. After that, the methane was turned off and left pure hydrogen plasma for 10 more minutes to clean the sample. The test sample was then

checked by scanning electron microscopy. Figure 4.3 shows the SEM picture of this sample. The particle size is about 12 μm, which indicates a growth rate of about 2 μm/h. Different nucleation densities on either side are clearly shown in the picture.

Table 4.1 Diamond growth parameters for test run

Pressure:	30 Torr
Temperature:	750 °C*
Microwave Power:	1000 W
Total Flow Rate:	900 Sccm
Methane Concentration:	0.8%
Growth Time:	6 hour

*This temperature is the surceptor temperature measured by the thermocouple. The real temperature of the sample is higher due to the plasma heating. We measured the sample temperature using an optical pyrometer and revealed that the sample temperature was about 180 °C higher than the thermocouple reading under the microwave power of 1000W and total pressure of 40 Torr.

(a)   (b)

Figure 4.3   CVD diamond grown on quartz substrate with (a) low nucleation density,

(b) high nucleation density

4.2.4 Raman Spectrum

It is rather fortuitous that Raman spectroscopy is used to characterize the quality of the

CVD diamond. An ideal Raman spectrum close to natural diamond is also the aim of our

diamond deposition. The Raman spectra of all CVD diamond samples are obtained with

the micro-Raman system, which is a Nic-Plan Raman Microscope interfaced to a

Chromex Spectrograph with a CCD detector. A schematic drawing of the micro-Raman

system is shown in Fig. 4.4. The excitation laser (argon ion, 514.5 nm) is directed by the
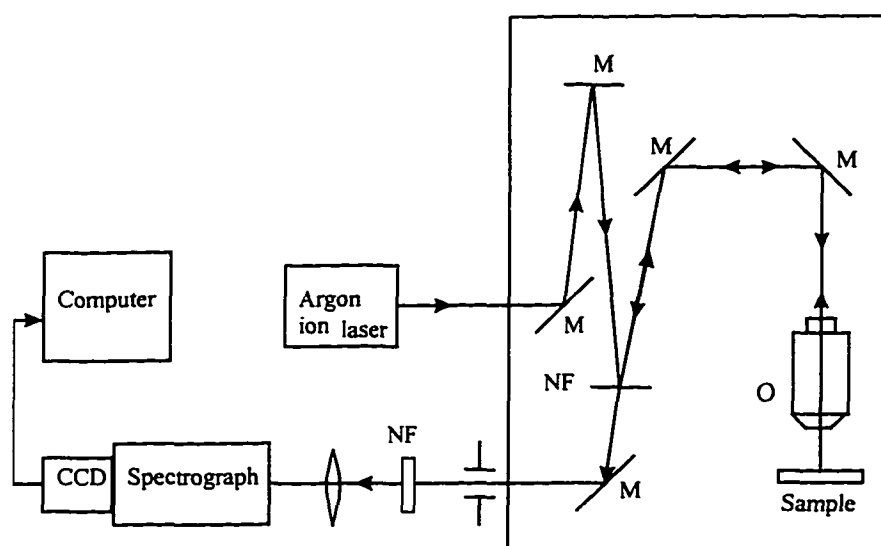
Figure 4.4 A schematic drawing of micro-Raman system

M— mirror , NF – notch filter, O – objective

mirrors, reflected at the notch filter, and then focused to the sample through the objective.

The scattered Raman signal is then collected by the same objective, and guided by the

mirrors to pass through the notch filter. The Rayleigh scattering is filtered out with this

notch filter. The Raman signal is then focused into a spectrograph attached with a CCD. The output signal from the CCD can be accumulated to increase the signal-to-noise ratio of the spectrum. An integration time, which determines the time of accumulation, can be set through the computer, which is interfaced to the CCD. The spatial resolution of this system is about 2 μm, such that the Raman spectrum of different facets of a diamond particle can be taken to analyze the sample.

A Raman spectrum of the test sample was taken and shown in Fig. 4.5. The integration time is 2 minutes with a slit width of 50 nm. A peak at 1332 cm^{-1} clearly
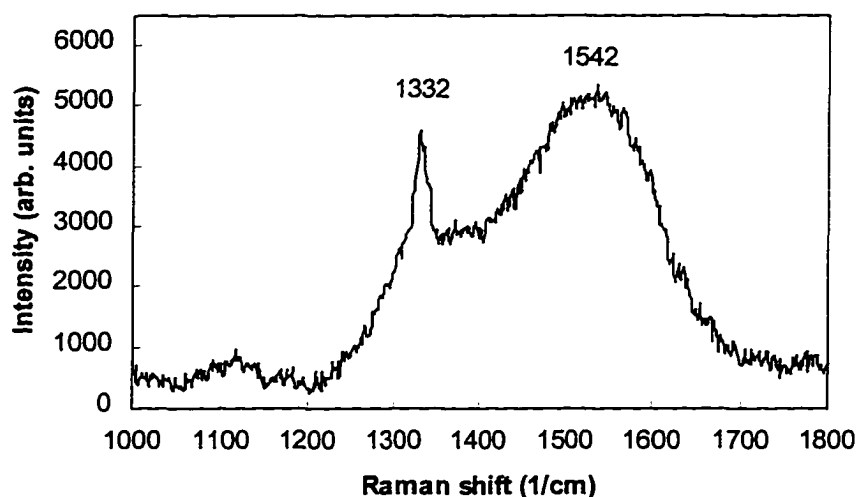
Figure 4.5   A Raman spectrum of the test sample

shows the existence of diamond. However, this peak is weak compared to the broad peak centered at 1540 cm^{-1}, which is an indication of graphitic carbon. It has been reported by Tuinstra and Koenig [97] that the peak intensity ratio of the 1332 cm^{-1} diamond line to 1540 cm^{-1} graphite line (D/G) is linearly proportional to the reciprocal of graphite particle

size. Thus, a measure of D/G can be used as an indication of the diamond quality. For this test sample, the D/G is measured as 0.54, which shows that the quality of the CVD diamond needs to be improved.

4.3 Quality Improvement of CVD Diamond

It appears that variations in Raman spectra of CVD diamond, as compared with common types of natural diamond, are caused by the presence of appreciable amount of sp^2 carbons. The quality of CVD diamond depends strongly on the growth conditions, most critically on the gas composition and substrate temperature: when the condition deviates from an optimum range, non-diamond structures increase in amount, and further deviation results in the composition of graphite phase. The optimization of deposition parameters such as temperature, pressure, microwave power, etc. is very complicated. One of the reasons is that most of the parameters are coupled together, which gives a large space for optimization. An exhaustive combination of different parameters is almost impossible. As Anthony [98] points out that, the empirical optimization of all parameters requires millions of growth experiments. On the other hand, the optimized parameters also strongly depend on the growth system, such as the growth method and the chamber size, which make the published results not reproducible for different systems.

The optimization in this research is mainly focused on pressure, substrate temperature, and gas compositions. The aim is to get the high quality diamond while keeping a reasonable growth rate. The best first search method, which varies only one parameter in one set of experiments, is used to get the optimum result. This approach,

although not guaranteed, is however a reasonable approach to get the optimized result using a limited number of experiments.

4.3.1 The Effect of Pressure

Pressure itself does not play a very important role in the quality of diamond growth as stated by Clausing [99]. However, pressure can change the gas temperature and the plasma composition thus changes the growth rate. Pressure determines the recombination length, the lifetime, and the drift distance of atomic hydrogen [100]. When the plasma pressure is low, electrons move much faster than ion due to lighter mass, results in a non-thermal equilibrium. However, due to the large electron mean free path, there is no energy redistribution between electrons and molecules, leading to a relatively low gas temperature. Atomic hydrogen and neutral carbon-containing radicals, necessary for diamond growth, are mainly generated by the high-energy electrons whose concentration is relatively small. Thus growth rate in low-pressure plasma is expected to be small. For high-pressure plasma, the mean free path of electrons becomes small. Energy redistribution between electrons and gas molecules is expected due to collision, thus bring the gas temperature as high as the electron temperature. In this case, both electron and gas molecules are expected to generate atomic hydrogen and neutral carbon-containing radicals. Hence, growth rate is expected to be higher for higher pressure.

The pressure effect of our growth system was experimentally investigated with pressure varying from 20 to 60 Torr. Other parameters were fixed during these experiments, which are listed in Table 4.2. After growth, the film color of these samples appeared dark gray, which showed the presence of graphite carbon contamination. The

diamond quality was further checked by Raman spectroscopy. Figure. 4.6 shows the

Raman spectrum of the three samples.

Table 4.2   Diamond growth parameters for pressure experiments

Pressure:	20, 40, 60 Torr
Temperature:	750 °C
Microwave Power:	1000 W
Total Flow Rate:	900 Sccm
Methane Concentration:	0.7%
Growth Time:	8 hour

To quantitatively determine the quality of the CVD diamond, the D/G ratio was

calculated. The D/G ratio for 40 Torr sample was 7.42, which was the largest compared

to the 2.11 and 4.78 for 20 Torr and 60 Torr samples, respectively. Fig. 4.7 shows the

SEM photographs of these three samples. As predicted, an increase in diamond growth

rate was observed, which was graphed in Fig. 4.8. However, the growth rate increment

from 40 Torr to 60 Torr was not so significant. The diamond quality also could be

checked by looking at the crystal structure under SEM. The 20 Torr sample showed

multifaceted and ball like crystals. The facets appear rough indicating poor quality of the

diamond. The 40 Torr sample shows cleaner and smoother facets compared to the other

two.

The saturation in growth rate and the degradation in quality at high pressure can be explained as the effect of the pressure induced temperature change. As stated before, the gas temperature will become higher at high pressure. The temperature effect will be further investigated in the next section. Considering the Raman spectrum and growth rate together, the gas pressure will be fixed at 40 Torr for further parameter studies.
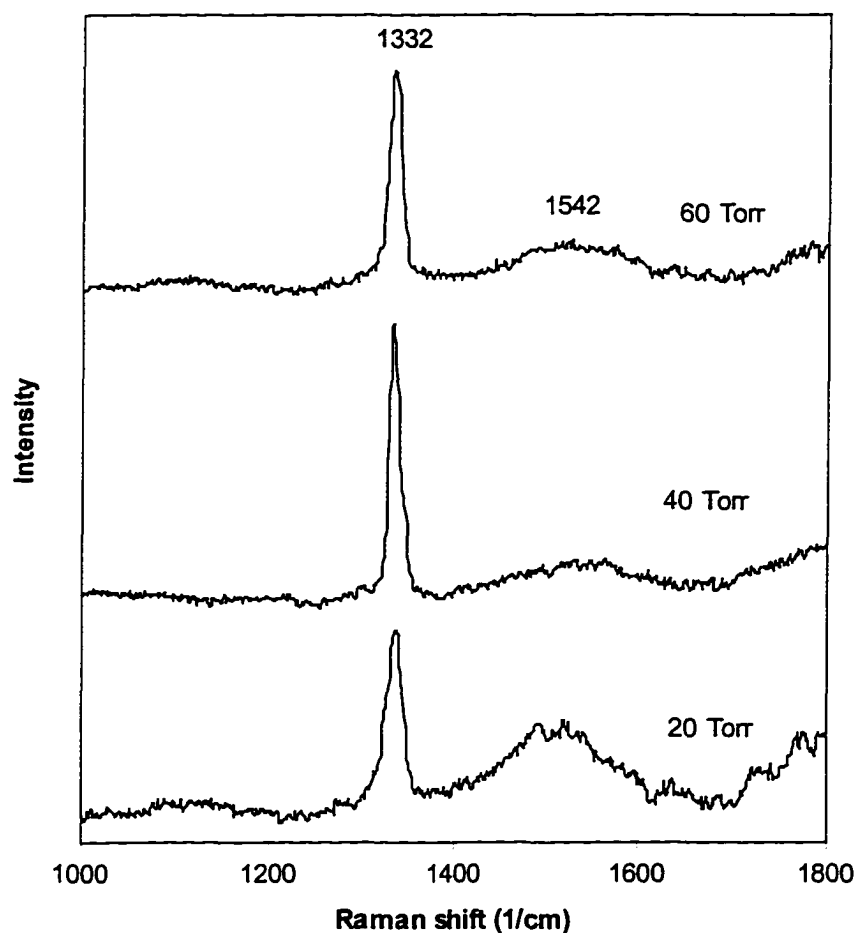
Figure 4.6   Raman spectra of CVD diamond under different growth pressure

(a)

(b)
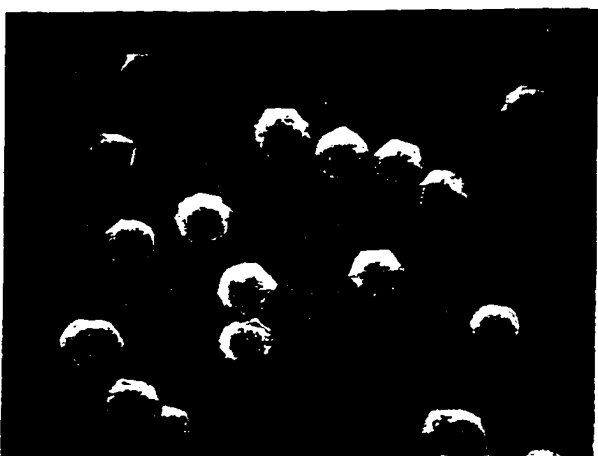
(c)

Figure 4.7   The pressure effect on the diamond growth: (a) 60 Torr, (b) 40 Torr, and (c) 20 Torr.
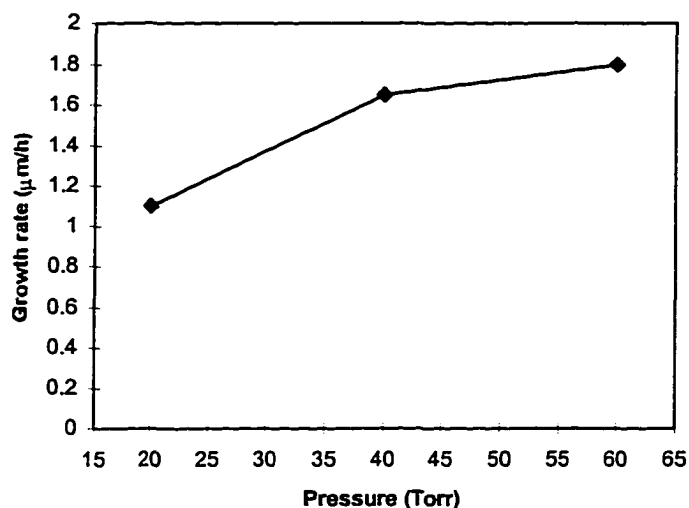
Figure 4.8   Growth rate versus pressure

4.3.2 The Effect of Substrate Temperature

Substrate temperature plays an important roll in both quality and growth rate of

diamond. A typical substrate temperature range for diamond growth is 500-1200°C.

Diamond growth at substrate temperature above 1200°C was found to result in high

graphite contamination, while growth below 500°C was found to lead to diamond-like

carbon deposits [101-103]. The substrate temperature was also found to control the

diamond growth rate. Growth rate increases with the increase of substrate temperature at

low temperature, which follows an Arrhenius behavior. However, growth rate starts to

decrease above the temperature of 1000°C. The surface reaction leading to such a

behavior has been modeled by many researchers [104-106].

To find an optimum temperature for our system, a series of experiments were

executed by varying the substrate temperature from 550 to 750°C and fixing the other

parameters. The growth parameters for these experiments are listed in Table 4.3. The

color of these films varies from dark gray to pure white when the temperature is

Table 4.3   Diamond growth parameters for substrate temperature experiments

Pressure:	40 Torr
Temperature:	550, 600, 650, 700, 750* °C
Microwave Power:	1000 W
Total Flow Rate:	900 Sccm
Methane Concentration:	0.7%
Growth Time:	8 hour

- Growth experiment with temperature 750 °C has been done in the pressure experiments.

decreased from 750°C to 550°C. However, the best Raman spectrum was found for the

sample with substrate temperature at 600°C, this result is shown in Fig. 4.9. The D/G

ratio was calculated and graphed in Fig. 4.10, which shows that the 600°C sample has the

highest D/G ratio. The samples were further examined under SEM to determine the

growth rate and crystal structure. Fig. 4.11 shows the SEM pictures of these samples.

The growth rate was measured and graphed in Fig. 4.12. As expected, the growth rate

decreased as temperature decreased. The crystal structure in the SEM pictures shows that

secondary growth and irregular shape happened for higher temperature. When the

temperature was lowered, the crystal surface became smoother and well faceted. This is
also an indication of diamond quality in addition to the Raman spectra.
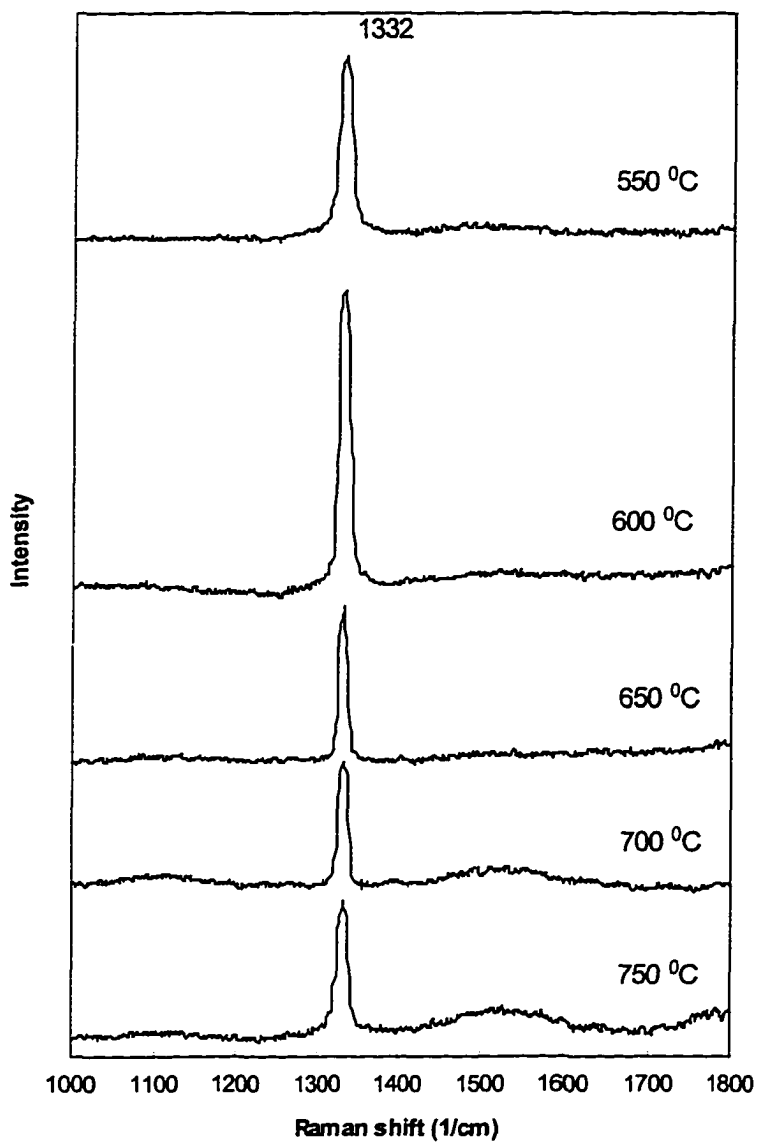
Figure 4.9   Raman spectra of CVD diamond under different growth temperature
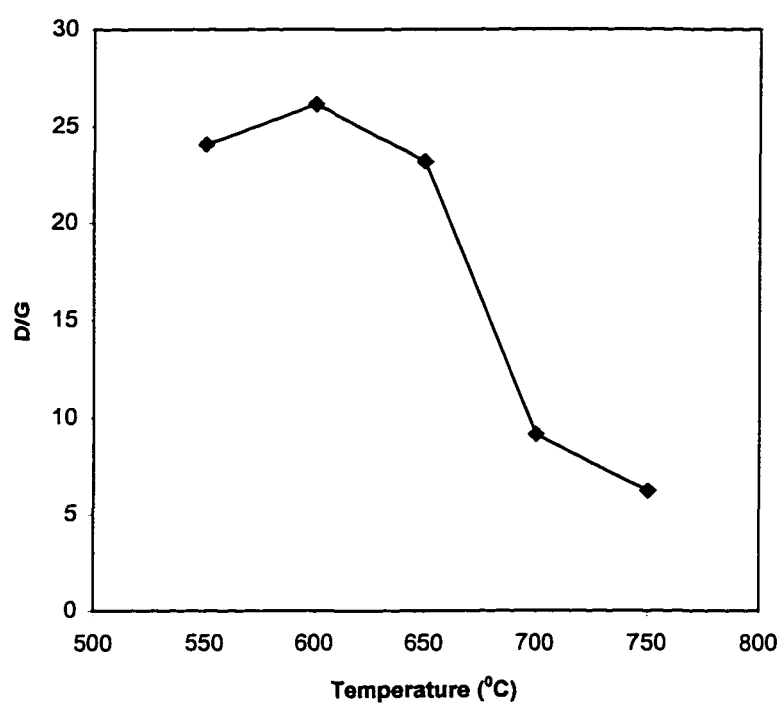
Figure 4.10 The D/G ratios of the CVD diamond sample under different substrate temperature

(a)

(b)

(c)

(d)

(e)
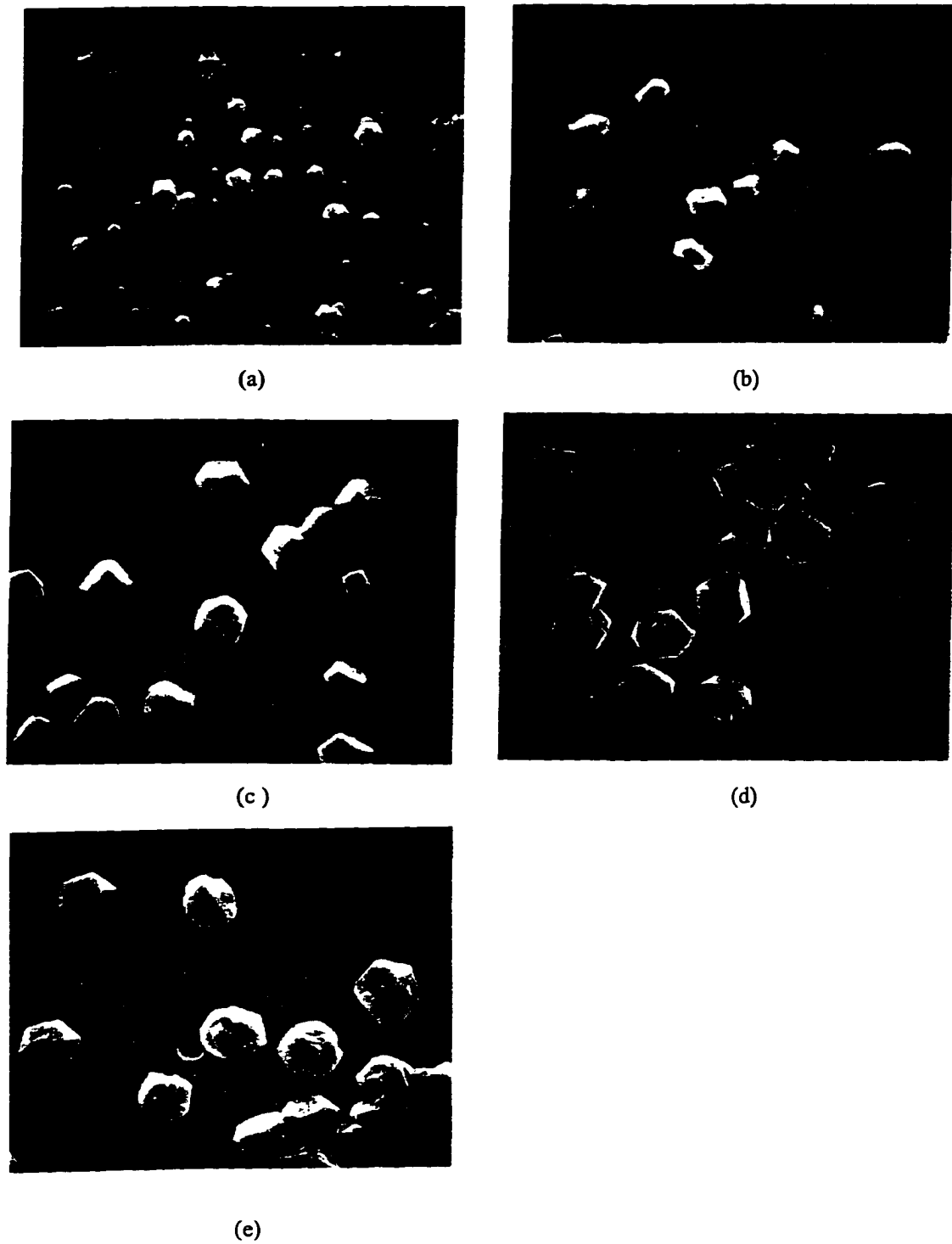
Figure 4.11 Temperature effect on diamond growth:

(a) 550°C, (b) 600°C, (c) 650°C, (d) 700°C, and (e) 750°C
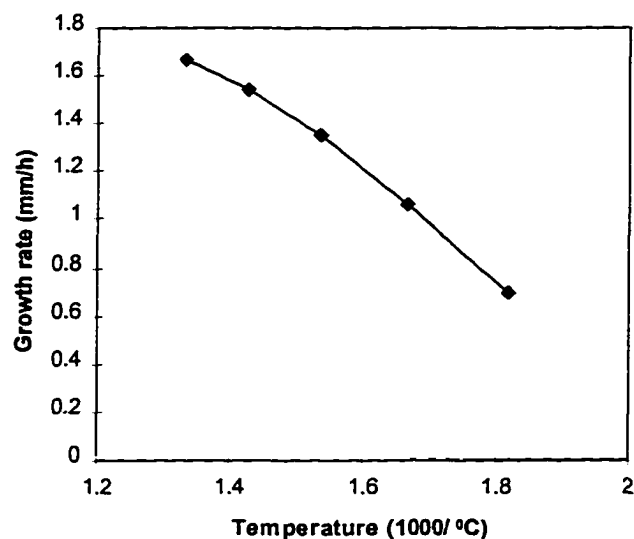
Figure 4.12 Temperature effect on the diamond growth rate

In conclusion, the best Raman spectrum occurs at 600 °C although growth rate is lower than those of the higher temperature experiments are. Therefore, substrate temperature is fixed at 600 °C for the further experiments.

4.3.3 The Role of Hydrogen

Hydrogen plays a very important role in the CVD diamond growth. It is only after a large excess of hydrogen was used in the process that microns per hour growth rates were obtained. It is well recognized that within a certain range, increasing the percentage of hydrogen improves the quality of diamond, but decreases the growth rate. Several factors have been suggested to explain the role of hydrogen dilution. The most

notable proposal is the preferential etching of graphite over diamond by atomic hydrogen, Advanced by Angus and Hayman [107] and Fedoseev *et al.* [108]. They proposed that a superequilibrium concentration of atomic hydrogen at the growth surface behaves like a solvent for graphite. Their studies of relative etching rates of diamond and graphite were confirmed by Saito *et al.* [109] and showed that the removal of graphite by activated hydrogen was orders of magnitude faster than diamond. However, as the growth temperature is lowered, the model of Frenklach and Wang [110] predicted that the rate of gasification of sp^2 carbon by H atoms will become too slow to remove these species, compared to the rate of other processes, such as hydrogeneration of sp^2 to sp^3 carbons by H atoms.

Besides the selective etching of graphitic carbon, another role of hydrogen is stabilization of the diamond surface by satisfying the dangling bonds of surface carbons, thereby keeping these carbons in an sp^3 configuration and preventing the surface reconstruction into graphite sp^2 structures [111]. Hydrogen atoms also play an extremely important role in the hydrogen abstraction reaction in diamond growth process. These reactions remove hydrogen from surface C_d- H bonds to create active growth sites (C_d •), and remove H from the growth surface to avoid trapping of hydrogen in the solid, which can be expressed as:

$$C_d\,H + H \rightarrow C_d \bullet + H_2$$
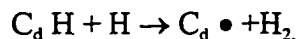
Here C_d represents the carbon on a diamond surface. Other suggested roles of atomic hydrogen are to promote the gas phase production of growth precursors [112], to promote the sp^3 configuration of gaseous radical precursors and surface clusters, and to remove oxygen chemisorbed on the substrate [113].

A growth run was executed to show the effect of the methane-hydrogen ratio. The methane concentration was reduced from 0.7% to 0.4% with other parameters listed in Table 4.4. Since the growth rate was reduced significantly for reduced methane

Table 4.4   Diamond growth parameters for CH_4/H_2 ratio experiments

Pressure:	40 Torr
Temperature:	600 °C
Microwave Power:	1000 W
Total Flow Rate:	900 Sccm
Methane Concentration:	0.4%
Growth Time:	16 hour

concentration, the growth time was increased to 16 hour. The SEM picture of the sample (Fig. 4.13) shows that the crystal has a very smooth and clean surface. The Raman spectrum in Fig. 4.14 shows an improved diamond quality compared to the 0.7% methane concentration sample. The D/G ratio was calculated as 34.29 and 26.15 for 0.4% and 0.7% methane concentration sample respectively. However, the growth rate was reduced to 0.7 μm/h compared to 1.15 μm/h for 0.7% sample.

Figure 4.13   Diamond particles grown at 0.4% CH₄ concentration
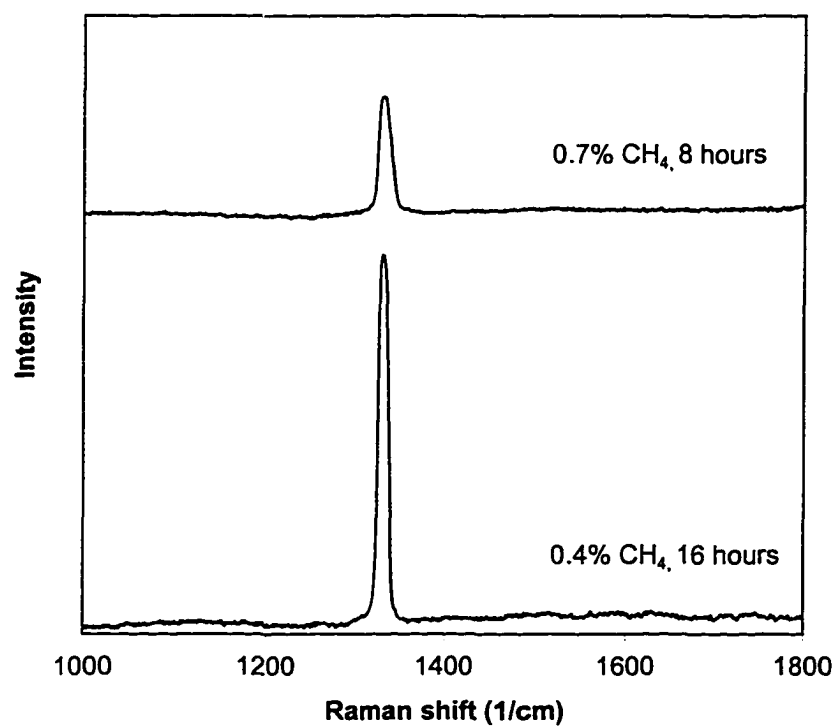
Figure 4.14   Raman spectra of CVD diamond with different methane concentration

4.3.4 The Addition of Oxygen

As presented in previous sections, low substrate temperature within a particular range and high hydrogen percentage can effectively improve the diamond quality. However, both of these mechanisms are found to reduce the growth rate. The addition of oxygen to hydrogen-hydrocarbon growth mixtures is believed to improve both the quality and the growth rate of CVD diamond [114-116], especially for the higher input hydrocarbon concentrations. The primary influence of oxygen is to enhance the quality of the deposited diamond, probably through O and O_2 or OH radicals, which effectively etch non-diamond carbon species and thus prevent poisoning of active surface sites. Hydroxyl radicals can also activate surface sites by reactions such as

$$C_d H + OH\bullet \rightarrow C_d \bullet + H_2O$$
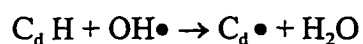
However, this reaction will probably not dominate over hydrogen abstraction. Other factors attributed to the role of oxygen are reduction in the concentration of acetylene, which was assumed to be the precursor of graphitic and amorphous carbon, reduction in the effective initial hydrocarbon mole fraction, increase in the concentration of H atoms, and removal of aromatic hydrocarbons in the gas phase.

The oxygen addition experiments are conducted using the mixture of hydrogen, methane, and carbon dioxide. The reason for introducing oxygen through carbon dioxide is for the safety concerns in mixing H_2 and O_2. The ratio of each species in the C-H-O growth system is critical for diamond growth [117]. The addition of oxygen allows higher methane concentration than the CH_4-H_2 growth system while still maintaining the high quality of the deposited diamond; thus higher growth rate can be achieved. The carbon atom in the carbon dioxide can also contribute to the diamond growth. However, too much oxygen will etch both graphite and diamond, leading to a decrease in growth rate [116]. Bachmann and coworkers [118] have constructed a

C-H-O phase diagram based on the experimental results to determine the appropriate ratio of the carbon, hydrogen, and oxygen for successful diamond growth. It has been found that diamond growth happens only within a particular region of this phase diagram. To determine the optimal concentration of the carbon dioxide for a particular methane concentration in our system, four diamond growth experiments were conducted with the growth parameters listed in Table 4.5. In these experiments, the methane concentration was fixed at 0.8%, while the carbon dioxide concentration was varied from 0.5% to 1.5%.

Table 4.5   Diamond growth parameters for $CH_4/CO_2/H_2$ ratio experiments

Pressure:	40 Torr
Temperature:	600 °C
Microwave Power:	1000 W
Total Flow Rate:	900 Sccm
Methane Concentration:	0.8%
Carbon Dioxide Concentration	0.5%, 1.0%, 1.2%, 1.5%
Growth Time:	4 hour

Fig. 4.15 shows the SEM pictures of the first three samples. No diamond growth was observed for the last sample (1.5% CO_2) due to excess oxygen. A decrease in growth rate was observed when concentration of carbon dioxide was increased (Fig. 4.16). This is due to the increased oxygen induces a higher etch rate on graphite as well as on diamond. The quality of diamond was checked by the Raman spectra, which is shown in Fig. 4.17. The 1.0% CO_2 sample shows much better D/G ratio (62.63)

(a)

(b)
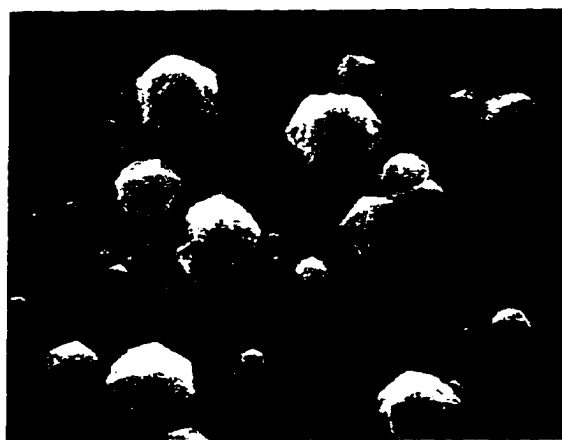
(c)

Figure 4.15   The effect of CO_2 concentration on diamond growth:

(a) 1.2% CO_2, (b) 1% CO_2, and (c) 0.5% CO_2.
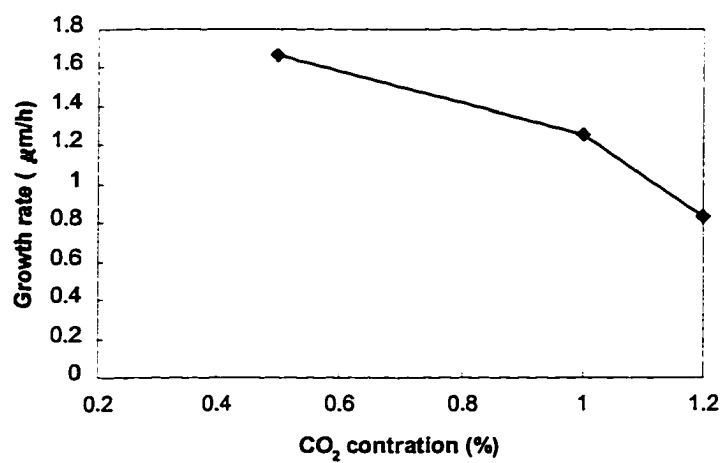
Figure 4.16   The effect of CO_2 concentration on the diamond growth rate
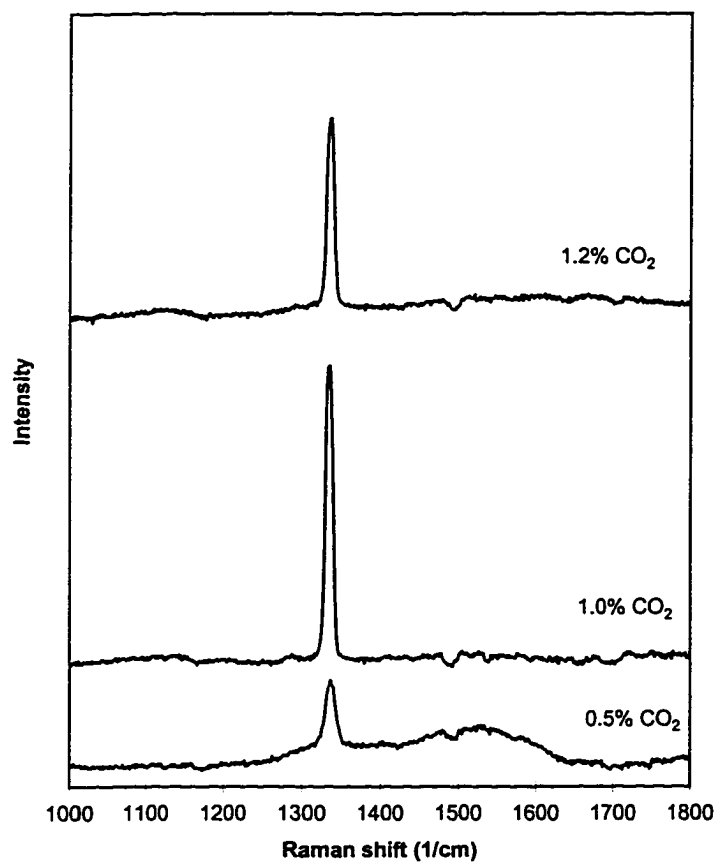
Figure 4.17   Raman spectra of CVD diamond under different CO_2 concentration

compared to that of the 0.5% CO_2 sample (3.57). But further increasing of CO_2 concentration (1.2%) does not lead to better Raman spectrum, however, decreases the growth rate.

The growth rate can be further increased by increasing the methane concentration. However, to keep the diamond quality, CO_2 concentration also needs to be increased, but should not be overdosed to upset the growth rate. A series of experiment was performed with different methane concentrations. For each methane concentration, CO_2 concentration is adjusted such that the Raman spectrum for the deposited diamond remains good while a high growth rate is obtained. Table 4.6 shows the optimized CO_2 concentrations for different CH_4 concentrations and the growth rate

Table 4.6   The optimized CO_2 concentration for different CH_4 concentration and their growth rate

Sample number:	1	2	3	4
CH_4 concentration (%):	1.5	3	5	6
CO_2 concentration (%):	2.0	3.5	5.2	6
Growth rate (μm/h):	1.67	2.5	3.17	3.8

under these conditions. Other growth parameters were kept the same as in Table 4.5. Figure 4.18 shows the SEM pictures of these samples. Note that different magnification is used for these SEM pictures as marked on the top of each picture. As expected, growth rate increases when methane and carbon dioxide concentration increase

simultaneously because more carbon species are available. However, the increment of

CO_2 is less than that of CH_4, which means the selective etching of graphite over

diamond by oxygen is very effective. The Raman spectra of these samples are shown in

Fig. 4.19. For all four samples, the 1540 cm^{-1} graphitic band had almost disappeared,

(a)

(b)

(c)

(d)
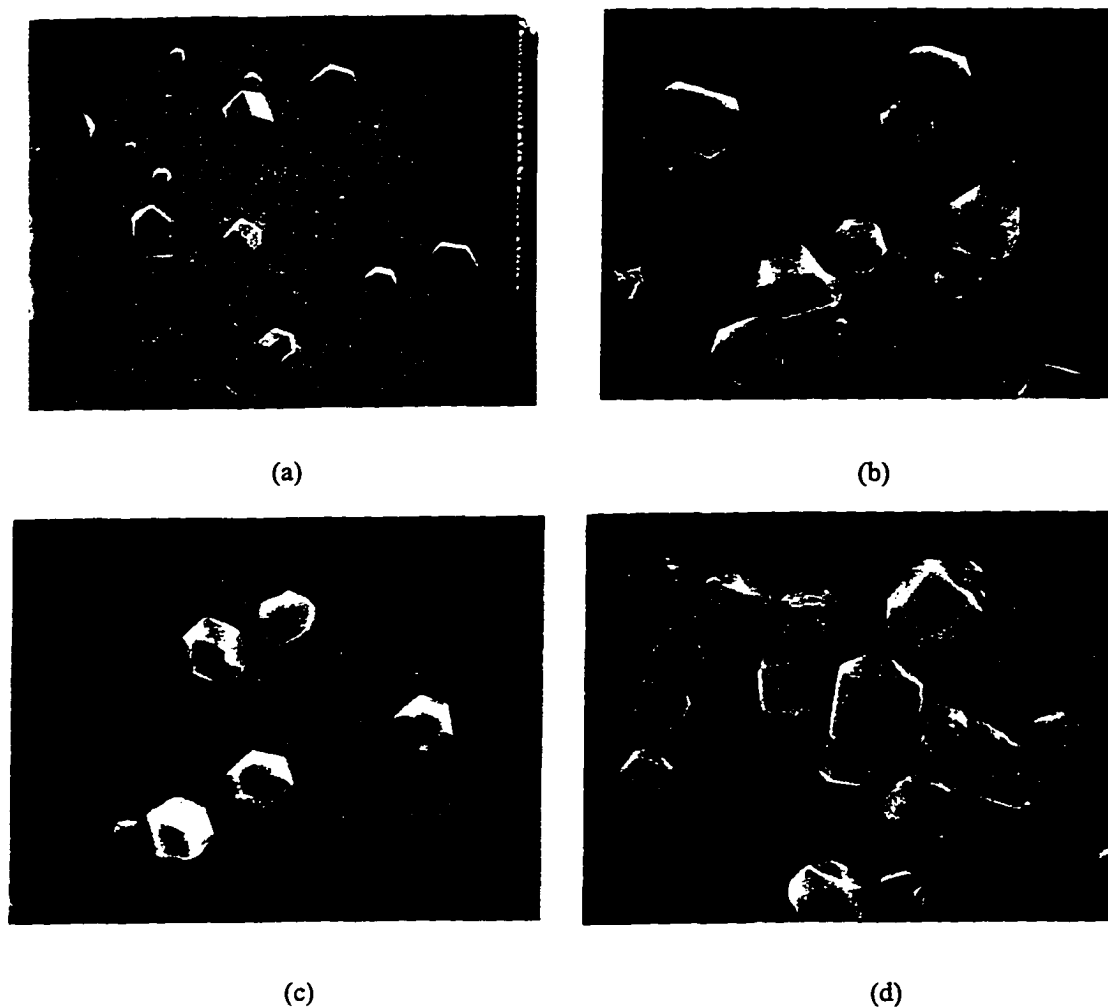
Figure 4.18 The effect of different CH_4 concentration with optimized CO_2 concentration: (a) 6% CH_4, 6% CO_2, (b) 5% CH_4, 5.2%CO_2, (c) 3% CH_4, 3.5 CO_2, and (d) 1.5 % CH_4, 2% CO_2. Note, different scales are used in the SEM as marked on top of each picture. Higher growth rate is obtained with higher CH_4 concentration, while the quality can be controlled by CO_2 concentration.
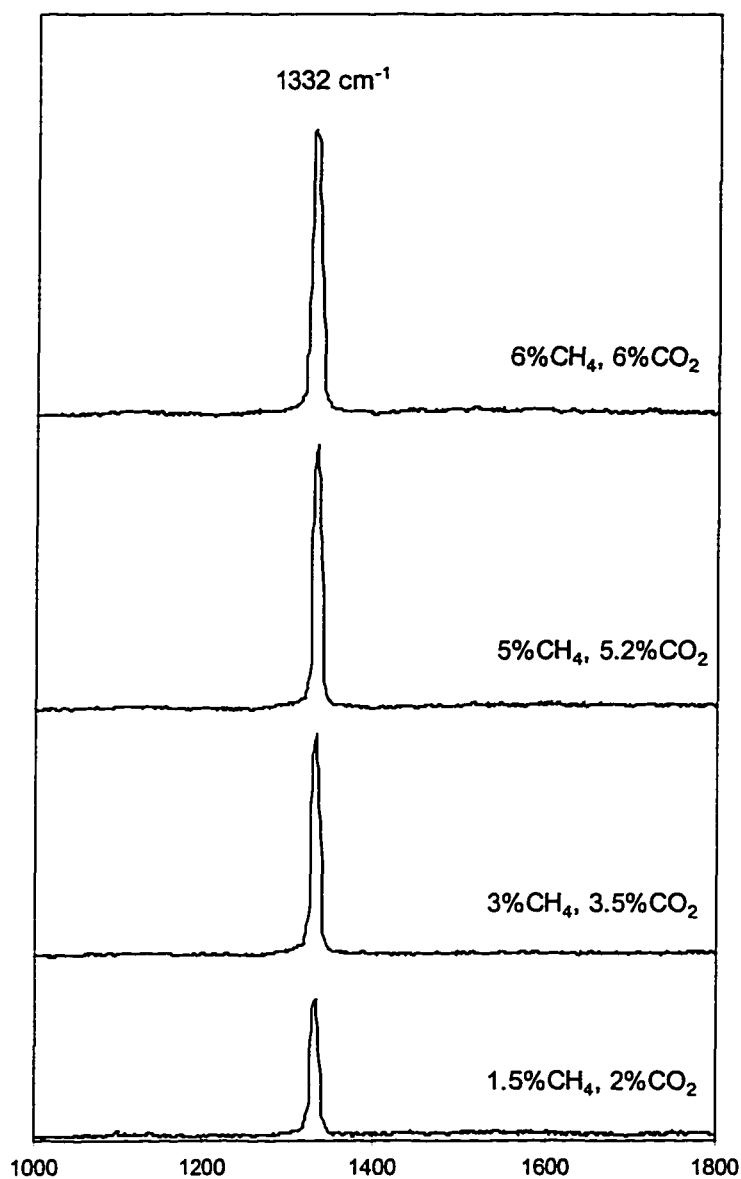
Figure 4.19   Raman spectra of CVD diamond under different optimized gas compositions

showing the good quality of diamond. The best result is given by sample #4, which has

the highest diamond band in Raman spectrum and highest growth rate. Further

investigation of increasing more CH_4 and CO_2 is limited by the maximum range of the

mass flow rate controller of our system.

In summary, it is found experimentally that pressure controls the diamond growth rate, it also affects the diamond quality through the gas temperature effect. Substrate temperature should be optimized to get the best quality of diamond. Higher or lower temperature results in graphite carbon or diamond-like carbon deposition. Increasing hydrogen percentage improves the diamond quality, however reduces the growth rate. Growth rate can be increased by increasing the methane concentration, and the diamond quality can be controlled by introducing a certain amount of CO_2. Based on the experimental results, the optimized parameters and gas composition for diamond growth in our system are listed in Table 4.7.

Table 4.7   Optimized diamond growth parameters and gas composition

Pressure:	40 Torr
Temperature:	600 °C
Microwave Power:	1000 W
Total Flow Rate:	900 Sccm
Methane Concentration:	6%
Carbon Dioxide Concentration	6%
Hydrogen	92%

4.4 Quantitative Raman Analysis using CVD Diamond as Reference

A fiber optic Raman probe was made using CVD diamond as the standard (Probe D5). Diamond was deposited on the quartz substrate using the optimized parameters listed in Table 4.7. This CVD diamond was then placed in front of the fiber optic Raman probe using the same structure of Probe D3 (Fig. 3.23). The gap between fiber end and CVD diamond is 2mm. A Raman spectrum was acquired when the probe was in air (Fig. 4.20). Compared to the Raman spectra acquired by Probe D3 , the glass Raman signal
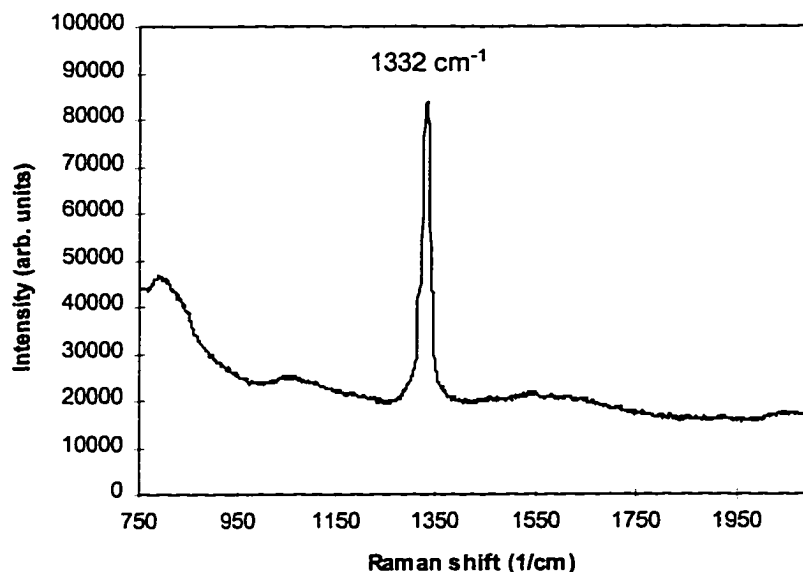
Figure 4.20   Raman spectrum of CVD diamond probe in air

around 750 cm^{-1} becomes larger. This glass Raman signal is generated inside the glass fiber by the excitation laser and scattered at the rough surface of the CVD diamond film. This rough surface scattered light has more chance to reach the collection fibers compared to the smooth surface of bulk in Probe D3 as shown in Fig. 4.21. Also the

1332 cm^{-1} diamond band becomes weaker and broader due to the small crystal size of the CVD diamond. Besides the glass Raman signal, the background of the Raman spectrum from the probe is not as flat as the micro-Raman spectrum. This is because micro-Raman
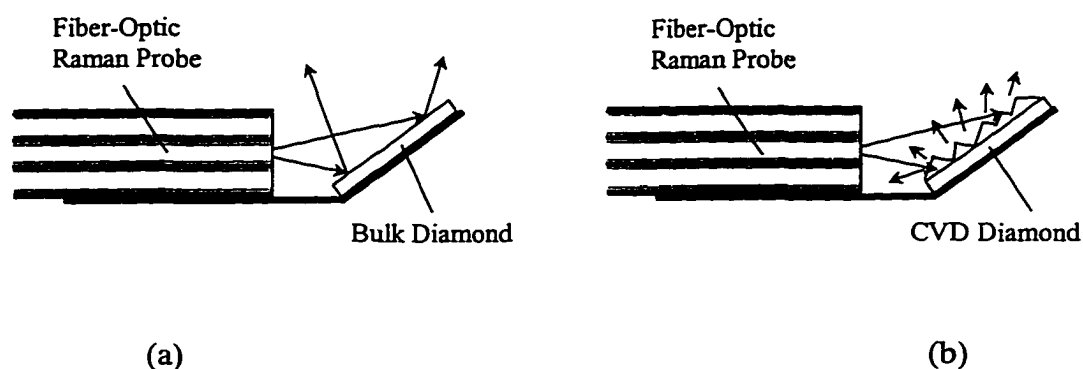
Figure 4.21 The reflection and scattering of glass Raman signal on (a) a smooth bulk diamond surface, and (b) a rough CVD diamond surface, respectively.

spectrum is acquired from a single diamond crystal, while fiber optic Raman is acquired within a relatively large area, and usually, graphite contamination at the boundary of crystals is more than that within the crystal.

Again, the probe performance was tested using the ethanol-water solution. A series Raman spectra were acquired with this probe as shown in Fig. 4.22. The 883.3 cm^{-1} ethanol peak area was calculated and normalized by the diamond peak area. A linear model built by regression was then used to predict the percentage of the ethanol. The result is shown in Table 4.8 and Fig. 4.23.
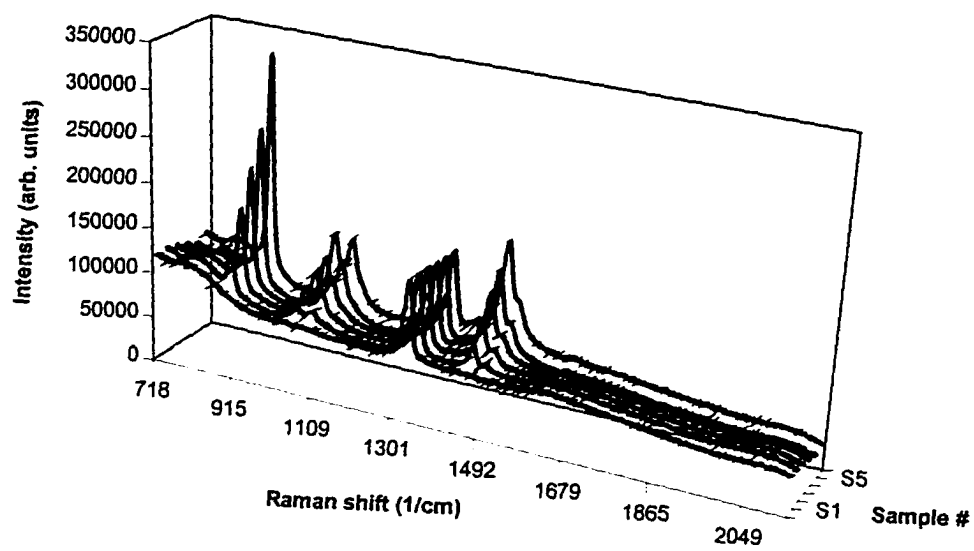
Figure 4.22 Raman spectra of ethanol-water solutions with different ethanol percentage acquired by the

CVD diamond probe

Table 4.8   Predicted ethanol volume percentage based on peak area method

after normalization with CVD diamond band

Sample Number	1	2	3	4	5	6
Measured Percentage (%)	0	19.50	39.51	57.79	78.15	100
Normalized Ethanol Peak Area	-0.01035	0.414645	0.87366	1.36733	1.84452	2.39798
Predicted Percentage (%)	1.41	18.93	37.85	58.20	77.87	100.69
error (%)	1.41	-0.57	-1.66	0.41	-0.27	0.68
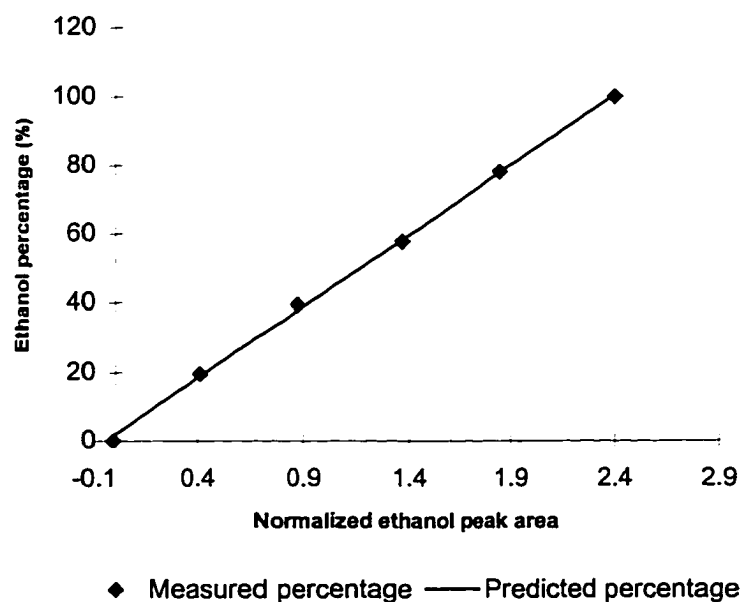
Figure 4.23   Predicted and measured ethanol percentages *vs.* peak area for the CVD diamond probe

Compared to the results for the bulk diamond probe in Table 3.7, larger prediction errors occur for the CVD diamond probe. This could be due to the interference between the glass Raman signal and the ethanol Raman band. Another reason for the error is that the weak CVD diamond Raman band reduces the S/N ratio for the standard, leading to a larger prediction error. However, no obvious non-linearity is observed between the normalized ethanol peak area and measured ethanol percentage.

To further investigate the probe performance in compensating the laser fluctuation and optical alignment, the laser power is intentionally changed and optical alignment is redone for the sample #4 (57.79% ethanol). Raman spectra are acquired using the CVD diamond referenced probe, and normalized ethanol peak area is used to predict the ethanol percentage using the same linear model. A standard deviation of 0.51% is observed when laser power coupled into the excitation fiber is varied form 4 mW to 8mW; and a standard deviation of ±0.58% is obtained when the optical alignment is redone 5 times. These results are comparable to the performance of the bulk diamond probe.

4.5 Summary

The concept of using CVD diamond as a standard in fiber optic Raman spectroscopy is investigated in this chapter. The quality of CVD diamond grown by a microwave assisted CVD system is optimized through different combinations of growth pressure, substrate temperature, and concentration of methane, hydrogen, and carbon dioxide. Under the optimized conditions, growth rate of 3.8 μm/h is achieved while high quality is maintained. The CVD diamond referenced fiber optic Raman probe is then

tested using the ethanol-water solution. Results similar to the bulk diamond referenced probe are obtained, however with a slightly larger prediction error. This error can be reduced by improving the CVD diamond quality and increasing particle size to enhance the diamond Raman intensity. The glass background can be reduced by smoothing the CVD diamond surface or using a band pass filter in the excitation fiber.

CHAPTER V

SUMMARY AND FUTURE RESEARCH

5.1 Summary

Raman spectroscopy is a useful tool for both species identification and concentration measurement. Its applications are extended to industrial on-line monitoring when fiber-optic technology is used. However, to perform quantitative analysis, an intensity standard is necessary.

In this work, a fiber-optic Raman probe with diamond as an intensity standard has been developed. The self-referencing property of the probe provides a reliable and simple way to measure the species concentration without recalibration. The performance of the probe is dependent on the structure. Five different probe structures have been designed. Probe D1 attaches a diamond window directly to the fiber end, which is the simplest structure. But the Raman spectrum acquired with this probe has a large glass Raman background due to the reflection at the diamond surface. Probe D2 uses a diamond particle, which is sealed in a glass lens and attached to the fiber Raman probe. This design has a compact structure and a reduced glass background. The probe is not sensitive to the index of refraction of the outside media and can successfully eliminate the power fluctuation in the excitation laser source. However, this design is not very effective to eliminate the effect due to different optical alignment. Probe D3 places a bulk diamond in front of the fiber with a 45-degree angle to eliminate the glass Raman background. This design has a good performance; however, an expensive big diamond is needed. Probe D4 is designed for remote sensing a diamond window directly attached,

and optical filters are employed to eliminate the glass background. Results from this probe show a good performance, however show a non-linearity due to the dependence on the refractive index of the tested media.

Research in CVD diamond growth provided an alternative to the expensive bulk diamond. A diamond growth method based on MPECVD system is investigated to get high quality CVD diamond. It has been found that the growth pressure controls the growth rate, and it affects the diamond quality through the gas temperature. Substrate temperature directly controls the diamond quality, high temperature leads to high graphite contamination, and low temperature results in diamond-like carbon deposition. Increasing hydrogen improves the diamond quality, however reduces the growth rate. High growth rate can be achieved by increasing methane concentration, and the diamond quality can be improved by introducing oxygen.

Probe D5 is a design based on CVD diamond film. The results from this probe are attractive although larger prediction error occurs compared to the results from the Probe D3. This error can be reduced if the quality of the CVD diamond can be further improved.

5.2 Future Research

Future research can be in the following areas:

5.2.1 Optimization of Probe Structure

The probe structures presented in this work have both advantages and disadvantages. Thus, a future effort could be the development of better probe structures for improved performance. One of the possible designs is shown in Fig. 5.1. In this design, the glass Raman signal is removed by a band pass filter, and the excitation

Band Pass Filter

Excitation Fiber

Glass Window
or coating

Collection Fiber

Diamond Window

0.25 Pitch GRIN Lens   Notch Filter
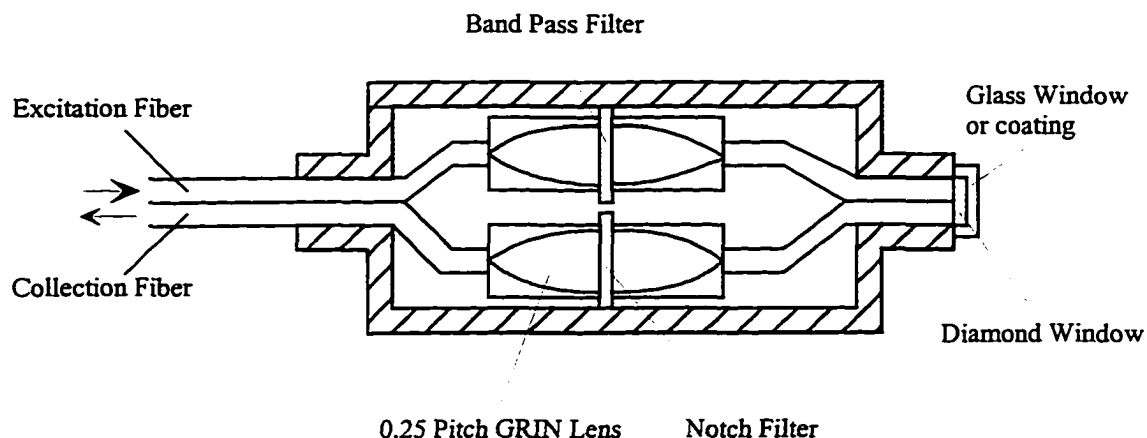
Fig. 5.1   A possible design for diamond referenced fiber-optic Raman probe

laser is filtered from the collection fiber through a notch filter. The use of GRIN lenses

reduces the probe size, leading to a compact structure. A small diamond window is

placed in front of the two fibers to provide an intensity reference. This diamond can be a

high quality CVD diamond with two sides polished to reduce surface scattering. In order

to reduce the refractive index dependence of the probe on the outside medium, the

diamond can be covered with a glass window or thin film coating, since refractive index

of glass (1.333) is close to most aqueous or organic solutions.

5.2.2 Sensitivity Enhancement

With a fixed excitation laser power and integration time, the sensitivity of the

measurement depends on the Raman intensity, which is controlled by the collection

efficiency of the probe. The output light form the excitation fiber has a diverging

cornical shape, therefore, the excitation volume is diverged and only the Raman signal

close to the probe can be collected. A possible solution to this problem is to increase the

effective excitation and collection volume by confining the excitation laser and scattered

Raman signal into a waveguide [12]. This structure is shown in Fig. 5.2. A transparent

tube is placed in front of the fiber Raman probe. The testing solution is sent through this
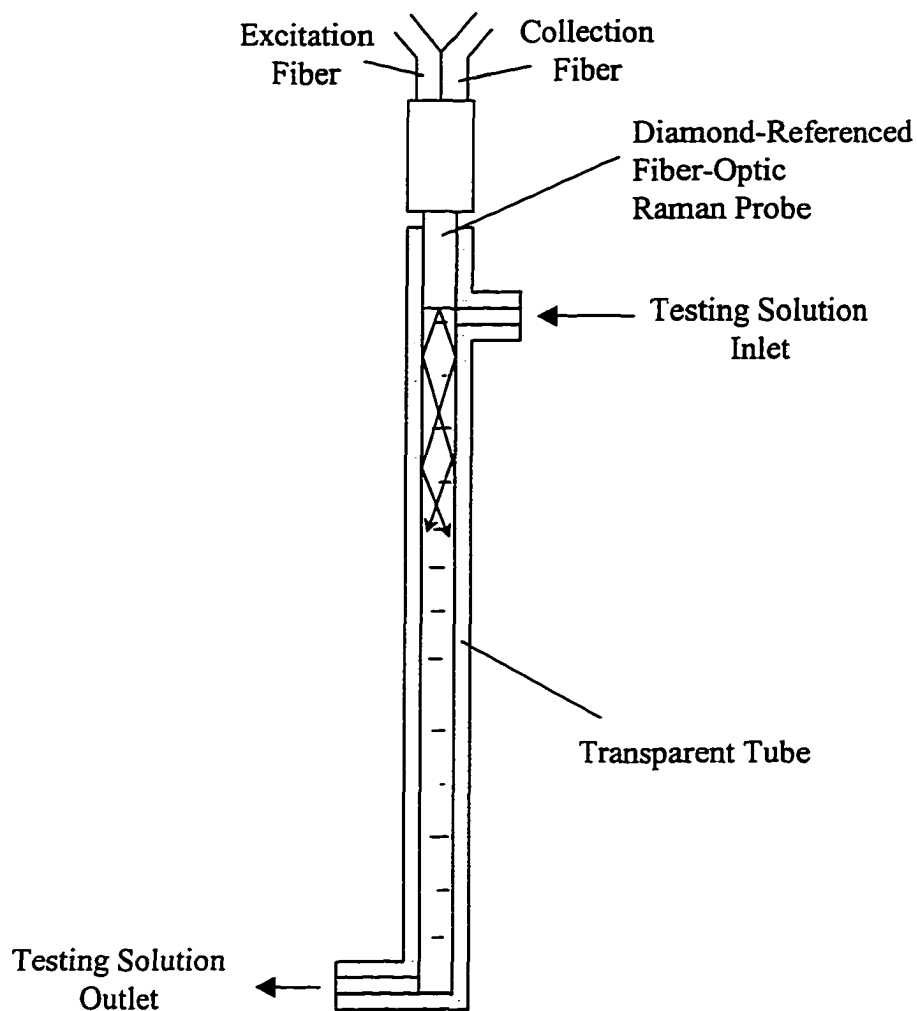
Figure 5.2   Sensitivity enhancement through a transparent tube to form a wave guide

tube. To form a waveguide, the measured solution should have a refractive index higher

than the tube material. Thus the collection efficiency can be largely improved since all of

the light is confined inside the waveguide. A preliminary experiment has been done for

DMSO solution in an 18-cm long, 0.5-cm inner diameter glass tube. The result in Fig.

5.3 shows that Raman signal with the waveguide is 3.5 times stronger than that of a
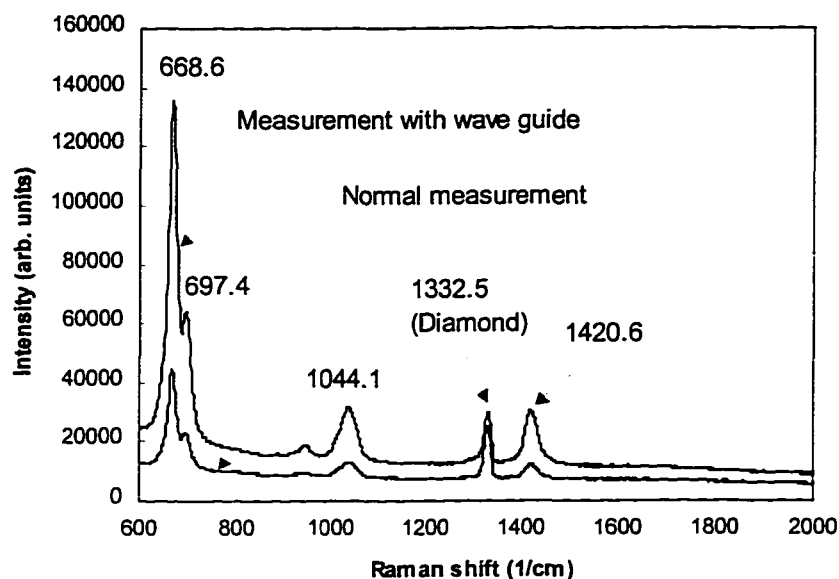
Figure 5.3   Raman spectra of the DMSO with and without waveguide

regular measurement. The signal can be enhanced further by increasing the length and

decreasing the inner diameter of the tube. For solution with index of refraction lower

than glass, polymer tube can be used. Further research in this area may lead to a highly

sensitive measurement technique.

5.2.3 SERS

It is possible to perform Quantitative SERS experiment on the rough surface of

CVD diamond if the CVD diamond surface is coated with silver. Since the surface grain

size of CVD diamond film can be easily controlled by different growth time, the surface

enhancement can be optimized, while an intensity standard is available from the diamond itself.

5.2.4 High Quality, High Growth Rate for CVD Diamond

The investigation of CVD diamond is far from enough to approach optimized quality and growth rate. For microwave assisted CVD process, different gas combination and different growth parameters still need to be explored. Other than microwave enhanced CVD process, it has been reported that high quality and high growth rate is achieved using oxygen-acetylene flame [119-124]. A preliminary growth experiment using O_2-C_2H_2 flame has been done in microelectronics laboratory [125], which shows an attractive result. As shown in Fig. 5.4, 15 µm diamond particles are grown within 15

Figure 5.4   SEM picture of diamond particles grown by oxygen-acetylene flame technique

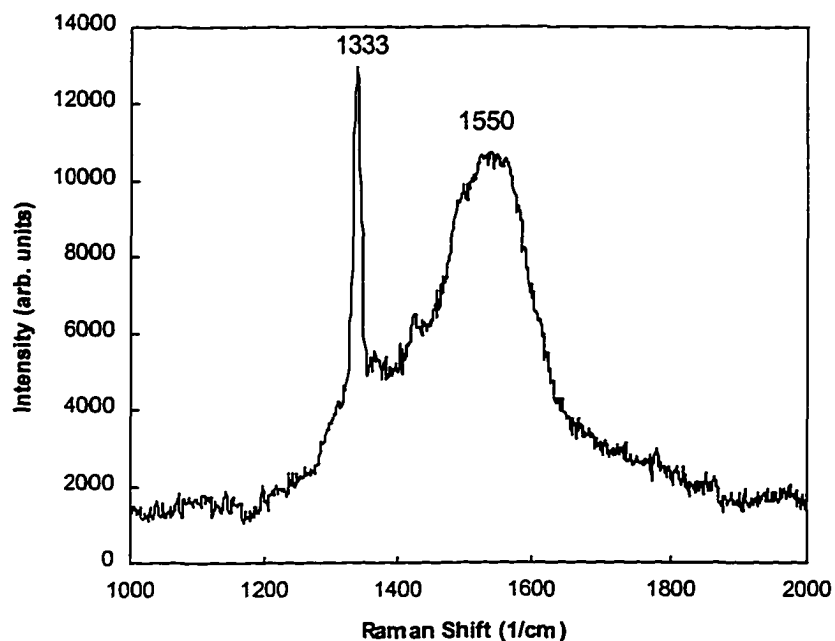Figure 5.5   Raman spectrum of the diamond shown in Fig.5.4

minutes, leading to a growth rate around 60 μm/h. This growth rate is much higher than

that obtained in MPECVD process. The Raman spectrum in Fig. 5.5 shows a clear

diamond peak at 1332 cm⁻¹ although high graphite contamination exists as indicated with

a hump around 1540 cm⁻¹. Further research needed to improve the quality of the flame

grown diamond.

REFERENCES

[1]   C. V. Raman and K. S. Krishnan, *Nature* (London) **121**, 501 (1929).

[2]   J. H. Hibben, *The Raman Effect and Its Chemical Applications*, Reinhold, New York (1939).

[3]   S. P. S. Porto and D. L. Wood, *J. Opt. Soc. Am.* **52**, 251 (1962).

[4]   P.R. Carey, *Biochemical Application of Raman and Resonance Raman Spectroscopies*. Academic Press, New York (1982).

[5]   A. B. Harvey, ed., *Chemical Applications of Non-Linear Raman Spectroscopy*, Academic Press, New York (1981).

[6]   R. L. Garrel, *Anal. Chem.*, **61**(6), 401A (1989).

[7]   D. B. Chase and J. F. Rabolt ed., *Fourier Transform Raman Spectroscopy*, Academic Press, San Diego (1994).

[8]   N. Q. Dao and M. Jouan, *Sensors and Actuators B*, **11**, 147 (1993).

[9]   G. R. Trott and T. E. Furtak, *Rev. Sci. Instrum.* **51**, 1493 (1980).

[10]   R. L. McCreery, M. Fleischmann and P. Hendra, *Anal. Chem.*, **55**, 146 (1983).

[11]   S. D. Schwab and R. L. McCreery, F. T. Gamble, *Anal. Chem.*, **58**, 2486 (1986).

[12]   S. D. Schwab and R. L. McCreery, *Appl. Spectrosc.*, **41**, 126 (1987).

[13]   C. D. Allred and R. L. McCreery, *Appl. Spectrosc.*, **44**, 1229 (1990).

[14]   K. I. Mullen, D. X. Wang, L. G. Crane, and K. T. K. Carreon, *Spectrosc.* **7** (5), 24 (1992).

[15]   C. Wang, T. J. Vickers, J. B. Schlenoff, and C. K. Mann., *Appl. Spectrosc.* **46** (11), 1729 (1992).

[16]   D. D. Archibald, L. T. Lin, and D. E. Honigs, *Appl. Spectrosc.*, **42**(8), 1558 (1988).

[17]   E. N. Lewis, V. F. Kalasinsky and I. W. Levin, *Anal. Chem.*, **60**, 2658 (1988).

[18]   M. L. Myrick and S. M. Angel, *Appl. Spectrosc.* , **44** (4), 565 (1990).

[19]   C. L. Schoen, T. F. Cooney, S. K. Sharma, and D. M. Carey, *Appl. Opts.* **31** (36), 7707 (1992).

[20]   J. R. Ferraro and K. Nakamoto, *Introductory Raman spectroscopy*, Academic Press, Boston (1994).

[21]   A. Anderson, *The Raman Effect*, Marcle Dekker, Inc., New York (1971).

[22]   M.Fleishmann, P.J.Hendra and A.J.McQuillan, *Chem. Phys. Lett.*, **26**, 163 (1974).

[23]   K. O. Christe, E. C. Curtis, D. A. Dixon, H. P. Mercier, J. C. P. Sanders, and G. J. Schrobilgen, *J. Am. Chem. Soc.*, **113**, 3351 (1991).

[24]   L. D. Ziegler, Y. C. Chung, P. G. Wang, Y. P. Zhang, *J. Phys. Chem.*, **94**, 3394, (1990).

[25]   S.Sun, R.L.Birke, and J.R.Lombardi, *J. Phys. Chem.*, **94**, 2005 (1990).

[26]   E. Koglin, H. H. Lewinsky, and J. M. Sequarts, *Sur. Sci.*,**158**, 370 (1985)

[27]   J. G. Grasselli and B. J. Bulkin, *Analytical Raman Spectroscopy*, John Wiley & Sons, New York (1991).

[28]   T. Hirschfeld and B Chase, *Appl. Spectrosc.* **40**, 133 (1986).

[29]   S. Zheng, A. T. Tu, *Appl. Spectrosc.* **41** (4), 696 (1987).

[30]   H. Ishida, R. Kamoto, S. Uchida, A. Ishitani, Y. Ozaki, K. Iriyama, E. Tsukie, H. Shibata, F. Ishihara, and H. Kameda, *Appl. Spectrosc.* **41**, 407 (1987).

[31]   N. T. Yu, and E. J. East, *J. Mol. Chem.* **250**, 2196 (1975).

[32]   T. G. Shiro and C. A. Grygon, *J. Mol. Struct.*, **173**, 79 (1988).

[33]   J. W. Petrich and J. L. Martin, *Chem. Phys.*, **131** (1), 31 (1989).

[34]   J. Lugtenburg, R. A. Mathies, R. G. Griffin, and J. Herzfeld, Trends. *Biochem. Sci.*, **13** (10), 388 (1988).

[35]   B. Jolles, L. Chinsky, and A. J. Laigle, *Raman Spectrosc.*, **19** (3), 155 (1988).

[36]   Y. Nonaka, M. Tsuboi, and K. Nakamoto, *Raman Spectrosc.*, **21**, 133 (1990).

[37]   D. L. Gerrard and J. Birnie, *Anal. Chem.*, **62**, 140R (1990).

[38]   Wagner, *J. Appl. Surf. Sci.*, **50**, 79 (1991).

[39]   T. Hara, H. Hagiwara, R. Ichikawa, S. Nakashima, K. Mizoguchi, W. L. Smith, C. Welles, S. K. Hahn, and L. Larson, *IEEE Electron Device Lett.*, **11** (11), 485 (1990).

[40]   W. M. Duncan, R. J. Matyi, H. Shiqijo, Y. C. Kao, and H. Y. Liu, *Appl. Phys. Lett.*, **57** (16), 1631 (1990).

[41]   J. Wagner, M. Ramsteiner, H. Seelewinder, and J. Clark, *J. Appl. Phys.*, **64** (2), 802 (1988).

[42]   S. Zhang, M. V. Klein, J. Klem, H. Morkoc, *Phys. Lett. A,* **64** (2), 802 (1988).

[43]   G. Landu, R. Carles, C. Fontaine, E. Bedel, and A. Munoz-Yague, *J. Appl. Phys.*, **66** (1), 196 (1989).

[44]   T. P. Humphreys, J. B. Posthill, K. Das, C. A. Sukow, R. J. Nemanich, N. R. Parikh, and A. Majeed, *Jpn. J. Appl. Phys. Part2*, **28** (9), L1595 (1989).

[45]   K. I. Mullen, D. X. Wang, L. G. Crane, and K. T. K. Carreon, *Spectrosc.* **7** (5), 24 (1992).

[46] K. Xi, S. K. Sharma, G. T. Taylor, and D. W. Muenow, *Appl. Spectrosc.*, **46**, 189 (1992).

[47] G. Ellis, M. Claybourne, and S. E. Richards, *Spec. Acta.*, **46A**, 227 (1990).

[48] Y. Ozaki, R. Cho, K. Ikegawa, S. Muraishi, and K. Kawauchi, *Appl. Spectrosc.*, **46**, 1503 (1992).

[49] C. M. Hodges and J. Akhavan, *Spec. Acta.*, **46A**, 303 (1990).

[50] D. P. Strommen and K. Nakamoto, *Laboratory Raman Spectroscopy*, John Wiley & Sons, New York (1984).

[51] T. B. Shope, T. J. Vickers, and C. K. Mann, *Appl. Spectrosc.*, **41** (5), 908 (1987).

[52] D. A. Gilmore, D. Gurka, and M. B. Denton, *Appl. Spectrosc.*, **49** (4), 508 (1995).

[53] J. D. Womack, T. J. Vickers, and C. K. Mann, *Appl. Spectrosc.*, **41** (1), 117 (1987).

[54] L. Lin, C. K. Mann, and T. J. Vickers, *Appl. Spectrosc.*, **41** (3), 422 (1987).

[55] C. K. Mann, T. J. Vickers, and J. D. Womack, *Appl. Spectrosc.*, **41** (8), 1324 (1987).

[56] J. E. Field, *The properties of diamond*, Academic Press, Oxford (1979).

[57] G. Davies, *Properties and growth of diamond*, INSPEC, London, UK (1994).

[58] C. Ramaswamy, *Indian J. Phys.*, **5**, 97 (1930).

[59] R. Robertson and J. J. Fox, *Nature* (London) **125**, 704, (1930).

[60] S. A. Solin and A. K. Ramdas, *Phys. Rew. B*, **1** (4), 1687 (1970).

[61] J. B. Dennison, M. Holtz, and G. Swain, *Spectroscopy*, **11** (8), 38 (1996).

[62] J. Wagner, C. Wild, and P. Koild, *Appl. Phys. Lett.*, **59**, 779 (1991).

[63] S. D. Schwab, and R. L. McCreery, *Anal. Chem.*, **56**, 2199 (1984).

[64] P. Plaza, N. Q. Dao, M. Jouan, H. Fevier, and H. Saisse, *Appl. Opt.*, **25**, 3448 (1986).

[65] S. D. Schwab and R. L. McCreery, *Appl. Spectrosc.*, **41** (1), 126 (1987).

[66] P. L. Hendra, G. Ellis, and D. J. Culter, *J. Raman Spectrosc.*, **19**, 413 (1988).

[67] D. Heiman, X. L. Zheng, S. Sprunt, B. B. Goldberg, and E. D. Isaacs, *SPIE*, **1055**, 96 (1989).

[68] S. A. Soper, and T. Kuwana, *Appl. Spectrosc.*, **43**, 1180 (1989).

[69] M. Jiaying and L. Zong, *Appl. Spectrosc.*, **45**, 1302 (1991).

[70] C. K. Chong, C. Shen, Y. Fong, J. Zhu, F. Yan, S. Brush, C. K. Mann and T. J. Vickers, *Vibrational Spectroscopy.*, **3**, 35 (1992).

[71] S. K. Sharma, C. L. Schone, and T. F. Cooney, *Appl. Spectrosc.*, **47** (3), 377 (1993).

[72] J. Ma and Y. Li, Appl. *Spectrosc.*, **48**(12), 1529 (1994).

[73] J. B. Cooper, P. E. Flecher, T. M. Vess, and W. T. Welch, *Appl. Spectrosc.*, **49** (5), 586 (1995)

[74] P. Plaza, Nguyen Quy Dao, M. Jouan, H. Fevrier and H. Saisse, *Appl. Opts.*, **25**, 3448 (1986).

[75] C. K. Mann, J. R. Goleniewski, and C. A. Sismanidis, *Appl. Spectrosc.*, **36**, 223 (1982).

[76] L. L. Tyson, Y. -C. Ling, and C. K. Mann, *Appl. Spectrosc.*, **38**, 663 (1984).

[77] P. Geladi and B. R. Kowalski, *Anal. Chem. Acta.*, **185**, 1 (1986).

[78] K. R. Beebe and B. R. Kowalski, *Anal. Chem.*, **59**, A1007 (1987).

[79] D. M. Haaland, and E. V. Thomas, *Anal. Chem.*, **60**, 1193 (1988).

[80] J. G. Grasselli, M. A. Hazle, and L. E. Wolfram, *Molecular Spectroscopy*, A. West, Ed., Heyden, New York (1977).

[81] J. D. Womack, C. K. Mann, and T. J. Vickers, *Appl. Spectrosc.*, **43** (3), 527 (1989).

[82] J. Wagner, C. Wild, and P. Koidl, *Appl. Phys. Lett.*, **59**, 779 (1991).

[83] D. S. Knight, and W. B. White, *J. Mater. Res.*, **4**, 385 (1989).

[84] P. K. Bachmann and H. Lydtin, *Diamond and Diamond-like Carbon*, edited by J. Angus, R. Clausing, L. Horton, and P. Koidl. Plenum, New York (1991).

[85] S. P. Chauhan, J. C. Angus, and N. C. Gardner, *Appl. Phys. Lett.*, **47**, 4746 (1976).

[86] T. D. Moustakas, *Synthetic Diamond: Emerging CVD Science and Technology*, edited by K. E. Spear and J. P. Dismukes, John Wiley & Sons, Inc. New York (1994).

[87] Y. Liou, A. Inspector, R. Weimer, and R. Messier, Appl. Phys. Lett., 55, 631 (1989).

[88] W. Zhu, C. A. Randale, R. A. Badzian, and R. Messier, *J. Vac. Sci. Technol. A*, 7, 2315 (1989).

[89] H. Eto, Y. Tamou, and N. Kikuchi, *Diamond and Diamondlike and Related Coatings,* edited by P. K. Bachmann and A. Matthews. Elsevier, Amsterdam, pp. 373-379 (1992).

[90] Y. Sato and M. Kamo. *The Principles of Natural and Synthetic Diamond*, edited by J. E. Field. Academic, Orlando, FL (1992).

[91] S. Iijima, Y. Arakawa, and K. Baba, *Appl. Phys. Lett.*, **57**, 2646 (1990).

[92]   K. Suzuki, A. Sawabe, H. Yasuda, and T. Inuzaka, *Appl. Phys. Lett.*, **50**, 728 (1987).

[93]   A. Sawabe and T. Inuzaka, *Thin Solid Films*, **137**, 89 (1986).

[94]   C. P. Chang, D. L. Flamm, D. E. Ibbotson, and J. A. Mucha, *J. Appl. Phys*, **63**, 1744 (1988).

[95]   P. K. Bbachmann, W. Drawl, D. Knight, R. Weimer, and R. F. Messier, *Diamond and Diamond-Like Materials Synthesis*, edited by G. H. Johnson, A. R. Badzian, and M. W. Geis, Material Research Society, Pittsburgh (1988).

[96]   S. Iijima, Y. Arakawa, and K. Baba, *J. Mater. Res.*, **6**, 1491 (1991).

[97]   F. Tuinstra, J. L. Koenig, *J. Chem. Phys.* **53**, 1126 (1979).

[98]   R. T. Anthony, *Diamond and Diamond-like Films and Coatings*, edited by R. E. Clausing. Plenum, New York (1991).

[99]   R. E. Clausing, L. Heatherly, and E. D. Specht, *Diamond, Diamond and Diamond-like Films and Coatings*, edited by R. E. Clausing. Plenum, New York (1991).

[100]   B. V. Spitsyn, L. L. Bouilov, and B. V. Derjagin, *J. Crystal Growth*, **52**, 219 (1981).

[101]   S. Matsumoto, Y. Sato, M. Kamo, and N. Setaka, *Jpn. J. Appl. Phys.*, **21**, L183 (1982).

[102]   S. Matsumoto, Y. Sato, M. Tsatsumi, and N. Setaka, *J. Mater. Sci.*, **17**, 3106 (1982).

[103]   M. Tsuda, M. Nakajima, and S. Oikawa, *J. Am. Chem. Soc.*, **108**, 5780 (1986).

[104]   D. Huang, M. Frenklach, and M. Maroncelli, *J. Phys. Chem.*, **92**, 6379 (1988).

[105] S. J. Harris, *Appl. Phys. Lett.*, **56**, 2298 (1990).

[106] S. J. Harris and M. R. Marata, *J. Mater. Res.*, **5**, 2313 (1990).

[107] J. C. Angus and C. C. Hayman, *Science*, **241**, 913 (1988).

[108] D. V. Fedoseev, V. P. Varnin, and B. V. Deryagin, *Russ. Chem. Rev.*, **53**, 435 (1984).

[109] Y. Saito, K. Sato, H. Tanaka, K. Fujita, and S. Matsuda, *J. Mater. Sci.*, **23**, 842 (1988).

[110] M. Frenklach and H. Wang, *Phys. Rev. B* **43**, 1520 (1991).

[111] K. E. Spear, *J. Am. Ceram. Sci.*, **72**, 171 (1989).

[112] M. Frenklach and K. E. Spear, *J. Mater. Res.*, **3**, 133 (1988).

[113] E. S. Machlin, *J. Mater. Res.*, **3**, 958 (1988).

[114] T. Kawato and K. Kondo, *Jpn. J. Appl. Phys.*, **26**, 1429 (1987).

[115] Y. Liou, R. Weimer, D. Knight, and R. Messier, *Appl. Phys. Lett.*, **56**, 437 (1990).

[116] T. Kim and T. Kobayashi, *Jpn. J. Appl. Phys.*, **33**, L459 (1994).

[117] M. Marinelli, E. Milani, M. Montuori, A. Paoletti, and A. Tebano, *J. Appl. Phys.*, **76** (10), 5720 (1994).

[118] P. K. Bachmann, D. Leers, and H. Lydtin, *Diamond and Related Materials*, **1**, 1 (1991).

[119] Y. Hirose and S. Amanuma, *J. Appl. Phys.*, **68** (12), 6410 (1990).

[120] R. S. Yalamanchi and K. S. Harshavardhan, *J. Appl. Phys.*, **68** (11), 5941 (1990).

[121] T. Abe, M. Suemitsu, and N. Miyamoto, *J. Appl. Phys.*, **74** (5), 3531 (1993).

[122] W. Zhu, B. H. Tan, J. Ahn, and H. S. Tan, *J. Mater. Sci.*, **30**, 2130 (1995).

[123] T. Abe, M. Suemitsu, N. Miyamoto, and N. Sato, *J. Appl. Phys.*, **73** (2), 971

(1993).

[124] M. Murayama, S. Kojima, and K. Uchida, *J. Appl. Phys.*, **69** (11), 7924 (1991).

[125] Microelectronics Laboratory internal report.

VITA

Jianli Zheng

1120 Bolling Avenue, 181-C

Norfolk, Virginia 23508

USA

Jianli Zheng was born in Tongxiang, Zhejiang province, People's Republic of China, in December 1964. He received his B. S. and M. S. degrees in Optical and Scientific Instrumentation Engineering at Zhejiang University, Hangzhou, P. R. China, in 1984 and 1987, respectively. From 1987 to 1994, he joined the Institute of Measurement Technique and Instrumentation in Zhejiang University as an assistant professor. Since 1994, he has been a doctoral candidate with the Electrical and Computer Engineering Department at Old Dominion University, Norfolk, Virginia, majoring in Electrical Engineering and minoring in Computer Science. He will receive his Ph.D. degree in December 1997. He has two patents pending and is the co-author of two books in optical and sensing technologies, co-translator of one book in computer software, and has published 12 journal papers and 7 conference articles. His research interests include sensor technology and semiconductor processing.